UNIVERSITA DEGLI STUDI DI PISA
FACOLTA' DI INGEGNERIA

Dipartimento Ingegneria Aerospaziale
Laurea Specialistica in Ingegneria Aerospaziale
Curriculum Aeronautico/Aerodinamico

Sediment transport models for Shallow Water equations

Anno Accademico 2011/2012

Candidato:
Cinat Paolo

Relatore:
M.V. Salvetti
H. Guillard
M. Bilanceri

A mio zio Angelino.

Non è possibile riprodurre i nostri pensieri in parole,
queste rimangono troppo rapidamente indietro,
come ombre, dietro le sensazioni.
[Friedrich Nietzsche]

Abstract

The numerical simulation of sediment transport problems is considered. The physical problem is modeled through the shallow-water equations coupled with the Exner equation to describe the time evolution of the bed profile. Three different models of solid transport discharge are considered. The spatial discretization of the governing equations is carried out by a finite-volume method and a modified Roe scheme designed for non-conservative systems. Linearized implicit schemes for time advancing are built through a recently proposed strategy, based on automatic differentiation to compute the flux Jacobians and on the defect correction approach to reach second-order accuracy. Explicit schemes for time advancing are compared with implicit ones in one-dimensional sediment transport problems, characterized by different time scales for the evolution of the bed. It is shown that, independently of the model used for the solid transport discharge, for slow and intermediate speeds of interaction between the bedload and the water flow, for which the use of large time steps is compatible with the capture of the bed evolution, implicit time advancing is far more efficient than explicit one with a CPU reduction up to more than four orders of magnitude. In the last part, a realistic test is proposed, concerning the sediment transport in Tunis Lake. This lake is divided into two main parts, the North Lake and South Lake. The simulations are performed setting input values to be consistent with reality, in order to have a good representation of sediment transport in Tunis Lake.

Contents

List of Symbol

A_g sediment constant which expresses the fluid-sediment interaction for Grass model.

A_d sediment constant which expresses the fluid-sediment interaction for modified Grass model.

$\tilde{A}$ sediment constant which expresses the fluid-sediment interaction for MPM model. It is the same as A_g.

$\tilde{A}_d$ sediment constant which expresses the fluid-sediment interaction for modified MPM model. It is the same as A_d.

a constant introduced in MPM simplification, which is 8 for MPM e 5.7 for FLV model.

$\tilde{a}$ the same as Ψ

C express the linear connection between shear stress and the square of velocity (Chezy form). It can be calculated with different theories (Chezy, Manning, etc.)

$\mathcal{C}$ Chezy constant for shear stress.

$c_s = \frac{c_s}{c}$ ratio between the volume occupied by the sediment and the water.

d grain diameter.

d_{50} mean grain diameter for a sediment cluster.

Fr Froude number.

$G = \frac{\rho_s}{\rho}$ ratio between the sediment density and the fluid density.

g gravity constant

H indicates the depth. It is taken positive from the reference level too the bottom. [7] [8]

h indicates the water column height. It is taken positive from the reference level too the bottom. [7] [8]

$K = (G-1)gd_{50}$ constant used to simplify MPM model

L_ref indicates a reference level. [7] [8]

m_g Grass model exponent.

N_p number of particle which fall from a fixed area.

N_s number of particle which separate from a fixed area.

p porosity.

p_r transport probability .

$\tilde{p}$ separation probability for sediment particles in a fixed area.

q global sediment flow rate.

q_b bedload sediment flow rate.

q_f mass flow rate.

q_s suspension and saltation sediment flow rate.

R_h hydraulic radius.

u velocity on x direction. [7] [8]

$\tilde{u}$ critical velocity which express the Shield condition assuming the shear stress expressed in Chezy form.

V volume occupied by water.

V_s volume occupied by sediment.

v velocity on x direction. [7] [8]

w_s sediment falling velocity settling velocity.

Z bed slope. Using the same notation as in [7] [8], it is expressed as $Z = L_{ref} - H$.

ρ fluid density.

ρ_s sediment density.

γ specific water weight.

γ_s specific sediment weight.

η Manning coefficient.

Φ intensity of sediment load.

Ψ load threshold for sediment transport.

θ non dimensional shear stress.

θ_{cr} Shields parameter, which expresses the non dimensional critical shear stress (Shields theory).

τ shear stress at the bed.

τ_{cr} critical shear stress.

ξ porosity factor $\frac{1}{1-p}$.

ζ distance between the free surface and the reference level. Using the same notation as in [7] [8], it is expressed as $\zeta = h - H$.

Introduction

The numerical simulation of bedload sediment transport processes caused by the movement of a fluid in contact with the sediment layer is of significant interest for many environmental and engineering problems. The hydrodynamic part is usually modeled through the classical shallow-water equations coupled with a continuity or Exner equation, expressing the conservation of the sediment volume, in which the solid transport discharge is provided by a closure model. Many different models of solid transport discharge are available in the literature (see, e.g., [7] [32] for a review). Moreover, a huge amount of work has been done in the last decades to develop numerical methods for the simulation of sediment transport problems (see, e.g., the references in [19] [7]). In previous works executed by Aerospace Engineering Department of Pisa, in collaboration with INRIA Sophia, they focused on the development and on the validation of a strategy for implicit time advancing of the the shallow-water equations coupled with the Exner equation, based on a defect-correction approach and on a time linearization, in which the flux Jacobians are computed through automatic differentiation [36] [31] [28]. This time advancing strategy was coupled with two different finite-volume methods for space discretization, viz. the SRNH predictor-corrector scheme [19] and a modified Roe scheme for non-conservative systems of equations [7]. The Grass expression [16], which provides one of the most popular and simple models for solid transport discharge, was used. Different 1D and 2D numerical experiments showed that, if the time scales characterizing the evolution of the hydrodynamic and morphodynamic components are not too small, implicit time advancing leads to large reductions of the computational costs with respect to those of explicit schemes, while preserving the result accuracy.

The aim of the present work is to investigate the behavior of the proposed implicit time advancing strategy, in terms of accuracy and efficiency, when the model of solid transport discharge is varied.

As a first step, it is considered a correction of the Grass model [10], to improve the accuracy of the physical model. The Grass model describes bedload as a function of the water velocity, considering an incompressible fluid in a 1D channel. For the Grass model, the maximum discharge value is where the fluid velocity reaches its maximum, i.e. near the free water surface. This is not in agreement with the physical reality, for which bedload is manifested at the bottom. The same correction proposed in [10] is investigated in this work, considering the water column, with good results from the numerical point of view.

Moreover, in addition to the Grass model, it is considered herein the Meyer-Peter-Müller (MPM) model [35], which is also widely used in numerical simulations of this type of problems. The main difference with respect to the Grass model is that the

MPM model takes into account the fact that the bottom movement starts when the shear stress exceeds a given critical value, as from a numerical viewpoint, the presence of a threshold in the bottom evolution may be a source of stiffness and, therefore, it is interesting to investigate whether and to which extent the efficiency of the proposed implicit linearized schemes is affected. Note that automatic differentiation together with the defect-correct approach allow the numerical method to be easily adapted to changes in physical modeling in general, and, in particular, in the modeling of the solid transport discharge. As for numerical discretization in space, the present study is limited to the modified Roe scheme. This is motivated by the fact that in a previous studies indicated that overall performance of the implicit time advancing is practically independent of the space discretization scheme to which it is coupled [37] [31]. Furthermore this analysis is completed investigating what happens varying the intensity of the threshold, considering 3 different value of the velocity magnitude.

Finally, the same correction analyzed for Grass model is proposed to MPM model, to investigate if this leads an overall improvement in computational efficiency and physical accuracy. Also in this case, results were compared between implicit and explicit scheme, varying the threshold magnitude.

The different time advancing schemes and physical models are appraised in the numerical simulation of one-dimensional test problems, characterized by different time scales for the interaction between the water flow and the the bed evolution. The same numerical schemes used in the 1D case are finally applied to 2D simulations of realistic sediment transport problems. As a first step, the Grass model it is used to study the sediment transport in the North and South Tunis lake.

Part I

Sediment transport problem

Chapter 1

Physical Model

Sediment transport model in a depth of water is solved coupling a morphodynamical component and an hydrodynamical component. The hydrodynamical component is modeled by Shallow Water equations, described in Sec. 1.1. The morphodynamical component is modeled by Exner equation, described in Sec. 1.2, where also some sediment transport model are presented.

1.1 Shallow water equations

Shallow Water equations are used to study fluid movement in rivers, channel and coastal areas. They are a set of hyperbolic partial differential equations which describes the fluid motion in a depth of water. The general characteristic of shallow water flows is that the vertical dimension is much smaller than the typical horizontal scale. The name shallow derives from that characteristic. The Shallow Water equations are derived from the Navier-Stokes equations, which describes the motion of fluids, presented in system (1.1). In an inertial frame of reference, the general form of the equations of fluid motion is:

$$\begin{cases} \frac{\partial \rho}{\partial t} + div(\rho \vec{u}) = 0 \\ \frac{\partial (\rho \vec{u})}{\partial t} + div(\rho \vec{u}\vec{u}) = \rho \vec{b} + \bar{\bar{T}} \end{cases} \tag{1.1}$$

where $\vec{u}$ is the flow velocity, ρ is the fluid density, $\bar{\bar{T}}$ is the Cauchy stress tensor and $\vec{b}$ represents body forces acting on the fluid. Energy equation is omitted. Gravity forces are negligible if the fluid is a gas. For water, these forces should be considered. The notation used herein is the one proposed by Castro in [7] and presented in Fig (1.1), where:

L_{ref} is the reference level

H is the bathymetry

h is the water column height

Z is the bed slope, expressed as $Z = L_{ref} - H$

Generally, the fluid flow is taken as incompressible. Also, salinity and temperature can be assumed as constant. So, fluid density ρ is constant in all the domain. Cauchy stress

tensor is it divided in two parts: an isotropic one, with pressure terms, and a deviatoric part, which consider shear stress. After those consideration, system (1.1) can be written as:

$$\begin{cases} div(\vec{u}) = 0 \\ \frac{\partial(\rho\vec{u})}{\partial t} + div(\rho\vec{u}\vec{u}) = \rho\vec{g} + -\nabla p + \Delta\vec{\tau} \end{cases} \tag{1.2}$$

According to the hypothesis of shallow water, conservation of mass implies that the vertical velocity of the fluid is small. The momentum conservation in the z direction is expressed as:

$$\frac{\partial p}{\partial z} = \rho g \tag{1.3}$$

So, according to Fig. (1.1), pressure variation in the z direction is:

$$p(z) = \rho g h + p_0 \tag{1.4}$$

The vertical pressure gradients are nearly hydrostatic and the horizontal pressure gradients are expressed as:

$$\begin{cases} \frac{\partial p}{\partial x} = \rho g \\ \frac{\partial p}{\partial y} = \rho g \end{cases} \tag{1.5}$$

So, with this pressure distribution, equation (1.5) can be integrated in the z direction with appropriate boundary conditions. On the free surface, i.e. for $z = \zeta = h - H$, which indicates the distance between the free surface and the reference level, must be specified the reference value of the pressure. Furthermore, it is not present normal mass flow and the shear stress remain on the free surface. So, for $z = \zeta$, conditions are:

- $p_0 = p_{atm}$
- $\frac{\partial \zeta}{\partial t} + u\frac{\partial \zeta}{\partial x} + v\frac{\partial \zeta}{\partial y} = 0$
- $- \tau_{xx}\frac{\partial \zeta}{\partial x} - \tau_{xy}\frac{\partial \zeta}{\partial y} + \tau_{xz} = \tau_{\zeta x}$

At the bottom, no-slip condition must be imposed. For $z = H$, conditions are:

- $u = v = 0$

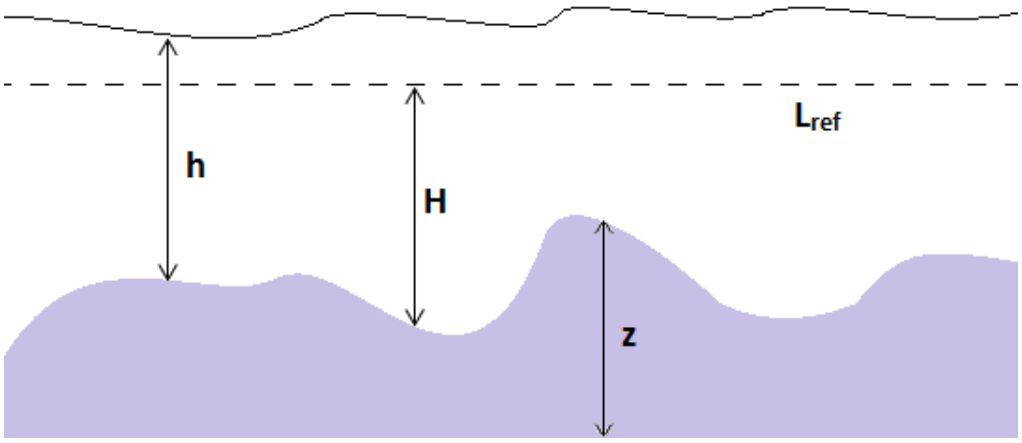

Figure 1.1: *Physical variables considered for Shallow Water equations.*

- $\frac{\partial H}{\partial t} + u\frac{\partial H}{\partial x} + v\frac{\partial H}{\partial y} = 0$
- - $\tau_{xx}\frac{\partial H}{\partial x} - \tau_{xy}\frac{\partial H}{\partial y} + \tau_{xz} = \tau_{Hx}$

So, integrating system (1.2) with respect to z, from $z = H$ to $z = \zeta$, it is obtained:

$$\begin{cases} \frac{\partial h}{\partial t} + \frac{\partial hu}{\partial x} + \frac{\partial hv}{\partial y} = 0 \\ \frac{\partial (hu)}{\partial t} + \frac{\partial}{\partial x}(hu^2 + gh^2) + \frac{\partial huv}{\partial y} = -\rho g \frac{\partial Z}{\partial x} \\ \frac{\partial (hv)}{\partial t} + \frac{\partial huv}{\partial x} + \frac{\partial}{\partial v}(hv^2 + gh^2) = -\rho g \frac{\partial Z}{\partial y} \end{cases} \tag{1.6}$$

System 1.6 are Shallow Water equations system for 2D case. To obtain Shallow Water equations for 1D case, it should be noted that partial derivate $\frac{\partial}{\partial v}$ is zero:

$$\begin{cases} \frac{\partial h}{\partial t} + \frac{\partial hu}{\partial x} = 0 \\ \frac{\partial (hu)}{\partial t} + \frac{\partial}{\partial x}(hu^2 + gh^2) = -\rho g \frac{\partial Z}{\partial x} \end{cases} \tag{1.7}$$

System 1.7 are Shallow Water equations for 1D case.

1.2 Exner equation. Theory of incipient motion

In the case of mobile bed, it is necessary to describe the movement of the granular sediment with an appropriate equation. The solid concentration is defined as:

$$c = \frac{V_s}{V} \tag{1.8}$$

where V_s is the solid volume and V the total volume. According to Castro notation in Fig. (1.1), the solid mass conservation is written as:

$$(1-p)\frac{\partial Z}{\partial t} + \frac{\partial q}{\partial x} = \frac{\partial (c\rho_s)}{\partial t} \tag{1.9}$$

$Z = Z(x, n)$ is the function defining the slope of the depth and q is the sediment flux. The first term indicates the variation of solid mass flow caused by movement at the bottom of the channel from x_2, while the second indicates the variation of the flow range between x_1 and x_2. The term on the right side of the equation defines the variation of the solid material concentration in the control volume, where ρ_s is the sediment density. Assuming that the solid concentration is constant, the system becomes:

$$(1-p)\frac{\partial z}{\partial t} + \frac{\partial q}{\partial x} = 0 \tag{1.10}$$

is known as Exner equation and connects the sediment flux with the depth form. Generally it is defined a porosity factor as $\xi = \frac{1}{1-p}$, and Exner equation became:

$$\frac{\partial z}{\partial t} + \xi\frac{\partial q}{\partial x} = 0 \tag{1.11}$$

The Exner equation needs a closure model for the sediment transport q, a matter studied by Shields (1936), who developed the theory of incipient motion. According to this theory, the movement begins when the shear stress exceeds a critical shear value. Above this value, the current is able to transport the granular sediment. Various physicals parameters should be considered:

- shear stress at the bottom τ

- sediment density ρ_s and fluid density ρ or their ratio $G = \frac{\rho_s}{\rho}$
- diameter of the sediment d
- characteristics of fluid dynamic motion

As it is possible to understand, the problem is complex because it is affected by local phenomena. Shields studied an average depth, composed of granular and non-cohesive sediments. This allowed him to avoid the influence of local phenomena. Thus, he imposed the balance of forces on a generic sediment particle, observing that the movement starts when the shear stress exceeds a given critical shear stress τ_c. Literature also shows different approaches to determine the incipient movement condition, based on a critical Froude number or a critical mass flow or a given mean speed of the fluid. This limit is obtained through several experiments, carried out on larger grains and then extrapolated for smaller cases. The shear stress is written as [7] :

$$\tau = \gamma_s R_H |SF| \tag{1.12}$$

γ_S is the specific water weight, R_H is the hydraulic ratio, usually equal to the water column h, and the form factor is defined according to the Manning Theory [7]:

$$SF = \frac{g\eta_0^2 u|u|}{R_H^{\frac{4}{3}}} \tag{1.13}$$

η_0 is the Manning coefficient and u is the fluid speed at the bottom used to calculate the fluid-dynamic forces. After several experiments, Shields obtained an incipient motion diagram (1.2), through the non-dimensional shear:

$$\theta = \frac{\tau}{(\gamma_s - \gamma)d} \tag{1.14}$$

where γ is the specific water weight. The incipient motion condition is expressed as:

$$\theta > \theta_{cr} \tag{1.15}$$

where:

$$\theta_{cr} = \frac{\tau_{cr}}{(\gamma_s - \gamma)d} \tag{1.16}$$

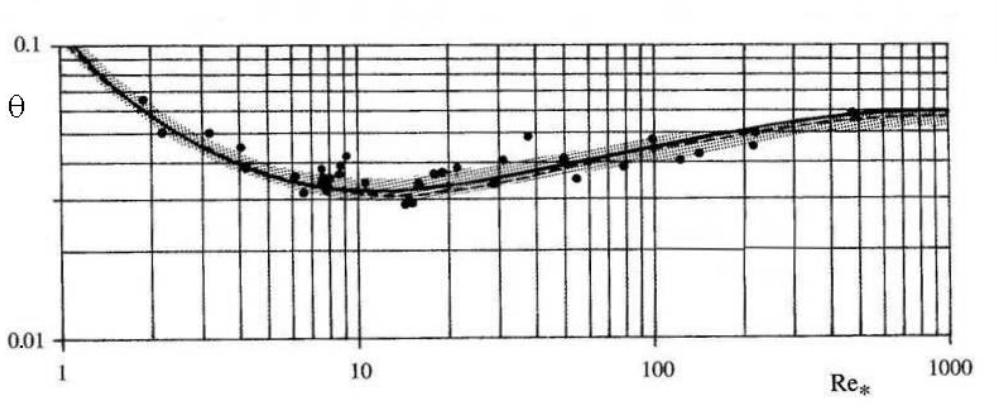

Figure 1.2: *Motion condition according to the Shields theory. The line represents the incipient movement condition, with respect to the Reynolds Number at the bottom.*

θ_{cr} is known as *Shields number*, which varies between 0.03 and 0.06. Therefore, Shields number could be imposed according to different theory, based on the physics of the problem. The diagram in Fig. 1.2 shows that a considerable amount of data is scattered but, after a given Reynolds, the Shields number is almost constant ($\simeq 0.04 \div 0.06$). The non dimensional shear stress can still be written following the non-dimensional form proposed by Chezy:

$$\theta = C_\tau \frac{u^2}{(G-1)\, g d_{50}} \tag{1.17}$$

where C_τ is called *Chezy parameter* which is generally of the order of 10^{-2}. It can be chosen depending on the specific case and is very often used in practice. Furthermore, θ is defined according to the mean diameter d_{50}, but it can also be expressed with respect to other characteristic parameters (e.g. the diameter of a similar particle with a higher weight).

1.3 Sediment transport models

Generally, the sediment transport is usually divided into three mechanisms, as Fig. 1.3 shows:

- Bedload: sediment grains roll or slide along the bed
- Suspension: fluid flux transports sediment grains over the bed, which lose contact with the bed
- Saltation: single grains jump over the bed

Generally, the Sediment falling velocity w_s (or Settling velocity) permit to differentiate between different cases [12]. It describes the ability of the sediment particle to move across the fluid: the maximum value is $\sqrt{2gh}$, obtained imposing the conservation of the energy in the channel. This value express the velocity with which a particle falls in a channel of height h, for sediment particle with an higher density value than water one. Settling velocity it is used to classify the sedimentation process, considering if its magnitude value remains constant or varies. Therefore, the solid flux q is divided into two portions:

$$q = q_s + q_b$$

and q_b is the transport terms related to bedload, and q_s is the suspensions terms including saltation, which is generally negligible. This distinction is not clear and it is difficult in

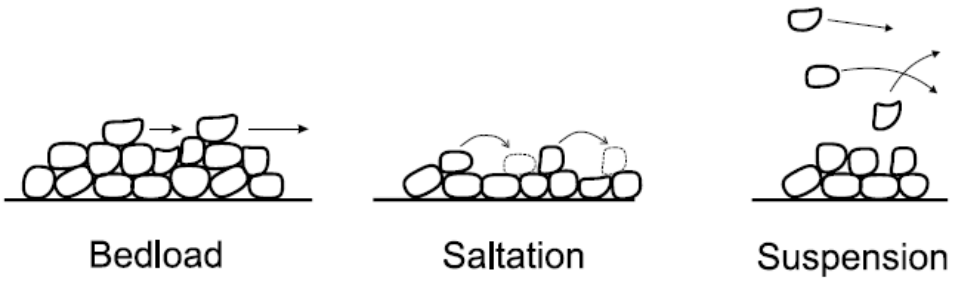

Figure 1.3: *Sketch of sediment transport mechanism.*

various cases. For example, in sandy areas the suspension term prevails, but bedload is also important and it could be difficult to define an accurate global model. Various deterministic or probabilistic approaches to model the sediment flux q are discussed in literature, in which different transport terms are developed. The models could be divided in in two types: empirical and hybrid model. All this model are obtained studying the sediment discharge in specific environmental conditions. The difference is between the form of model utilized. Some equations are obtained empirically based on the probabilistic theory of Einstein. These models have a well defined shape in the equation, derived from this theory, but they do set the parameters according to various studies. The principal issues of hybrid model are the consideration of a global discharge: Einstein introduce a new subdivision in sediment transportmechanism, the alveum.

1.4 Empirical sediment transport models

This model are empirically derivates, with some experiment conducted by the authors. Model are obtained for q_b or q_s singly, considering this mechanism as separate and independent. Below, the models are presented in chronological order.

1.4.1 Du Boys relation

The first sediment flux model was proposed by Du Boys in 1879, but it is not much used today. Du Boys divided the upper stream of the depth in N parts of height δ, with Colombian stress between these parts. After imposing the balance of shear stress of the control volume in each stream, he found:

$$N = \frac{\tau_0}{\tau_c} \tag{1.18}$$

where is the shear stress at the upper side and τ_0 is the shear stress at the lower side. Obviously, the velocity field decreases moving down, and defining v_s as the maximum velocity at the upper side, the Du Boys relation is:

$$q = \left(\frac{\delta v_s}{2\tau_c^2}\right) \tau_0 \left(\tau_0 - \tau_c\right) \tag{1.19}$$

where $(\frac{\delta v_s}{2\tau_c^2}) = f(d_{50}) = 0.54\frac{1}{\gamma_s - \gamma}$ (Schoklitsch, 1914).

1.4.2 Exner model

Exner, in 1925, as presented in [23], simplified his conservation sediment equation, observing that:

1. fluid mass flow rate is constant

$$q_f = hu = const$$

2. $\zeta \ll h \longrightarrow h = H - Z$ waves are lower than water level

3. the solid flux is linear with fluid velocity: $q = \alpha u$

Therefore, Exner equation became only function of the depth slope:

$$(1-p)\frac{\partial Z}{\partial t} + \frac{\partial f\left(Z\right)}{\partial x} = 0 \tag{1.20}$$

where $f(Z) = \frac{\alpha q_f}{h-Z}$. Exner developed a solution for a continuous and discontinuous slopes. For the continuous solution Exner added a diffusion term:

$$(1-p)\frac{\partial Z}{\partial t} + \frac{\partial f(Z)}{\partial x} = \epsilon \frac{\partial^2 Z}{\partial x^2} \tag{1.21}$$

The diffusion term ϵ is usually determined experimentally. A similar model is discussed in [1], investigating coupled solution of SWE system and Exner equation. The used expression is:

$$\frac{\partial \overline{Z}}{\partial \overline{t}} + c\frac{\partial \overline{Z}}{\partial \overline{x}} = 0 \tag{1.22}$$

where $\overline{Z} = \frac{Z}{D_0}$, where D_0 is a typical length of the water level, is non-dimensional seabed slope and c is the non-dimensional migration speed, or celerity, of the bed form:

$$c = \frac{m}{(1-\overline{\eta})^{m+1}} \frac{A_s^*}{1-p} Fr \tag{1.23}$$

where $A*_s$ and m are constants depending on the problem, V_0 is a velocity-scale and Fr is the Froude number expressed as $Fr = \frac{V_0}{\sqrt{gD_0}}$. It is expected $c \ll Fr$. That model is used only for the simplicity of the solution, but is not considered a valid solution of Exner equation: it introduces various physical parameters which are difficult to determine, occurring in several errors.

1.4.3 Meyer-Peter - Müller model

The MPM model is one of the most known relations for the solid discharge. After a series of experimental texts, conducted in Zurich in 1948, Laboratory of Hydraulic Research, Meyer-Peter and Müller [35] proposed the following relation between sediment flux and shear stress:

$$\frac{q_b}{\sqrt{(G-1)gd_{50}^3}} = 8sgn(u)(\theta - \theta_{cr})^{\frac{3}{2}} \tag{1.24}$$

Typically, it describes the sediment transport for rocky rivers, rather than for sandy areas as in Grass model (1.28). It is important the choice of the model for the shear stress τ, to well define the Shields condition. Generally, the motion condition is $\theta_{cr} = 0.047$ [35], according to the Bathurst theory. For different cases this value could be changed. This formula is set for coarse sediments ($d_{50} = 0.4429\ mm$), useful for coarse stream-beds and for depth inclination of less than 2. For higher inclinations, MPM formula overestimates sediment discharge [35]. Efficiency of relation (1.24) is significant, because it is based on a large experimental data set and it takes into account only the mean characteristic of the flow. In [30] an interesting correction of the MPM model is investigated:

$$\frac{q_b}{\sqrt{(G-1)gd_{50}^3}} = 8sgn(u)(\theta - \gamma\nabla\eta - \theta_{cr})^{\frac{3}{2}} \frac{\theta - \gamma\nabla\eta}{\|\theta - \gamma\nabla\eta\|} \tag{1.25}$$

where γ is a non-dimensional parameter, related to the bottom slope effects. The slope of the depth appears by its gradient, expressing the stabilizing effect of the seabed reshaping. In [30], the formula is used to investigate bedload in the case of significant breaking wave height (see Camenen Model). This correction is considered one of the best closure models of the Shallow Water equations system by the authors in [30].

1.4.4 Fernandez Luque - Van Beek model

FLV [7] proposed a similar model to MPM model (1.24):

$$\frac{q_b}{\sqrt{(G-1)gd_{50}^3}} = 5.7 sgn(u) \left(\theta - \theta_{cr}\right)^{\frac{3}{2}} \tag{1.26}$$

Only a coefficient varies between the two equation. Equation (1.26) is set for bigger grains than (1.24).

1.4.5 Grass model

Grass [16] proposed non linear expression, like:

$$q_s = \alpha u^n. \tag{1.27}$$

Shields theory was avoided by Grass, who proposed a non-linear relation for q, expressed as:

$$q_b = A_g \frac{q_f}{h} \left\| \frac{q_f}{h} \right\|^{m_g - 1} \tag{1.28}$$

where $1 \leq m_g \leq 4$ (generally 3) and $0 < A_g < 1$, usually determined experimentally. This term takes into account the dimension of the grain and fluid viscosity, and is smaller when there is a weak sediment-fluid interaction. Barry [22] (2004) proposed a similar solution, function only of fluid flow:

$$q_b = \alpha q_f^{\beta} \tag{1.29}$$

where α and β are empirical coefficients.

1.4.6 Modified Grass model

Hogg (2005) proposed a correction with water column h, observing that, in Grass Model, the maximum of sediment mass flow is on the upper side of the water, where $q_f = 0$. Authors in [10] investigated a linear relation between q and h, with good results. Thus resulted in the following model:

$$q_b = A_d h u \left\| u \right\|^2 \tag{1.30}$$

where A_d is a constant which depends on sediment features, and is usually determined experimentally. This model is more accurate that Grass Model and also with more complicated ones [10]. That model is compared to 1.24, one of the most used and accurate relation used today. Results are similar if $\theta < \theta_{cr}$ for few time. This model allows to correct an intrinsical error of Grass model, for which the sediment mass flow q_b depends only on the water velocity. So, in a simplified model, the maximum velocity value is on the free surface, where $h = 0$, according to Castro notation. This is not physically correct, because the Grass model simplifies bedload transport, which occurs mainly on the bottom. Thus, introducing the state h, it is possible to correct this impropriety, expecting then a maximum value of the sediment flow at the bottom, where h is maximum, consistent with the physical reality.

1.4.7 Nielsen model

Nielsen [34] proposed a model to similar (1.24):

$$\frac{q_b}{\sqrt{(G-1)gd_{50}^3}} = 12 sgn(u) \left(\theta - \theta_{cr}\right) \sqrt{\theta} \tag{1.31}$$

with $\theta_{cr} = 0.05$, generally. Equation (1.31) is set for smaller grains than the MPM one.

1.4.8 Camenen model

Camenen [29] proposed a formula for only suspended load:

$$q_s = uC_r \frac{\epsilon}{w_s}[1 - \exp(-\frac{w_s d}{\epsilon})] \tag{1.32}$$

where $\epsilon = kd\left(\frac{D}{\rho}\right)^{\frac{1}{3}}$ is the sediment diffusivity and D is the total dissipation in the water flux. The Sediment ratio C_r is:

$$C_r = A_{C_r}\theta_T \exp(-\frac{\theta_M}{\theta_{cr}}) \tag{1.33}$$

where θ_T is the mean non-dimensional stress and θ_M the maximum stress at the bed. A_{cr} is a parameter depending on grain dimension. It is difficult to define C_r, which depends also on the characteristics of waves and currents. Therefore, relation is often used because it matches accurately the problem of suspension load. In [30], this model is used to investigate suspension load in the case of significant breaking wave height, comparing global transport with experimental data obtained in [3]. Bedload is expressed by eq. 1.25. Results are very accurate.

1.5 Hybrid sediment transport models

In this section are considered model which consider a different subdivision in sediment transport mechanism. Those model consider the transport as an unique item, according to the alveum theory proposed by Einstein [13]. The discharge is approached with a probabilistic idea, and a generical expression of sediment global flux it is found. This formula it is used by different authors. setting parameter differently. Also are considered model which takes into account the alveum theory. Below, the models are presented in chronological order.

1.5.1 Einstein approach

Einstein proposed a new approach for sediment transport discharge, by a probabilistic model [13]. He also avoided the distinction between bedload and suspended load, defining a streambed structure (alveum). The transport probability in the stream varies from 0 to 1: there is no threshold imposed directly to the discharge, so Einstein does not take into account Shields theory. There is probability on motion condition, connected to the Shields theory, but is related to the force which produce the movement of the particle. This is in contrast with most bedload formulas, both preceding and following Einstein approach, which are based on Shields Theory of incipient motion and formulas are obtained empirically through experimental field data. Einstein's theory considers a grain diameter d_i, a number of particles N_p which separate from an area Ω (long L the mean shift of the particle), a number of particles N_a which fall in Ω. Einstein imposed that number of the particles which fall in Ω are the same of those which separates:

$$N_p = N_a \tag{1.34}$$

and observed that solid discharge must overrun a threshold $\tilde{a}$. For simplicity, this parameter is connect to the Shields parameter but has not the same physical meaning:

$$\tilde{a} = \frac{1}{\theta_{cr}} = \Psi \tag{1.35}$$

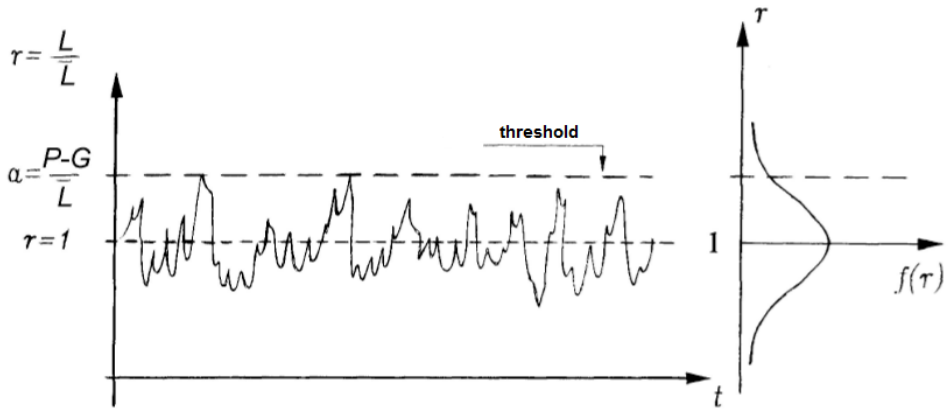

Figure 1.4: *The Einstein Theory of sediment transport.*

Therefore, taking into account a mean normal force and a fluctuating force as $L = \overline{L}+L'$, where $r = \frac{L}{\overline{L}}$, Einstein defined the transport condition as:

$$r > a \tag{1.36}$$

The solid transport happens with a probability p_r, defined as:

$$p_r = \int f(r)\, dr \ [-\infty, a-1] \tag{1.37}$$

where $f(r)$ is a Gauss function for the force. Therefore, the separation probability $\tilde{p}$ of a sediment grain is $\tilde{p} = 1-p_r$. The number of particles N_p which separate from the bottom is equal to the percentage of particles of diameter d_i in Ω multiplied by the separation probability $\tilde{p}$. Einstein proposed this relation for the total sediment transport:

$$\frac{q}{g\rho_s\sqrt{(G-1)gd_{50}^3}} = \frac{I_b}{I_s}\frac{\alpha_L\alpha_2}{\alpha_1\alpha_3}p \tag{1.38}$$

where parameters in α represent geometrical features of the grain, I_s is the percentage of particles of diameter d_i which cross a unit area normal to Ω and I_b is the percentage of particles of diameter d_i which breaks off from Ω [5]. Einstein defined the intensity of sediment load as:

$$\Phi = \frac{q}{g\rho_s\sqrt{(G-1)gd_{50}^3}} \tag{1.39}$$

which is called Einstein parameter. He also defined $A' = \frac{\lambda\alpha_2}{\alpha_1\alpha_3}$. , $B* = \frac{1}{\sigma\sqrt{2}} = \frac{1}{\eta_0}$, $\Phi' = \Phi\frac{I_b}{I_s}$, $\xi = \frac{r-1}{\sigma\sqrt{2}}$ (σ is the variance of $f(r)$). It could be shown as $\alpha_L = \frac{\lambda}{1-p}$, where λ is derived experimentally. Einstein obtained the following integral expression:

$$\frac{A'\Phi'}{1+A'\Phi'} = p = 1 - \frac{1}{\sqrt{\pi}}\int \exp\left(-\xi^2\right) d\xi \ \left[-\left(B*\Psi+\tfrac{1}{\eta_0}\right); B*\Psi-\tfrac{1}{\eta_0}\right] \tag{1.40}$$

This relation was developed in the following years and inspired other probabilistic theories such as Kalinske's one [2]. A solution proposed by Einstein was obtained supposing Φ' as a constant, where the separation probability p is known. Therefore, Einstein expression is:

$$q = \Phi'\frac{I_s}{I_b}\rho_s g\sqrt{(G-1)\, gd_{50}^3} \tag{1.41}$$

Furthermore, when sediment grains are regular, it results that $I_b = I_s = 1$. In this form, the equation 1.41 is similar to 1.24. Otherwise, Einstein and Brown [6], in 1950, proposed the following solution:

$$\Phi = \begin{cases} \frac{K}{0.465}\exp(\frac{-0.391}{\theta}) & \theta < 0.182 \\ 40K\theta^3 & \theta > 0.182 \end{cases} \tag{1.42}$$

where $K = \sqrt{\frac{2}{3} + \frac{36}{d_0^3}} - \sqrt{\frac{36}{d_0^3}}$ and $d_0 = d\left[\frac{(G-1)g}{\nu^2}\right]^{\frac{1}{3}}$ is the non-dimensional diameter.

1.5.2 Engelund - Hansen model

The EH model [1], the total sediment load is calculated as:

$$q = \overline{u}0.05C_\tau \frac{\tau_{b,c}^2}{(G-1)^2 d_{50}\rho^2 g^{\frac{5}{2}}}\left[1 + \frac{1}{2}\left(\xi\frac{u_0}{\overline{u}}\right)^2\right] \tag{1.43}$$

this formula is set for smooth sediment grains and is derived calculating an energy balance for waves and tidal current. The average velocity of water flux is $\overline{u}$, and u_0 is the velocity of waves at the free surface. The shear stress due only to current effect is $\tau_{b,c}$, where ξ is a damping coefficient. The shear stress due to current and wave effect is:

$$\tau_{b,wc} = \tau_{b,c}\left[1 + \frac{1}{2}\left(\xi\frac{u_0}{\overline{u}}\right)^2\right] \tag{1.44}$$

1.5.3 Bijker model

Bijker formula is one of the earliest for global discharge for waves and tidal currents [14]. It is based on Kalinske probabilistic theory of sediment transport [2]. Bijker divided bedload, which depends on bottom shear stress, and suspension, which depends on the integral of velocity shape and sediment concentration, without considering Shields Theory. Bedload is expressed as:

$$q_b = Ad_{50}\frac{\overline{u}}{C_\tau}\sqrt{g}\exp\left[\frac{-0.27(G-1)d_{50}\rho g}{\mu\tau_{b,wc}}\right] \tag{1.45}$$

where A is an empirical coefficient depending on waves typology, $\overline{u}$ the mean current velocity, μ depends on wave shape. All those coefficients are expressed in [32]. The first part of the formula 1.45 represents a transport term and the second part a mixing term. The suspension formula is calculated assuming that bedload is confined in a little layer, at constant concentration. The dimension of this layer is proportional to depth roughness κ. Integrating in water height:

$$q_s = 1.83q_b\left[I_1\ln\left(\frac{33h}{\kappa}\right) + I_2\right] \tag{1.46}$$

where I_1 and I_2 are Einstein Integrals, explained in [27].

1.5.4 Ackers and White model

Ackers and White [39] developed a solution for smooth or coarse sediments, in the case of multidirectional currents. Bedload is only considered for coarse sediments, depending on the shear stress at the bottom. Suspension is only considered for smooth sediments,

depending on the turbulent flow. In the first model proposed by AW (1967), only the effects of tidal current are considered:

$$q = \overline{u}\frac{1}{1-p}d_{35}\left(\frac{\overline{u}}{u_*}\right)^n \frac{C_{d,gr}}{A^m}\left(F_C - A\right) \tag{1.47}$$

where d_{35} is the grain diameter of a particle added of the 65% of weight, u_* the stream velocity at the bottom and n, m, $C_{d,gr}$, A are non-dimensional parameters depending on grain diameter [39]. F_c is the sediment mobility number. All parameters are expressed in [32]. In [17], an expression including waves effects is proposed and is identical to relation 1.47, but the velocity term $\overline{u}$ is expressed as:

$$\overline{u}_{wc} = \overline{u}\sqrt{1 + \frac{1}{2}\left(\xi\frac{u}{\overline{u}}\right)^2} \tag{1.48}$$

while the same expression is used for u_*.

1.5.5 Engelund - Fredsoe model

The EF formula [20] is a deterministic sediment discharge model, which takes into account Einstein model:

$$\Phi = \begin{cases} 0 & \theta < \theta_{cr} \\ 18.74\left(\theta - \theta_{cr}\right)\left(\sqrt{\theta} - 0.7\sqrt{\theta_{cr}}\right) & \theta > 0.182 \end{cases} \tag{1.49}$$

In [18], an interesting correction of Shields parameter is investigated, proposed by Brors (1999) and reshaped for 3D case:

$$\theta_{cr} = \theta_{cr0}\frac{\sin\left(\alpha - sgn(\vec{\tau}\cdot\vec{S})\vartheta\right)}{\sin\alpha} \tag{1.50}$$

These parameters define the dune geometry. Furthermore, bedload is divided into different directions as Brors relation:

$$q_i = q\frac{\theta_i}{\|\theta\|} - C\,\|q\|\,\frac{\partial\eta_i}{\partial x_i}\;i = 1,2] \tag{1.51}$$

The constant C, introduced by Brors, which varies from 1.5 to 2.3, takes into account the slope of the dune.

1.5.6 Bailard and Inman approach

Bailard and Inman [11] developed a relation based on Bagnold theory [9], for which the global work for sediment transport is equal to the total energy dissipation in the water mass flow. This formula became very frequently used in engineering issues because of its accuracy and simplicity in computational solution. For smooth depth, considering wave and tidal currents effects, the proposed relation is the following:

$$q = \frac{1}{2}f_w\frac{u_0^3}{(G-1)}\left[\frac{e_b}{\tan\gamma}\left(\frac{\delta_v}{2} + \delta_v^3\right) + \frac{e_s}{w_s}\left(\delta_v u_3^*\right)\right] \tag{1.52}$$

where e_b and e_s are generally constant, depending on the shear stress at the bottom and the particle diameter. The first term is related to bedload while the second term is related to suspension load. The two efficiency parameters δ_v and u_3 are expressed in [32], which contains an extended version of formula 1.52, in vectorial form.

1.5.7 Van Rijn model

Taking into account experimental data, Van Rijn [25] [24] [26] proposed a very important sediment transport model for rivers. In fact, this model is one of the most used together with the MPM equation. According to Bagnold theory [9] [25], in Van Rijn model the interaction between fluid forces and sediment grain weight produces bedload and saltation:

$$q_b = c_b u_b \delta_b \tag{1.53}$$

where c_b is sediment concentration for bedload, u_b is grain velocity and δ_b the dimension of the layer where sediments are transported. Analytical expressions are available in [32]. Otherwise, Van Rijn proposed a simpler model for bedload which includes Shields parameter [27]:

$$\frac{q_b}{\sqrt{(G-1)g d_{50}^3}} = \frac{0.005}{C_d^{1.7}} \left(\frac{d_{50}}{h}\right)^{0.2} \left(\sqrt{\theta} - \sqrt{\theta_{cr}}\right)^{2.4} \sqrt{\theta} \tag{1.54}$$

that is easy to solve but also accurate, as most author have shown [32] [7] [30]. If bedload is expressed as the flux of sediment in a little layer, suspension load is expressed similarly, integrating the average solid concentration c in the water height:

$$q_s = \int_0^h vcdz = c\overline{u}hF \tag{1.55}$$

$\overline{u}$ is a mean velocity in the field, F is an integral function of the problem, expressed with empirical coefficients as in [33]. These relations are often use because the empirical coefficient can be set according to the problem.

1.5.8 Watanabe approach

The total sediment discharge for Watanabe depends on waves and tidal currents and starts after the Shields threshold [4]. The total sediment load is transported by the mean flow as:

$$q = A_W (G-1)(\theta - \theta_{cr})\overline{u} \tag{1.56}$$

This relation is typically used to investigate coastal evolution, shipping channels and harbor. The parameter is a coefficient function of the wave. Generally, it is set constant, but A_w varies according to waves and grain typology, as it was observed experimentally [4].

1.5.9 CERC, Inman - Bagnold and Kamphuis approaches

In [32], some formulas presented here are compared with a series of experimental field data such as Duck85, SuperDuck and SandyDuck. These data were obtained by the U.S. Army in Duck harbor, North Carolina, where sediment discharge of $d_{50} > 0.1\,mm$ grain, was investigated in relation with waves and tidal current. The U.S. Army proposed the following relation, known as CERC:

$$q = \frac{1}{16}\frac{K_0}{(1-p)}\frac{\sqrt{\frac{g}{\gamma_b}}}{(G-1)}\tilde{H}^{2.5}\sin 2\theta_b \tag{1.57}$$

where global load is proportional to the energy of waves, while K_0 is a constant. This happen because γ_b, θ_b and $\tilde{H}$ are indeed coefficients related to waves. In particular, θ_b,

not to be confused with Shields parameter, indicates a medium angle of wave brake. This expression were modified by Inman-Bagnold, which proposed the following

$$q = \frac{K_b}{(1-p)} \frac{C_{gb} E_b}{(\rho_s - \rho)} \left(\frac{\overline{u}}{u_{max}} \right) \cos \theta_b \tag{1.58}$$

where C_{gb}, E_b and u_{max} are still coefficients related to waves, while K_b is a constant. The relation (1.58) was also verified by U.S. Army in various areas of America and Japan. These two field experiment were then developed in 2002 by Kamphuis, who proposed the following relation:

$$q_{,t} = \frac{2.27}{\sqrt[4]{d_{50}}} T_p^{1.5} m_b^{0.75} H^2 \sin^{0.6}(2\theta_b) \tag{1.59}$$

expressed in unit time. T_p is the peak time of waves, m_b is the coastal slope. Relations (1.57), (1.58) and (1.59) are developed for strong breaking waves. In fact, Duck85, SuperDuck and SandyDuck databases [38] are obtained in surf zones, where the suspension term prevails.

1.5.10 CHSH Approach

The Defense Chinese Minister proposed, analogously to the U.S. Army, the Code of Hydrology for Sea Harbor of China (CHSH) for total sediment transport in harbors:

$$q = 0.05059 K' (H_{rms})^2 C_{gb} \sin \theta_b \tag{1.60}$$

This formula is similar to (1.57). K' is a parameter depending on the mean diameter of a sediment grain d_{50}. In [21] relation (1.60) and (1.57) in were applied to investigate the sediment transport in the Shijiu harbor. This harbor have got a particular conformation, where sediment load is bidirectional and the mean grain dimension are smaller than other cases, about $d_{50} \cong 0.12\, mm$. Formulas are tested comparing simulation with experimental data. CHSH relation results more accurate than CERC from the analysis. In fact, CHSH is set for mean value of the sediment grain and waves. Therefore, that model produce a smaller error because K' varies considerably with d_{50}, not as for K in CERC model. For an accurate analysis, it should be investigated the two formulas for bigger grains.

1.5.11 Yang and Liu approach

Following Einstein, Yang and Liu developed in 2005 a formula for the global load [18]:

$$\Phi = 1.25 \sqrt{\frac{1}{G-1}} T_0 \tag{1.61}$$

where $T_0 = \frac{\tau_0 \left(u_*^2 - u_{*c}^2 \right)}{(\gamma_s - \gamma) w_s \sqrt{g d_{50}^3}}$ is a non-dimensional parameter, function of the fluid-dynamic characteristics. All those parameter are available in [18], where different terms of T_0 are presented and authors applied this model in various scenarios, like rivers or tidal currents.

1.5.12 Bayrman Model

In 2007, Bayrman proposed a formula [17] for global transport discharge, adding more recent databases (1993-2004) to the studies which define formulas (1.57), (1.58) and (1.59). Bayrman assumed that the work W done by waves keeps the solid suspension

concentration at a constant value. He defined an efficiency parameter ε which he supposed to be a universal constant:

$$W = F\varepsilon$$

where F is the energy flux of waves. Bayram expressed W as the energy required to avoid the sediment fall:

$$q = \frac{\varepsilon F \overline{u}}{(\rho_s - \rho)(G-1) w_s} \tag{1.62}$$

This expression aims to incorporate most of the physical parameters involved, such as tidal currents, sediment influence (in the falling velocity w_s) and effects of interaction fluid-sediment. Furthermore, $\overline{u}$ is the mean flow velocity, which takes into account waves, currents and harbor slope. This relation is even simpler than CERC (1.57): its results one more accurate for strong winds and tsunamis, as Bayrman shows in [17].

1.6 General remarks on sediment transport models

Einstein's conception of the streambed structure permits to bypass the distinction between bedload and suspension. Therefore, the sediment transport is considered as a single unit and can be useful in the case of a granular smooth seabed. It is to be noted that the expression of parameter Φ proposed by Einstein is maintained in other relations. For example, MPM and Van Rijn models are more suitable for sediment transport in rocky rivers, although they are often used in coastal environment, because they are simpler to solve. In the case of sandy areas, Shields parameter θ_{cr} can be neglected and the use of simple models which do not take the incipient motion theory into account can be satisfying. As shown in [7], considering $\theta_{cr} = 0$, MPM equation can be written as the Grass model. Van Rijn's model provides a lower scatter compared to different fields measurement [32], although it does not represent a specific case, while other formulas (EF, EH, Watanabe, AW, Bijker) analyzed do. Bayrman's analysis shows that the Van Rijn equation is also effective in the case of tidal currents and strong waves (surf zones), although it is less accurate than the CERC relation (1.57) and the Bayrman model. MPM model (1.24) is commonly used and effective only for bedload, also when grains are smoother than those for which it was set. The correction model proposed in (1.25), in which bedload depends on the shape of the depth, is very interesting for practical applications. Watanabe model seems to guarantee simplicity and accuracy to describe global sediment transport. Among all the models analyzed, two were chosen to be implemented to analyze the transport in the case 1D. The first is the modified Grass model because it introduces a small modification in the already available Grass model, but ir has benne shown in [10] that thus may lead to substantial differences in sediment motion. Secondly, the Meyer-Peter Muller model was chosen for several reasons. In the first place for the introduction of a threshold in the sediment motion, in order to analyze the computational efficiency of the implicit time advancing in this case. Moreover, there are several example in the literature which shows his accuracy of MPM model. In this case it is necessary to define the model of the shear stress: for simplicity a linear relationship with the square of the speed is chosen. In this way the model MPM can be rewritten in a manner similar to that of Grass. Also in this case, the same correction proposed for the model of Grass is implemented.

Chapter 2

Modified Roe Scheme for Shallow Water

According to Castro notation, the system composed by Shallow Water equations and Exner equation is presented in the following section for 1D case (2.1) and for 2D case (2.2). The mathematical problem is solved with a finite volume approach (2.2) proposed by Castro [7] [8], according to the *modified Roe scheme* (MR). The time advancing is defined whit the Courant number (CFL)(2.4). Bilanceri in [28] implemented the Grass model (1.28) to solve Exner equation. Three additional sediment transport model are chosen and implemented in the present work. The implementation in the code is done by changing the partial derivates in the last line of the Roe Matrix.

2.1 Shallow water coupled system for 1D and 2D case

According to the simplified Navier Stokes system (1.7) and Exner equation (1.10), the Shallow water system for 1D case is:

$$\begin{cases} \frac{\partial h}{\partial t} + \frac{\partial hu}{\partial x} = 0 \\ \frac{\partial (hu)}{\partial t} + \frac{\partial}{\partial x}(hu^2 + gh^2) = -\rho g \frac{\partial \eta}{\partial x} \\ \frac{\partial z}{\partial t} + \xi \frac{\partial q}{\partial x} = 0 \end{cases} \tag{2.1}$$

where the porosity factor $\xi = \frac{1}{1-p}$. The 2D solution scheme proposed by Castro in [8] is the same presented for 1D solution scheme. The Shallow Water equations for bi-dimensional condition is presented as follows:

$$\begin{cases} \frac{\partial h}{\partial t} + \frac{\partial hu}{\partial x} = 0 \\ \frac{\partial (hu)}{\partial t} + \frac{\partial}{\partial x}(hu^2 + gh^2) = -\rho g \frac{\partial \eta}{\partial x} \\ \frac{\partial (hv)}{\partial t} + \frac{\partial}{\partial y}(hv^2 + gh^2) = -\rho g \frac{\partial \eta}{\partial x} \\ \frac{\partial z}{\partial t} + \xi \frac{\partial q_x}{\partial x} + \xi \frac{\partial q_y}{\partial x} = 0 \end{cases} \tag{2.2}$$

The solution scheme solve together Exner and SWE, coupling both systems. A different approach is obtained decoupling both equation. First, the fluid part is solved and, after that, the bed slope is upgraded according to the fluid dynamic solution.

2.2 Finite volume approach

The numerical methodology proposed in this work is based on a standard finite volume formulation. The computational domain $[a, b]$ is divided into the cells $C_i, i = 1, ..., N_c$ which are defined by $\left[x_{i-1/2}, x_{i+1/2}\right]$. The barycenter of each cell is denoted by x_i and its length is defined by $\Delta x_i = x_{i+1/2} - x_{i-1/2}$. Finally $\mathbf{W}_i(t)$, the mean value of the solution over each control volume, is defined as follows:

$$\mathbf{W}_i(t) = \frac{1}{\Delta x_i} \int_{x_{i-1/2}}^{x_{i+1/2}} \mathbf{W}(x,t)\mathrm{d}x \tag{2.3}$$

while $\mathbf{W}_i^n$, which denotes a generic unknown of the fully discretized problem, is an approximation of $\mathbf{W}_i$ at time $t = t^n$.

A Roe-like scheme for non-conservative systems

The numerical scheme proposed in [7] is used herein for space discretization. This approach is based on the following non-conservative form of the system of equations (**??**):

$$\frac{\partial \mathbf{W}}{\partial t} + \mathbf{A}(\mathbf{W})\frac{\partial \mathbf{W}}{\partial x} = 0 \quad \text{where} \quad \mathbf{A}(\mathbf{W}) = \frac{\partial \mathbf{F}(\mathbf{W})}{\partial \mathbf{W}} - \mathbf{B}(\mathbf{W}) \tag{2.4}$$

and

$$\left\{ \begin{array}{lllll} \mathbf{W} & = (& h, & hu, & H \quad)^T \\ \mathbf{F}(\mathbf{W}) & = (& hu, & hu^2 + \frac{1}{2}gh^2, & -\xi q_b \quad)^T \end{array} \right. ; \ \mathbf{B}(\mathbf{W}) = \begin{pmatrix} 0 & 0 & 0 \\ 0 & 0 & c^2 \\ 0 & 0 & 0 \end{pmatrix} \tag{2.5}$$

in which $c = \sqrt{gh}$, $H = L_{ref} - Z$ is the bathymetry function with respect to a fixed reference level L_{ref} and the matrix $\mathbf{A}$ is expressed as:

$$\mathbf{A} = \begin{pmatrix} 0 & 1 & 0 \\ c^2 - u^2 & 2u & -c^2 \\ -\xi \frac{\partial q}{\partial h} & -\xi \frac{\partial q}{\partial hu} & 0 \end{pmatrix} \tag{2.6}$$

In [7] [8] a Roe-like scheme for the non-conservative system (2.4) is proposed leading to the following semi-discrete formulation:

$$\frac{\partial \mathbf{W}_i}{\partial t} = \frac{1}{\Delta x_i}\left(\mathcal{F}_{i-1/2}^n - \mathcal{F}_{i+1/2}^n + \frac{1}{2}\tilde{\mathbf{B}}_{i-1,i}\left(\mathbf{W}_i^n - \mathbf{W}_{i-1}^n\right) + \frac{1}{2}\tilde{\mathbf{B}}_{i,i+1}\left(\mathbf{W}_{i+1}^n - \mathbf{W}_i^n\right)\right) \tag{2.7}$$

in which the Roe-like numerical flux function $\mathcal{F}(\mathbf{W}_j^n, \mathbf{W}_i^n)$ for $j = i \pm 1$ is expressed as:

$$\mathcal{F}_{\frac{i+j}{2}}^n = \mathcal{F}(\mathbf{W}_i^n, \mathbf{W}_j^n) = \frac{1}{2}\left(\mathbf{F}(\mathbf{W}_i^n) + \mathbf{F}(\mathbf{W}_j^n)\right) - \frac{1}{2}|\tilde{\mathbf{A}}|(\mathbf{W}_j^n, \mathbf{W}_i^n)\left(\mathbf{W}_j^n - \mathbf{W}_i^n\right) \tag{2.8}$$

where $|\tilde{\mathbf{A}}| = \tilde{R}\left|\tilde{\Lambda}\right|\tilde{R}^{-1}$, $\tilde{R}$ being the right eigenvector matrix of $\tilde{A}$ and $\left|\tilde{\Lambda}\right|$ the diagonal matrix whose diagonal coefficients are the absolute values of the eigenvalues of $\tilde{A}$. Moreover, $\tilde{A}$, the generalized Roe matrix and $\tilde{B}$, the matrix associated to the non-conservative term involved in (2.7) and (2.8), are expressed as:

$$\tilde{\mathbf{A}}(W_L, W_R) = \begin{pmatrix} 0 & 1 & 0 \\ \tilde{c}^2 - \tilde{u}^2 & 2\tilde{u} & -\tilde{c}^2 \\ \tilde{a}_{31} & \tilde{a}_{32} & 0 \end{pmatrix} \quad \tilde{\mathbf{B}}(W_L, W_R) = \begin{pmatrix} 0 & 0 & 0 \\ 0 & 0 & g\tilde{h} \\ 0 & 0 & 0 \end{pmatrix} \tag{2.9}$$

$\mathbf{W}_L$ and $\mathbf{W}_R$ being two generic states while $\tilde{h}$, $\tilde{u}$ and $\tilde{c}$ are the Roe averages for the Shallow Water equations, i.e.

$$\tilde{h} = \frac{h_L + h_R}{2}, \quad \tilde{u} = \frac{u_L\sqrt{h_L} + u_R\sqrt{h_R}}{\sqrt{h_L} + \sqrt{h_R}}, \quad \tilde{c} = \sqrt{g\tilde{h}}$$

Apart for simple models as the Grass one, the definition of the terms $\tilde{a}_{31}$ and $\tilde{a}_{32}$ to obtain a Roe linearization of system (2.4) can be challenging, and thus, as done in [7] [8], an approximated Roe-like matrix is considered by taken the partial derivatives of Q_b computed at the Roe average state, i.e.:

$$\tilde{a}_{31} \doteq -\xi \left.\frac{\partial q_b}{\partial h}\right|_{(\tilde{h},\tilde{u})} \qquad \tilde{a}_{32} \doteq -\xi \left.\frac{\partial q_b}{\partial hu}\right|_{(\tilde{h},\tilde{u})}$$

Second-order extension

Following [7] the second-order extension considered in this work is based on the introduction of a reconstruction operator $P_i(x)$ which depends on the solution on C_i and on its adjacent cells. The following second-order semi-discrete formulation of (2.4) is then proposed:

$$\frac{\partial \mathbf{W}_i}{\partial t} = \frac{1}{\Delta x_i}\left(\mathcal{F}(\mathbf{W}^-_{i-1/2}, \mathbf{W}^+_{i-1/2}) - \mathcal{F}(\mathbf{W}^-_{i+1/2}, \mathbf{W}^+_{i+1/2}) + \frac{1}{2}\tilde{\mathbf{B}}_{i-1,i}\left(\mathbf{W}^+_{i+1/2} - \mathbf{W}^-_{i+1/2}\right)\right.$$
$$\left. + \frac{1}{2}\tilde{\mathbf{B}}_{i,i+1}\left(\mathbf{W}^+_{i+1/2} - \mathbf{W}^-_{i+1/2}\right)\right) - \frac{1}{\Delta x_i}\int_{x_i}^{x_{i+1}} \mathbf{B}(P_i(x))\frac{\mathrm{d}P_i}{\mathrm{d}x}\mathrm{d}x \quad (2.10)$$

where $\mathbf{W}^{\pm}_{i\pm1/2}$ are the extrapolated values of the solution at the cell interfaces defined, for instance, for the case of the interface between cells C_i and C_{i+1} by

$$\mathbf{W}^-_{i+1/2} = \lim_{x\to x_{i+1/2}} P_i(x), \quad \mathbf{W}^+_{i+1/2} = \lim_{x\to x_{i+1/2}} P_{i+1}(x)$$

Due to the non-conservative formulation, the second-order approach is not only a function of the extrapolated values of the solution at the cell interfaces, but also function of the solution values inside the cells through the reconstruction operator $P_i(x)$. The order of the numerical formulation depends on $P_i(x)$ and on its derivative as well as the order of the quadrature formula used to approximate the integral in (2.10). Consequently, in order to maintain a second-order accuracy, the integral term has been approximated through the barycentre quadrature formula, that is:

$$\int_{x_i-1/2}^{x_{i+1/2}} \mathbf{B}(P_i(x))\frac{\mathrm{d}P_i}{\mathrm{d}x}\mathrm{d}x \simeq \Delta x_i\, \mathbf{B}(P_i(x_i))\left.\frac{\mathrm{d}P_i}{\mathrm{d}x}\right|_{x_i} \quad (2.11)$$

while a MUSCL-type reconstruction operator is used:

$$P_i(x) = \mathbf{W}_i + \nabla\mathbf{W}_i\,(x - x_i) \quad (2.12)$$

where the gradient $\nabla\mathbf{W}_i$ is computed by using the standard minmod limiter.

2.2.1 Discretization in time

First and second order explicit time advancing

A simple fully discretized formulation for system (2.4) can be obtained through the use an explicit Euler method for time advancing. The resulting first-order accurate

numerical scheme is expressed as

$$\mathbf{W}_i^{n+1} = \mathbf{W}_i^n + \Delta^n t\, \mathrm{RHS}_1^n \tag{2.13}$$

in which RHS_1^n corresponds to the right hand side of (2.7) and $\Delta^n(\cdot) = (\cdot)^{n+1} - (\cdot)^n$.

Moreover, in order to obtain an explicit scheme second-order accurate in time, the time discretization is carried out by using a second-order TVD Runge-Kutta method [15]. Thus, the following space and time second-order accurate numerical scheme is obtained:

$$\left\{ \begin{array}{lcl} \mathbf{W}_i^{n+1/2} & = & \mathbf{W}_i^n + \Delta t^n\, \mathrm{RHS}_2^n \\ \mathbf{W}_i^{n+1} & = & \dfrac{\mathbf{W}_i^{n+1/2} + \mathbf{W}_i^n}{2} + \dfrac{1}{2}\Delta t^n\, \mathrm{RHS}_2^{n+1/2} \end{array} \right. \tag{2.14}$$

RHS_2^n and $\mathrm{RHS}_2^{n+1/2}$ being the the right hand side of (2.10) considering the solution at time t^n and the one of the first Runge-Kutta stage respectively.

2.2.2 Linearized implicit time advancing: a first-order accurate approach

Generally speaking, the implicit counterpart of a first order explicit Euler method is obtained by considering the right-hand-side term as a function of the solution at time $n+1$ instead of n. Hence, a fully implicit first-order version of the scheme 2.13 can be obtained by using the following backward Euler method:

$$\mathbf{W}_i^{n+1} - \Delta^n t\, \mathrm{RHS}_1^{n+1} = \mathbf{W}_i^n \tag{2.15}$$

However, from a practical point of view this would require the solution of a large non-linear system of equations at each time step. The computational cost for this operation is in general not affordable in practical applications and, in general, significantly overcomes any advantage that an implicit scheme could have with respect to its explicit counterpart. A common technique to overcome this difficulty is to linearize the numerical scheme, that is to find an approximation of RHS_1^{n+1} in the form:

$$\mathrm{RHS}_1^{n+1} \simeq \mathrm{RHS}_1^n + \sum_{j=i-1}^{j=i+1} \mathcal{D}_{ij}^n \Delta^n \mathbf{W}_j \tag{2.16}$$

where $\mathcal{D}_{ij}^n$ are matrices depending on the solution in cells C_i and C_j. Using this approximation, the following linear system must be solved at each time step:

$$\frac{1}{\Delta^n t}\Delta^n \mathbf{W}_i - \sum_{j=i-1}^{j=i+1} \mathcal{D}_{ij}^n \Delta^n \mathbf{W}_j = \mathrm{RHS}_1^n \tag{2.17}$$

The implicit linearized scheme is completely defined once a suitable definition for the matrices $\mathcal{D}_{ij}^n$ is given. If the right hand side is differentiable, a common choice is to use the Jacobian matrices, hence:

$$\mathcal{D}_{ij}^n \simeq \frac{\partial \mathrm{RHS}_1^n}{\partial \mathbf{W}_j^n} \tag{2.18}$$

Nevertheless, it is not always possible nor convenient to exactly compute the Jacobian matrices. This problem has been solved herein through the use of the automatic differentiation software Tapenade. The operational principle of an automatic differentiation software is as follows: given the source code of a routine which computes the function

$y = F(x)$, the automatic differentiation software generates a new source code which compute the analytic derivative of the original program. In practice, each time the original program performs some operation, the differentiated program performs additional operations dealing with the differential values. Through an automatic differentiation software it is possible to quickly implement an implicit linearized scheme of the form 2.17, once a routine which computes the explicit flux function is available. As a consequence using an automatic differentiation tool, starting from a first-order explicit method, it is possible to automatically compute the matrices $\mathcal{D}_{ij}^n$ and then implement the linearized implicit methods 2.17 without additional modifications. Note that the use of an automatic differentiation tool is also convenient in the context of the study of sediment transport fluxes modeling since the increase of complexity for models does not give additional implementation difficulties for the implicit formulation.

A space and time second-order accurate linearized implicit formulation

A second-order implicit scheme is obtained, here, through the use of a second-order backward differentiation formula in time:

$$\frac{(1+2\tau)\mathbf{W}_i^{n+1} - (1+\tau)^2\mathbf{W}_i^n + \tau^2\mathbf{W}_i^{n-1}}{\Delta^n t\,(1+\tau)} - \mathrm{RHS}_2^{n+1} = 0 \tag{2.19}$$

where $\tau = \dfrac{\Delta^n t}{\Delta^{n-1} t}$. Similarly to the first-order case, a linearization of RHS_2^{n+1} must be carried out in order to avoid the solution of a nonlinear system at each time step. Clearly, the same approach as for the first-order scheme that is to find an approximated linearization of RHS_2^{n+1}, could be considered.

However, the linearization for the second-order accurate fluxes and the solution of the resulting linear system implies significant computational costs and memory requirements. This is a consequence of the more complex expression of second-order schemes with respect to their first-order counterparts and of the larger stencil of the second order flux function. In order to reduce the computational costs, an alternative approach is to use a defect-correction (DEC) technique. The DEC iterations write as:

$$\begin{cases} \mathcal{W}^0 = \mathbf{W}^n \\ \mathcal{L}_i^s \Delta^s \mathcal{W}_i - \displaystyle\sum_{j=i-1}^{j=i+1} \mathcal{D}_{ij}^s \Delta^s \mathcal{W}_j = \mathcal{C}_i^s \quad s = 0, \cdots, r-1 \\ \mathbf{W}^{n+1} = \mathcal{W}^r \end{cases} \tag{2.20}$$

in which:

$$\begin{cases} \mathcal{L}_i^s = \dfrac{(1+2\tau)}{\Delta^n t\,(1+\tau)}\, I - \mathcal{D}_{ii}^s \\ \mathcal{C}_i^s = -\left(\dfrac{(1+2\tau)\mathcal{W}_i^s - (1+\tau)^2\mathbf{W}_i^n + \tau^2\mathbf{W}_i^{n-1}}{\Delta^n t\,(1+\tau)} \right) + \mathrm{RHS}_2^s \end{cases} \tag{2.21}$$

$\mathcal{D}_{ij}^s$ being the generic matrices of the approximation (2.16) in which are involved the intermediate solutions $\mathcal{W}^s$. Thus, even if the flux function is computed using the second-order accurate numerical method, the linearization is based on the first-order flux function. In the basic approach, only one DEC iteration is used, i.e. $r = 1$, since only one defect-correction iteration is theoretically needed to reach a second-order accuracy ([28]). Nevertheless, form a practical point o view, the use of few additional DEC iterations (one or two) can improve the robustness.

2.3 Modified Roe Scheme for 2D solution

The 2D solution scheme proposed by Castro in [8] is the same presented for 1D solution scheme. So, the system (2.2) it could be reduced in the non conservative form as:

$$\frac{\partial W}{\partial t} + \mathtt{A}_1 \frac{\partial W}{\partial x} + \mathtt{A}_2 \frac{\partial W}{\partial y} = 0 \tag{2.22}$$

in the non conservative form. The matrix $\mathtt{A}_1$ and $\mathtt{A}_2$ are the Jacobian of the Shallow Water equations expressed by:

$$\mathtt{A}_1 = \begin{pmatrix} 0 & 1 & 0 & 0 \\ u^2 + gh & 2u & 0 & 0 \\ -uv & v & u & 0 \\ -\xi \frac{\partial q_b x}{\partial h} & -\xi \frac{\partial q_b x}{\partial q_x} & -\xi \frac{\partial q_b x}{\partial q_y} & 0 \end{pmatrix} \tag{2.23}$$

$$\mathtt{A}_2 = \begin{pmatrix} 0 & 0 & 1 & 0 \\ -uv & v & u & 0 \\ v^2 + gh & 0 & 2v & 0 \\ -\xi \frac{\partial q_b y}{\partial h} & -\xi \frac{\partial q_b y}{\partial q_x} & -\xi \frac{\partial q_b y}{\partial q_y} & 0 \end{pmatrix} \tag{2.24}$$

The *Roe-like Matrix* in the 2D dimensional case is expressed following eq. (2.22), as shown in [8], introducing the Roe averages as the 1D case. The expression of those averages are more complex than 1D case. The *Roe-like Matrix* $\mathtt{A}_1$ and $\mathtt{A}_2$ are defined for the right and the left cell and a *Roe-like Matrix* $\tilde{A}(W_L, W_R, n_{LR})$ is defined as follow:

$$\tilde{A}(W_L, W_R, n_{LR}) = n_{x,LR}\mathtt{A}_1 + n_{y,LR}\mathtt{A}_2 \tag{2.25}$$

Finally, introducing the diagonal matrix $|\Lambda|$, composed by the absolute values of the eigenvalues of $\tilde{A} = R|\Lambda|R^{-1}$, and $F_n = n_x F_1(W) + n_y F_2(W)$, the Roe-like numerical flux function $F(W_i, W_j, n_{LR})$ is introduced:

$$F(W_i, W_j, n_{LR}) = \frac{1}{2}(F_{n_{ij}}(W_i) - F_{n_{ij}}(W_i)) - \frac{1}{2}|\Lambda|(W_j - W_i) \tag{2.26}$$

2.3.1 Explicit solution

The complete formulation of MR scheme it could be expressed after the definition of the Roe-like numerical flux function 2.26. It is possible to write the non-conservative system (2.22) as:

$$\frac{\partial W}{\partial t} = \widehat{RHS}(F) \tag{2.27}$$

where $\widehat{RHS}(F)$ is a function of the Roe-like numerical flux function, which dependence will be omitted for simplicity (2.26) (for the complete formulation see [28]). The time discretization for the explicit Euler scheme is:

$$W^{n+1} = W^n + (\Delta t^n)\widehat{RHS} \tag{2.28}$$

This formulation express the solution for Shallow Water equations solved with the MR scheme. The second order extension is obtained introducing a reconstruction operator for each cell. Nevertheless, once (2.12) is defined, it is possible to extend the MR scheme to the second-order accuracy. The MR scheme presents for the second order extension is defined:

$$W^{n+1} = W^n + (\Delta t^n)\widehat{RHS_2} \tag{2.29}$$

It is considered a MUSCL-like reconstruction operator which at time t^n can be expressed as:

$$P_i(x; W_j^n) = W_i^n + \widehat{\Delta W_i^n}(x - G_i) \tag{2.30}$$

where $\widehat{\Delta W_i^n}$ is an approximation of the gradient in the i^{th}-cell, possibly taking into account flux-limiters. The same technique described in [8] is considered for the computation of $\widehat{\Delta W_i^n}$. A linear approximation of the gradient in each triangle T_j is considered, considering the barycentric coordinate λ_j associated for each k^{th} vertex of the j^{th} triangle. The gradient is approximated as:

$$\widehat{\Delta W_i^n} \simeq \frac{\sum_j |T_j| \Delta W_{T_j}}{\sum_j T_j} \tag{2.31}$$

In [8] is showed as eq. (2.31) is, for regular solution, a first-order approximation of ΔW shows [28].

2.3.2 Implicit solution. DEC correction

The implicit counterpart of a first order explicit method is obtained by considering the right-hand-side term as a function of the solution at time $n+1$ instead of n. It is possible to obtain a implicit method from an explicit using the following backward Euler method:

$$W^n = W^{n+1} - (\Delta t^n)\widehat{RHS} \tag{2.32}$$

However, from a practical point of view this would require the solution of a large nonlinear system of equations at each time step. A common technique to overcome this difficulty is to linearize the numerical scheme, that is to and an approximation of $\widehat{RHS}$:

$$\widehat{RHS}W^{n+1} \simeq \widehat{RHS}W^n + \sum D_{ij}\Delta^n W \tag{2.33}$$

where D_ij is a matrix depending on the solution in the i^th and the j^th- cell. Using this approximation, the following linear system must be solved at each time step for the MR scheme:

$$\frac{\Delta^n W}{\Delta t^n} - \sum D_{ij}\Delta^n W = \widehat{RHS} \tag{2.34}$$

The implicit linearized scheme is completely defined once a suitable definition for the matrices D_{ij} is given, similar at the one for the 1d case (2.18). If the right side is differentiable, a common choice is to use the Jacobian matrices, but it is not always possible or convenient to exactly compute the Jacobian matrices. In fact, it is not unusual to have some lack of differentiability of the numerical flux functions or in the source term. The implicit scheme is obtained using the automatic differentiation software TAPENADE. Through an automatic differentiation software it is possible to quickly implement an implicit linearized scheme of the form 2.34, once a routine which computes the explicit flux function is available. The implicit code is obtained from the explicit Roe solution. Therefore, the application of this method would require the solution of two non linear systems of equations at each time step, thus dramatically increasing the computational costs with respect to the explicit version. An alternative approach, generally more efficient in terms of computational costs, is to use a second-order backward differentiation formula in time:

$$\frac{(1+2\tau)W^{n+1} - (1+\tau)^2 W^n + \tau^2 W^{n-1}}{\Delta^n t(1+\tau)} - \widehat{RHS_2} = 0 \tag{2.35}$$

where $\tau = \frac{\Delta^n t}{\Delta^{n-1} t}$ Similarly to the 1^{rst}-order case, a linearization of $\widehat{RHS_2}$ must be carried out in order to avoid the solution of a nonlinear system at each time step, using the same approach for 1D solution of DEC correction (2.16). Indeed, it can be shown that only one defect correction iteration is theoretically needed to reach a second-order accuracy, while few additional iterations (one or two) can improve the robustness. DEC correction, as shown in [28], increase the simulation time efficiency without a deterioration of the solution accuracy.

2.4 CFL Condition

At the end, it is necessary for convergence of MR scheme to define the time interval Δt. In mathematics, it is used the Courant Friedrichs Lewy condition (CFL condition). Usually, it arises when explicit time-marching schemes are used for the numerical solution. As a consequence, the time step must be less than a certain time in many explicit time-marching computer simulations, otherwise the simulation will produce incorrect results. CFL condition it is necessary to define correctly the time step simulation. If a wave is moving across a discrete spatial grid and, it is necessary to compute its amplitude at discrete time steps of equal length. This length must be less than the time for the wave to travel to adjacent grid points. So, with CFL condition, the time step is set as the minor time for a wave to cross the spatial domain Δx. The intensity of the wave is given by the maximum eigenvalue λ_{max}. For 1D case, the CFL number used is defined as follows:

$$CFL = \frac{\lambda_{max} \delta t}{\delta x} \tag{2.36}$$

where λ_{max} is the maximum value of the eigenvalues of *Roe Matrix*. For 2D solution the CFL condition is expressed for MR scheme as the 1D case, and the maximum eigenvalue is taken from the global *Roe Matrix* $\tilde{A}$ and Δx is a characteristic length of each cell. As it possible to understand, for implicit solution CFL value must be higher than explicit solution. This mean that the time steps are higher, and the solution could result less accurate but faster than explicit one. The objective of this work is to improve the accuracy for implicit solution, with a different sediment transport model to solve Exner equation.

2.5 1D Model implementation

The implementation of the model chosen is herein presented.

2.5.1 Modified Grass Model

The first model chose is the modified Grass model (1.30), presented in Section 1.3, subchapter 1.4.6. The model is implemented only modifying the last line of Roe Matrix (2.9), which, for simplicity, is called $\vec{F}$. This vector is composed by the partial derivates of the sediment transport model q_b as follows:

$$F = -\frac{1}{1-p} \frac{\partial q_b}{\partial x} \tag{2.37}$$

where $\vec{x} = (x_1, x_2, x_3)$ is the state vector:

$$\vec{x} = \begin{pmatrix} h \\ hu \\ H \end{pmatrix} \tag{2.38}$$

So, the modified Grass model (1.30) can be rewritten as:

$$q_b(x_1, x_2, x_3) = A_d x_1 (\frac{x_2}{x_1})^3 \tag{2.39}$$

Therefore, according to eq. (2.37):

$$\vec{F} = \begin{pmatrix} \frac{1}{1-p} A_d \frac{u^{3/2}}{2} \\ -\frac{1}{1-p} \frac{3}{2} A_d \sqrt{u} \\ 0 \end{pmatrix} \tag{2.40}$$

and the last line of Roe Matrix is the transposed of vector $\vec{F}$. So, the first order explicit solution is derived and the implicit solution was implemented using automatic differentiation though TAPENADE. Second order terms are automatically calculated in the 1D code and defined the first order fluxes and the implicit 2^{nd} order version simply derives by using the DEC approach described in [28]

2.5.2 Meyer Peter Muller Model

The Meyer Peter - Muller model, expressed as eq. 1.24, in Section 1.3, subchapter 1.4.3 has also been implemented. That model, is defined by:

$$\frac{q_b}{\sqrt{(G-1)g d_{50}^3}} = sign(u) 8 (\theta - \theta_{cr})^{\frac{3}{2}}$$

is one of the most used in the literature and/or for ingegneristic/hydraulical problems. It is important the choice of the model for the shear stress τ, to well define the Shields condition. To simplify the computational problem, the shear stress are written in the Chezy form $\tau = Cu^2$ where C is a constant, which can be determined by different theories (e.g. Manning theory or Chezy theory, App. C.). So, the non-dimensional shear stress θ is:

$$\theta = \frac{C}{K} u^2 \tag{2.41}$$

It is possible to simplify eq. (1.24) by defining the parameter K as:

$$K = (G-1) g d_{50} \tag{2.42}$$

Therefore, substituting in eq. (1.24) the expression of the non-dimensional shear stress (2.41), MPM 1.24 equation is simplified as:

$$q_b = sign(u) \tilde{A} (u^2 - \tilde{u}^2)^{\frac{3}{2}} \tag{2.43}$$

where:

$$\tilde{A} = a \frac{C^{\frac{3}{2}}}{K} d_{50} \tag{2.44}$$

$$\tilde{u}^2 = \theta_{cr} \frac{K}{C} \tag{2.45}$$

Where, for MPM model, $a = 8$. For the Fernandez Luque and Van Beek model $a = 12$: in the code a is put as an input, so it is simple to switch between the two models. Consequently, it is possible to handle different physical conditions and to perform also the Fernandez Luque model. The incipient motion condition is thus a condition on the square of velocity u. So, if $u^2 > \tilde{u}^2$, sediment transport is present and expressed by eq. (1.24). Therefore, in the 1D code an *if control* is implemented to consider the threshold on the motion condition. The variables set as input are:

- a
- d_{50}
- $G = \frac{\rho_s}{\rho}$
- C
- θ_{cr}

The last line of Roe Matrix $\vec{F}$, as done for modified Grass model, is the transposed of vector $\vec{F}$, defined in [8], which can be expressed as follows:

$$\vec{F} = \begin{pmatrix} \frac{1}{1-p} 3\tilde{A}\sqrt{(u^2 - \tilde{u}^2)}\frac{u^2}{h} \\ -\frac{1}{1-p} 3\tilde{A}\sqrt{(u^2 - \tilde{u}^2)}\frac{u}{h} \\ 0 \end{pmatrix} \tag{2.46}$$

and the transposed vector (2.46) is the last line of Roe Matrix. It should be noted that $\frac{\partial q_b}{\partial h} = -u\frac{\partial q_b}{\partial hu}$. So, the first and second order implicit version can therefore be obtained as previously explained for the modified Grass model.

2.5.3 Modified Meyer Peter Muller Model

MPM model can oalso be modified in a similar way as the Grass model. As done for MPM model, the equation is reduced as:

$$q_b = sign(u)\tilde{A}h(u^2 - \tilde{u}^2)^{\frac{3}{2}} \tag{2.47}$$

The last line of the Roe Matrix is the transposed of vector $\vec{F}$ having the following expression:

$$\vec{F} = \begin{pmatrix} \frac{1}{1-p}\tilde{A}[(u^2 - \tilde{u}^2)^{\frac{3}{2}} - 3u^2\sqrt{(u^2 - \tilde{u}^2)}] \\ -\frac{1}{1-p} 3u\tilde{A}\sqrt{(u^2 - \tilde{u}^2)} \\ 0 \end{pmatrix} \tag{2.48}$$

Part II

1D Numerical Simulation

Chapter 3

Simulations with Grass model

In this Chapter, the test case used by Bilanceri in [28] for the Grass model is described. The results obtained with Grass model are briefly recalled the in Sec. (3.1). Next, in Sec. (3.2), simulations done with modified Grass model are presented.

3.1 Test case. Grass model results

A 1D test-case which corresponds to a standard problem already considered in several papers (see e.g. [7], [28]) is considered. It is a sediment transport problem in a channel of length $l = 1000$ m with a non constant bottom profile. The initial bottom topography is given by a hump shape function (Fig. 3.1):

$$\begin{cases} Z(0,x) = \begin{cases} 0.1 + sin^2(\frac{(x-300)\pi}{200}) & if\ 300 \leq x \leq 500 \\ 0.1 \end{cases} \\ h(0,x) = 10 - Z(0,x) \\ u(0,x) = \frac{10}{h(0,x)} \end{cases} \tag{3.1}$$

in which all the variables are in SI units. In [7] [28], two different uniform grids are considered for the discretization of the computational domain: a coarse grid, GR1, which is composed by 100 cells and a refined one, GR2, composed by 250 cells. The results computed by first and second-order MR schemes, both explicit and implicit, were compared in terms of accuracy and computational costs. Four sets of simulations, characterized by A_g equal to 0.001, 0.01, 0.1 and 1 respectively, A_g being the free parameter in the Grass model were carried out. Each value of the parameter A_g corresponds to a specific speed of interaction between the flow and the bedload and, as a consequence, to a specific time scale for the evolution of the bottom topography. The first value corresponds to a weak interaction between the flow and the bedload, the last to a strong one, while the other values to intermediate conditions. Therefore, in order to observe significant variations of the bed profile, the simulations corresponding to small values of A_g were advanced in time for longer periods, as table (3.1) shows. The largest CFL, allowing an accurate solution to be obtained are shown in Tab. (3.2). As it is possible to see, for second order implicit case, DEC correction permit to use a higher value of CFL. The implicit time advancing is computationally efficient even using only one DEC iteration for slow and intermediate speeds of interaction. The CFL limitation to avoid loss of accuracy is roughly inversely proportional to A_g and, in presence of unphysical oscillations, increasing the

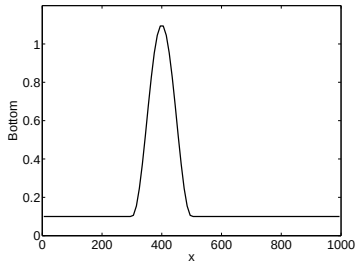

Figure 3.1: *Initial condition imposed for 1D numerical test.*

number of DEC iterations can significantly increase the accuracy. The implicit time advancing is computationally efficient even using only one DEC iteration for slow and intermediate speeds of interaction not shown here for the sake of brevity. In this work, the same problem and simulation set up are used, for all the models implemented. All the simulations have been carried out on a 2.5 GHz Intel Pentium Dual Core processor with 4 Gb RAM. Porosity is set as $p = 0.4$.

A_g	1	0.1	0.01	0.001
Simulation time	700	7000	50000	500000

Table 3.1: *Final simulation time (seconds) for the considered values of A_g.*

A_g	1	0.1	0.01	0.001
CFL Explicit	0.8	0.8	0.8	0.8
CFL Implicit DEC=1	10^0	10^1	10^2	10^3
CFL Implicit DEC=3	10^1	10^2	10^3	10^4

Table 3.2: *CFL value which allows the lower computational cost for Grass model.*

3.2 Simulation for modified Grass model

Numerical test are conduced to investigate the corrective effect of the state h in the Grass model GRH. The correction implies that the sediment constant A_g is modified as follows:

$$A_g = hA_d \tag{3.2}$$

so it varies along the local water column. A_g is not constant in the field and reaches its maximum values at the bottom, where h is maximum. In the field test case used, the maximum height is $h \cong 10$ meters, as presented in Section 3.1. Therefore, discharge constant A_d is set as in Tab. (3.3), in order that the maximum values of A_g be the same as those considered in [28] [31]. The local reduction of A_g could decrease the stiffness of the problem, reducing also the computational cost.

A_g	1	0.1	0.01	0.001
A_d	0.1	0.01	0.001	0.0001

Table 3.3: *Values imposed in input constant to obtain each fluid interaction.*

3.2.1 Weak interaction

Weak interaction corresponds to the smallest value of the sediment constant A_g. This type of interactions, when $0.001 \leq A_g \leq 0.003$, is typical for sandy areas, on costal environment. Figure 3.2 compares the solutions obtained with second order explicit scheme (CFL= 0.8) and implicit one (CFL= 10^3) for the Grass model and the modified Grass model. As for the model comparison, the sediment constant varies in the z direction, and thus the total discharge it is reduced, the bottom slope is more compact, and less advanced in the x direction. It can also be seen that the implicit solutions at CFL=10^3 coincide with the explicit ones for both grids and for both models. In order to better investigate the effects of the CFL number (a equivalently time step) Figs 3.3 and 3.4 show the solution obtained with 1^{st} and 2^{nd} order implicit schemes for the modified Grass model at various CFL numbers, compared to corresponding explicit solutions. In all cases at CFL=10^4 there is a deterioration of the implicit solution accuracy. Finally, Fig. 3.5 shows the effect of DEC iterations on the 2^{nd}-order implicit solution at CFL=10^4. It appears that with 3 or 4 DEC iterations accuracy problems are practically eliminated. Computational time are presented in Tab. (3.4). Implicit second order scheme for CFL= 10^4, DEC= 3, is clearly the best value which allows accuracy with small computational time. An important decrease of the CPU cost is anyway obtained with the implicit scheme also at CFL=10^3.

Method	GRID	
	100 el.	250 el.
Explicit 1^{st} CFL= 0.8	33.51 s	206.892 s
Explicit 2^{nd} CFL= 0.8	77.33 s	478.67 s
Implicit 1^{st} CFL= 10^3	0.228 s	1.44 s
Implicit 2^{nd} CFL= 10^3 DEC 1	0.232 s	1.468 s
Implicit 2^{nd} CFL= 10^4 DEC 3	0.072 s	0.444 s

Table 3.4: *Simulation time for modified Grass model when $A_d = 0.0001$. Comparison between Grid of 100 and 250 elements.*

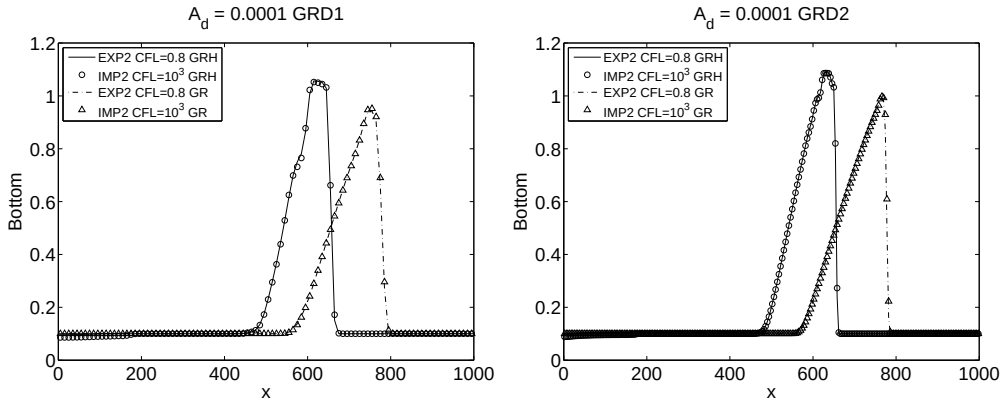

Figure 3.2: *Comparison between Grass model and modified Grass model for $A_d = 0.0001$. Second order solution, explicit solution with CFL= 0.8 and implicit solution with CFL= 10^3.*

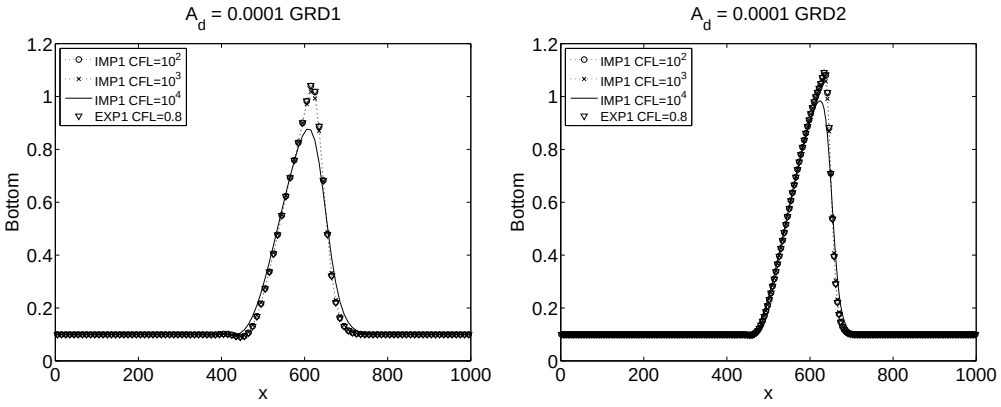

Figure 3.3: *Implicit case for modified Grass model for* $A_d = 0.0001$ *compared to explicit solution, CFL*$= 0.8$*. First order solution,CFL varies from* 10^2 *to* 10^4*.*

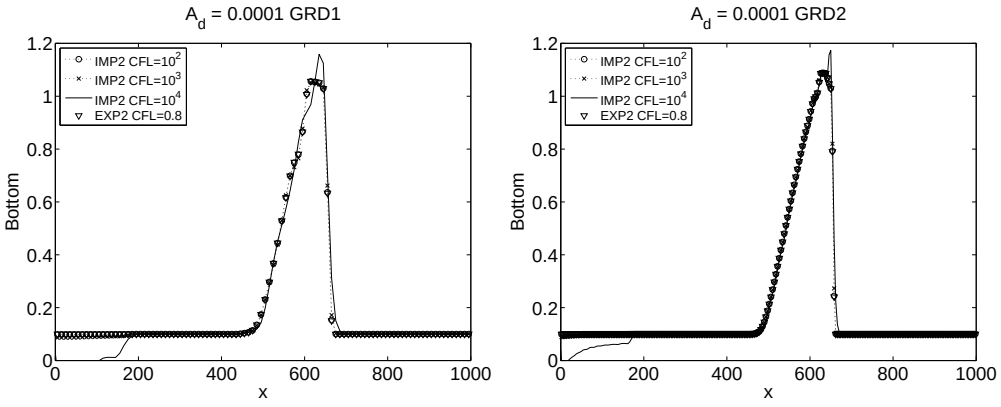

Figure 3.4: *Implicit case for modified Grass model for* $A_d = 0.0001$ *compared to explicit solution, CFL*$= 0.8$*. Second order solution,CFL varies from* 10^2 *to* 10^4*.*

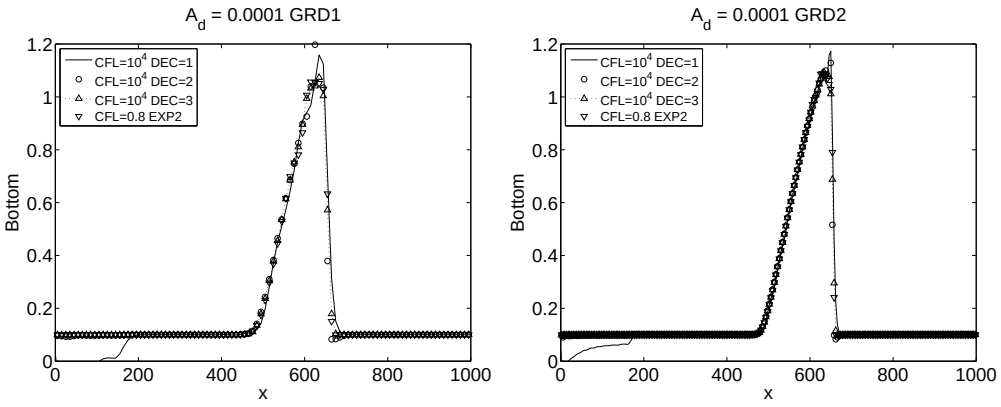

Figure 3.5: *Second order implicit case for modified Grass model for* $A_d = 0.0001$*, effects of the number of DEC iterations for CFL*$= 10^4$*.*

3.2.2 Weak/intermediate interaction

A weak/intermediate interaction, which correspond to $A_g = 0.001$ ($A_d = 0.0001$), is now considered. Weak/intermediate interactions are found in river areas, where the bed is more grainy, composed by sand and small stones. Fig. 3.6 shows the largest value of CFL (10^2) for second order implicit scheme with match explicit solution with DEC= 3. The modified Grass model present a more compact shape, with an higher peak, than Grass one. Moreover, the bottom slope is less advanced in the x direction. It can also be seen that the implicit solutions at CFL=10^2 coincide with the explicit ones for both grids and for both models. The same analysis proposed for weak interaction to investigate the CFL influence in implicit scheme is proposed in Figs. 3.7 and 3.8. For both 1^{st} and 2^{nd} order, explicit solution is reached by implicit scheme for CFL=10^2. Furthermore, a deterioration of the solution accuracy appears for CFL=10^3 and, for second order scheme, DEC iteration corretion is introduced in Fig. 3.9. For the second order implicit scheme, increasing DEC iterations, the accuracy is improved and, for DEC= 3, good accuracy is obtained also at CFL= 10^3. Finally, Tab. (3.5) shows the computational times. The largest gain obtained is obviously obtained at CFL=10^3 with 3 DEC iterations, but the implicit scheme is more efficient than the explicit one also at CFL=10^2.

Method	GRID	
	100 el.	250 el.
Explicit 1^{st} CFL= 0.8	3.384 s	20.737 s
Explicit 2^{nd} CFL= 0.8	7.828 s	47.939 s
Implicit 1^{st} CFL= 10^2	0.228 s	1.424 s
Implicit 2^{nd} CFL= 10^2 DEC 1	0.236 s	1.456 s
Implicit 2^{nd} CFL= 10^3 DEC 3	0.068 s	0.44 s

Table 3.5: *Simulation time for modified Grass model when* $A_d = 0.001$. *Comparison between Grid of 100 and 250 elements.*

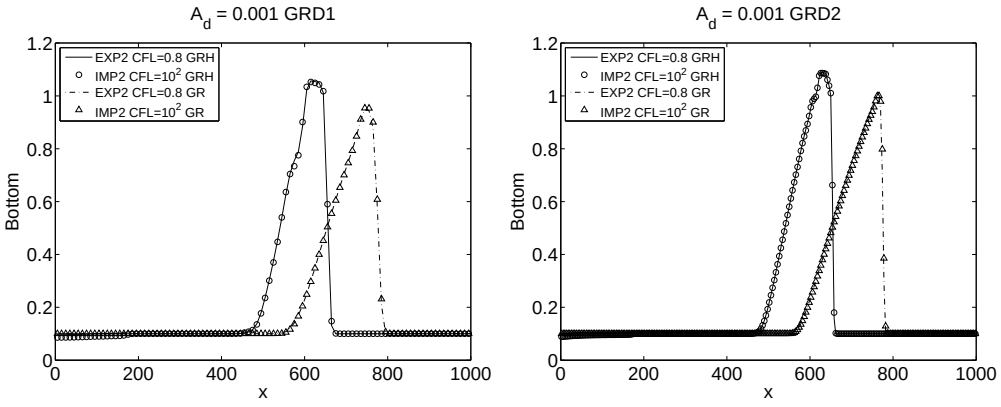

Figure 3.6: *Comparison between Grass model and modified Grass model for* $A_d = 0.001$. *Second order solution, explicit solution with CFL*= 0.8 *and implicit solution with CFL*= 10^2.

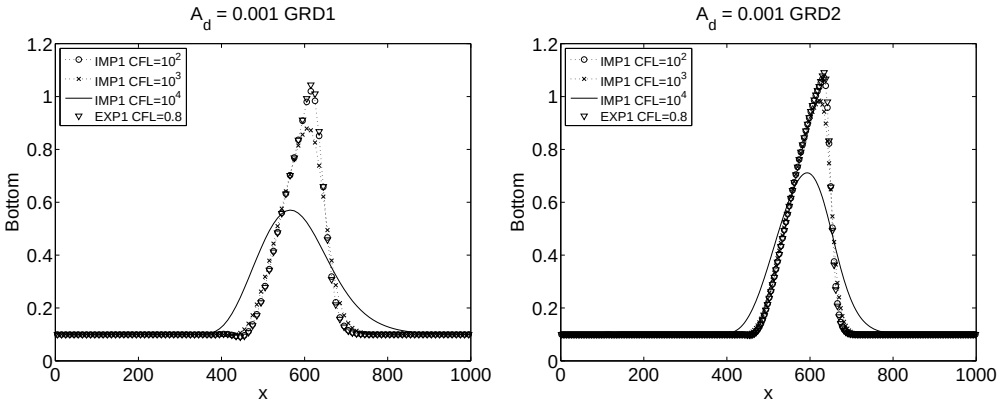

Figure 3.7: *Implicit case for modified Grass model for* $A_d = 0.001$ *compared to explicit solution, CFL*$= 0.8$*. First order solution, CFL varies from* 10^2 *to* 10^4*.*

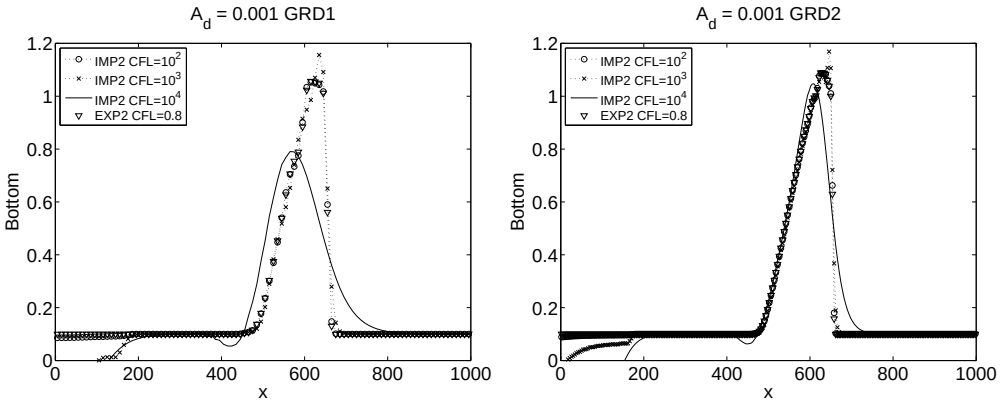

Figure 3.8: *Implicit case for modified Grass model for* $A_d = 0.001$ *compared to explicit solution, CFL*$= 0.8$*. Second order solution, CFL varies from* 10^2 *to* 10^4*.*

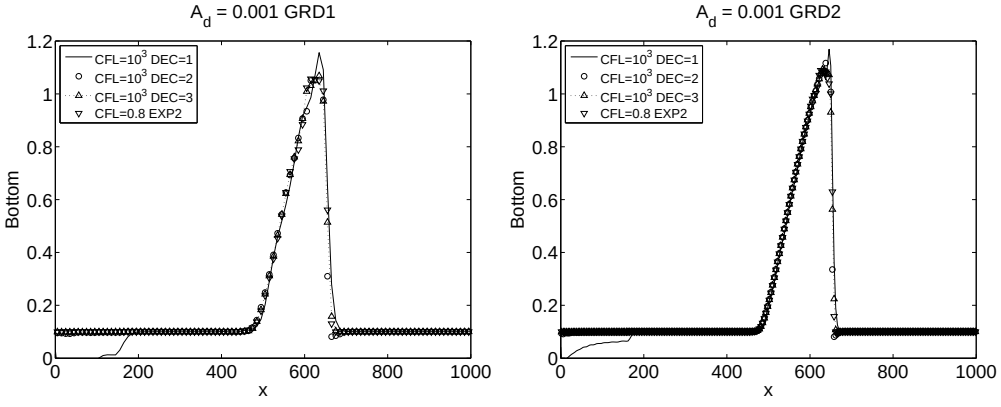

Figure 3.9: *Second order implicit case for modified Grass model for* $A_d = 0.001$*, effects of the number of DEC iterations for CFL*$= 10^3$*.*

3.2.3 Strong/intermediate interaction

This type of interaction is the highest value, physically speaking, considered valid for Grass model. However, the study of these interactions is useful at computational level since it allows to reduce the final time to observe a well defined sediment discharge. Moreover, considering strong/intermediate interaction, which correspond to $A_g = 0.1$ ($A_d = 0.01$), the modified Grass model compared to the Grass model is presented in Fig. 3.10. Implicit second order scheme with CFL=10^1 and explicit solutions with CFL=0.8 are compared. Implicit scheme match the explicit solution for both grid and condition. Also in this case, a reduction on displacement in x direction is found for the modified Grass model. Therefore, the CFL influence in implicit scheme is investigated in Fig. 3.11 for 1^{st} order and in Fig. 3.12 for 2^{nd} order. In all cases the implicit scheme accuracy deteriorates for CFL=10^2. Conversely, for CFL=10^1, implicit 1^{st} and 2^{nd} order scheme well match explicit solution with CFL=0.8 for both meshes. Finally, DEC iteration was investigated for CFL=10^2 and it is shown in Fig. 3.13 for both grid. It appears that with 3 DEC iterations accuracy problems are practically eliminated. In conclusion, computational times are presented in Tab. (3.6). Implicit second order scheme for CFL=10^2, DEC=3, is the best value which allows accuracy with with a negligible reduction in computational time. Explicit second order scheme CFL=0.8 gives accurate results with slightly higher times than implicit second order scheme with CFL= 10^2, DEC 3.

Method	GRID	
	100 el.	250 el.
Explicit 1^{st} CFL= 0.8	0.46 s	2.88 s
Explicit 2^{nd} CFL= 0.8	1.072 s	6.66 s
Implicit 1^{st} CFL= 10^1	0.316 s	1.968 s
Implicit 2^{nd} CFL= 10^1 DEC 1	0.324 s	2.012 s
Implicit 2^{nd} CFL= 10^2 DEC 3	0.1 s	0.608 s

Table 3.6: *Simulation time for modified Grass model when* $A_d = 0.01$. *Comparison between grid of 100 and 250 elements.*

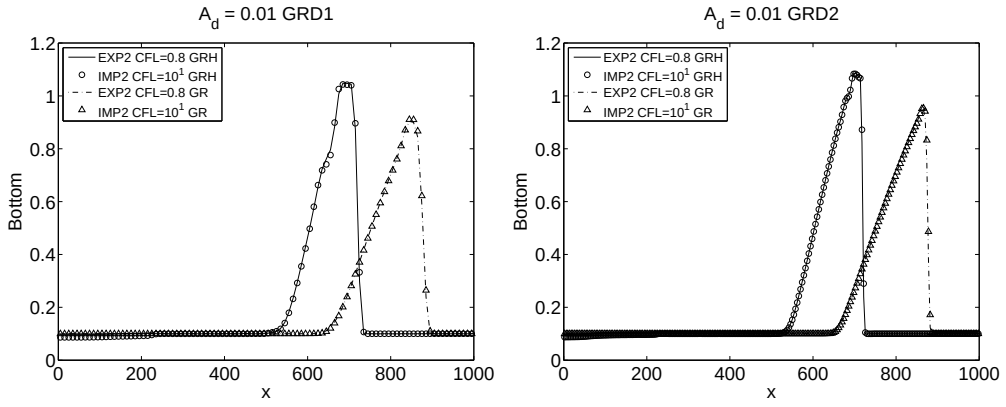

Figure 3.10: *Comparison between Grass model and modified Grass model for* $A_d = 0.01$. *Second order solution, explicit solution with CFL=* 0.8 *and implicit solution with CFL=* 10^1.

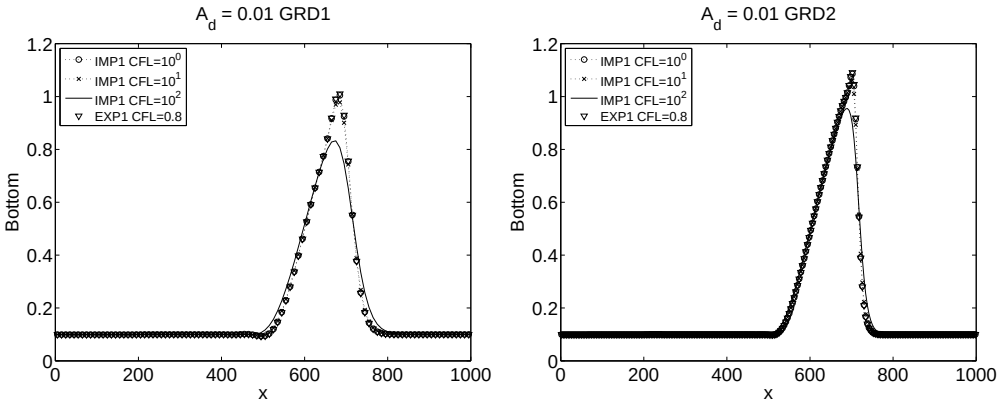

Figure 3.11: *Implicit case for modified Grass model for* $A_d = 0.01$ *compared to explicit solution, CFL*$= 0.8$*. First order solution, CFL varies from* 10^0 *to* 10^2*.*

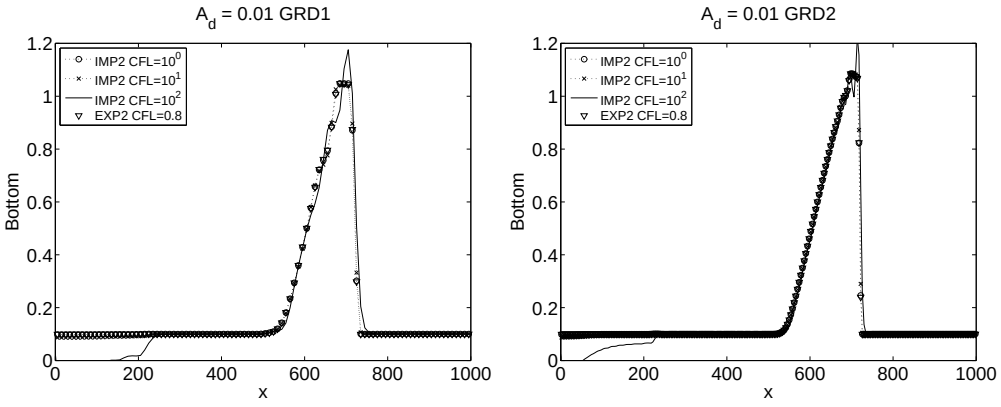

Figure 3.12: *Implicit case for modified Grass model for* $A_d = 0.01$ *compared to explicit solution, CFL*$= 0.8$*. Second order solution, CFL varies from* 10^0 *to* 10^2*.*

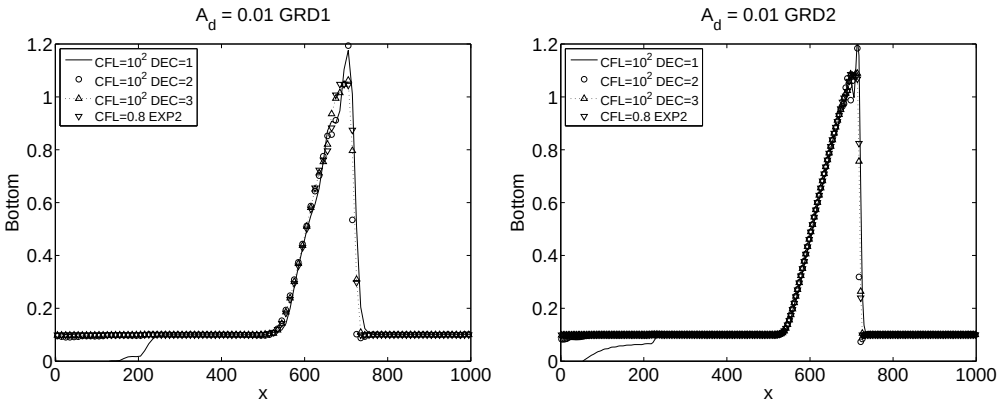

Figure 3.13: *Second order implicit case for modified Grass model for* $A_d = 0.01$*, effects of the number of DEC iterations for CFL*$= 10^1$*.*

3.2.4 Strong interaction

The last interaction value considered is for $A_g = 1$ ($A_d = 0.1$). In order to compare the modified Grass model and the Grass one for strong interaction, in Fig. 3.14 implicit solution obtained with CFL=1 is presented together with the one given by explicit scheme. In this case, a reduction in CFL for modified Grass model is found for the explicit scheme, which gives valid solution for CFL=0.6, instead of the value 0.8 used for Grass model. Again, for strong interaction a different discharge is found for the two considered models, for both grid. Modified Grass model presents a reduction of the x direction. Also for strong interaction, the influence in implicit solution of CFL is investigated for 1^{st} and 2^{nd} order scheme (Figs. 3.15 and 3.16). In all cases at CFL= 10^1 there is a deterioration of the implicit solution accuracy. Furthermore, increasing the number of DEC iterations for second order implicit scheme makes the solution more stable, as presented in Fig. 3.17. For 3 DEC iterations all accuracy problems completely disappear. Finally, computational time are presented in Tab. 3.7. Explicit scheme has a CPU time comparable to second order implicit scheme CFL= 10^1, with DEC= 3. For strong interaction, it is found a good computational gain using implicit scheme with DEC correction. Thus, for strong interaction, it is better to use the explicit scheme.

Method	GRID	
	100 el.	250 el.
Explicit 1^{st} CFL= 0.6	0.064 s	0.368 s
Explicit 2^{nd} CFL= 0.6	0.14 s	0.828 s
Implicit 1^{st} CFL= 10^0	0.28 s	1.756 s
Implicit 2^{nd} CFL= 10^0 DEC 1	0.288 s	1.792 s
Implicit 2^{nd} CFL= 10^1 DEC 3	0.084 s	0.536 s

Table 3.7: *Simulation time for modified Grass model when $A_d = 0.1$. Comparison between Grid of 100 and 250 elements.*

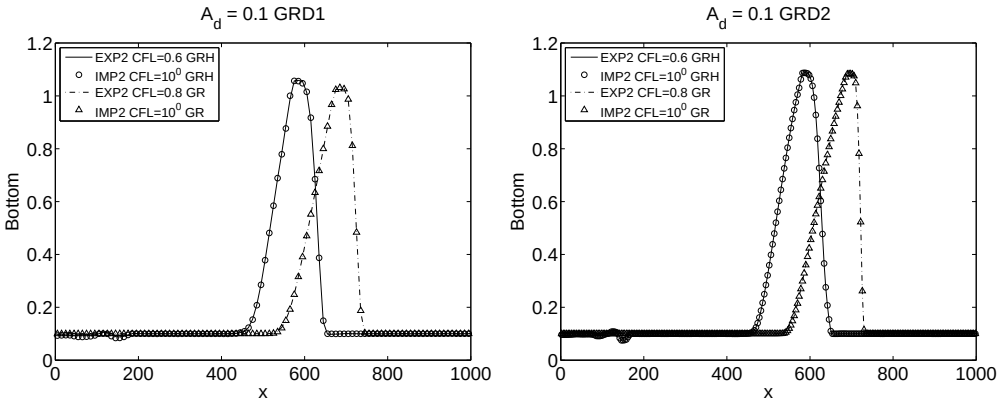

Figure 3.14: *Comparison between Grass model and modified Grass model for $A_d = 0.1$. Second order solution, explicit solution with CFL= 0.6 for modified Grass model and implicit solution with CFL= 10^1.*

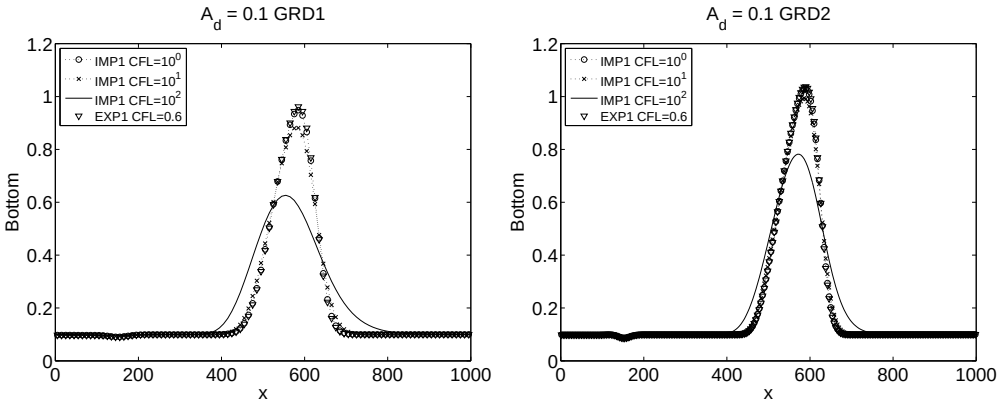

Figure 3.15: *Implicit case for modified Grass model for* $A_d = 0.1$ *compared to explicit solution,* $CFL = 0.6$*. First order solution,CFL varies from* 10^0 *to* 10^2*.*

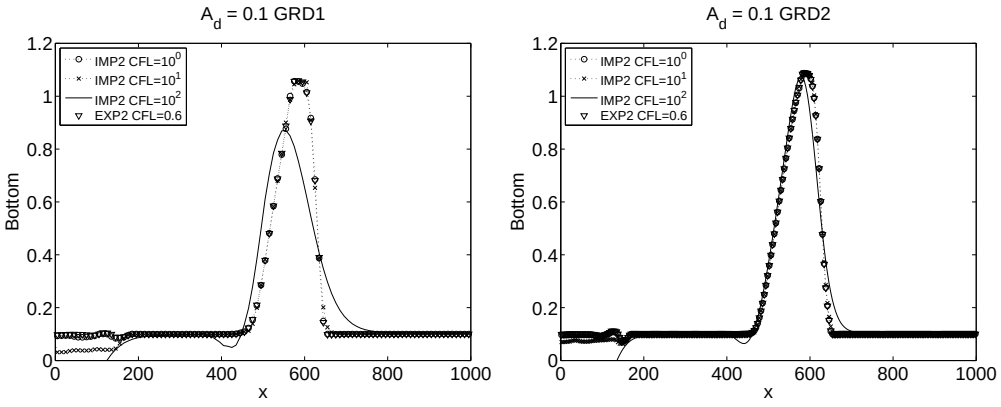

Figure 3.16: *Implicit case for modified Grass model for* $A_d = 0.1$ *compared to explicit solution,* $CFL = 0.6$*. Second order solution,CFL varies from* 10^0 *to* 10^2*.*

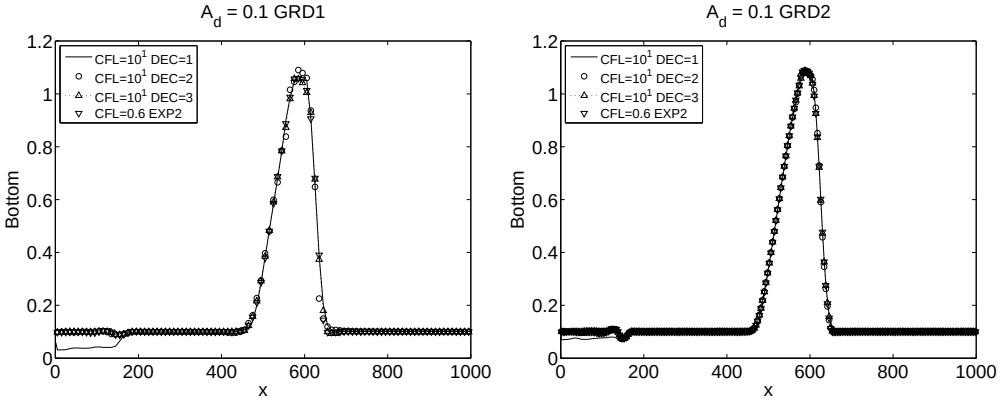

Figure 3.17: *Second order implicit case for modified Grass model for* $A_d = 0.1$*, effects of the number of DEC iterations for* $CFL = 10^1$*.*

3.2.5 Concluding remarks for the modified Grass model

As for the comparison between the implicit and explicit time advancing, the behavior of the modified Grass model is practically the same as the Grass one. The maximum CFL allowed for implicit time advancing to obtain an accurate solution is:

$$CFL =\simeq \frac{1}{A_g} \tag{3.3}$$

It could be increased of one order of magnitude at second order with 3 DEC iterations. Fig. 3.18 shows the ratio between explicit and implicit CPU time for all the values of A_g. Second order implicit scheme with 3 DEC iteration presents a strong decrease in computational efficiency for modified Grass model than the Grass one, especially for weak interaction, also if the CFL value is 10^4 for both model. Considering weak interaction for Grass model, the gain using implicit second order scheme is four time higher than using the modified Grass scheme. Moreover, also for weak/intermediate interaction this reduction it is found. The same decreasing trend is found for the solutions with only one DEC iteration.

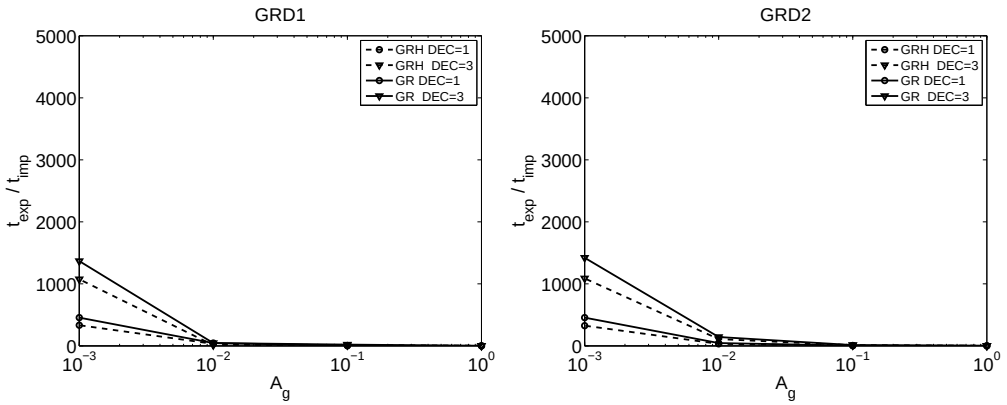

Figure 3.18: *Time ratio between second order implicit and explicit scheme, for modified Grass model (DEC= 3) and Grass model (DEC= 3) model for all the interaction analyzed.*

Chapter 4

Simulations with MPM model

In this Chapter, the analysis carried out for MPM model is presented. Simulations are presented in Sec 4.2. To well study the threshold influence in the problem, a set of test are carried out for MPM model and are presented in Sec. (4.3). After that, the MPM model is corrected like the Grass model. Simulations are presented in Sec. (4.4), and in Sec. (4.5) the analysis on threshold condition is reported.

4.1 Validation ($\tilde{u} = 0$)

First of all, to validate the work done, results obtained by Bilanceri [28] with Grass Model are used. The MPM model without threshold and Grass model must coincide. So, it is possible to compare those models by imposing in MPM, $\theta_{cr} = 0$. The results obtained with MPM match Grass results, also in CFL variation, as Fig. 4.1 shows for second order scheme and GR2. The considered values of A_g ($\tilde{A}$) constant in MPM model is obtained by imposing correctly the value of $G = \frac{\rho_s}{\rho}$ and Chezy constant C, following eq. (2.44). Table (4.1) resumes the constant value imposed in input to obtain all fluid interactions speed. The threshold θ_{cr} is also an input, so it is imposed equal to zero to have Grass model. As expected, the computational times for Grass model and MPM without threshold are comparable. The solution scheme is the same, only one therm change which does not produce relevant time gain. After no threshold analysis, threshold condition is verified, by imposing in input $\theta_{cr} = 0.047$. Obviously, to analyze the effect of the threshold, the incipient motion condition must be present in the test. Therefore, according to the Chezy expression of shear stress, it is simple to note that $\tilde{A}$

Interaction	$G = \frac{\rho_s}{\rho}$	C	$\tilde{u}$ $[m/s]$	d_{50} $[m]$
$A_g = 1$	1.8155	1	1.04	2.876
$A_g = 0.1$	9.1549	1	1.04	0.2877
$A_g = 0.01$	1.08155	0.01	1.04	0.287
$A_g = 0.001$	1.8155	0.01	1.04	0.0288

Table 4.1: *Values imposed in input parameter to obtain each fluid interaction.*

do not depend on mean diameter:

$$\tilde{A} = a\frac{C^{\frac{3}{2}}}{(G-1)g} \tag{4.1}$$

Consequently, it is possible to set only the value of C and G to have the value of $\tilde{A}$ required. The values presented in Tab. (4.1) are obtained by setting the Chezy coefficient, calculating G to obtain the corresponding speed interaction. After that, with an opportune value of d_{50}, the presence of the threshold is assured. This has got an important physical meaning, namely that the presence of sediment transport depends on the size of the sediment and not from the relative weight. Considering the same weight of two particle with different diameter the same weight, the size of the sediment defines the threshold of motion and, in turn, the type of scheme ($\tilde{A}$ is inversely proportional to density ratio G). Therefore, the threshold appears in the scheme used as a velocity condition. This because of the model of τ chosen. So, to obtain an optimal value, velocity shape at the bottom of Bilanceri result is analyzed. It is set as speed condition an average value:

$$\tilde{u} = 1.04 \tag{4.2}$$

which, guarantees the presence of the threshold in the test.

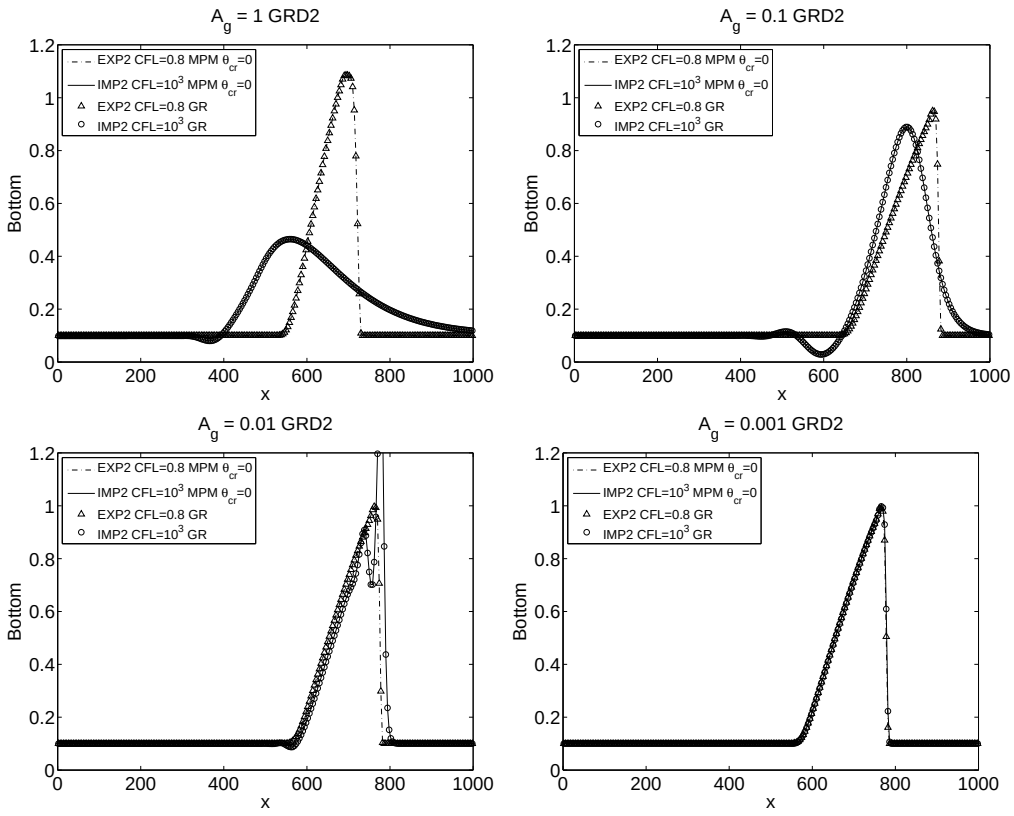

Figure 4.1: *Results obtained for MPM model with no threshold. All A_g values matches results with Grass model.*

4.2 Simulation with $\tilde{u} = 1.04$

In this section, results obtained with the MPM model with threshold set as $\tilde{u} = 1.04$ are presented. The presence of the threshold must change the bottom slope, and it is important to understand the effect on the stiffness of the code.

4.2.1 Weak interaction

Considering weak interaction, first and second order explicit solution, compared to Grass results, are shown in Fig. 4.2 for $\tilde{u} = 1.04$. It is possible to see the difference in the displacement of the bottom slope or the MPM, which is smaller and the hump near the threshold condition. Implicit first order solutions are compared with explicit first order in Fig. 4.3 for $\tilde{u} = 1.04$. Solutions seems to be stable, with an excellent accuracy of the solution up to CFL=10^4. At CFL=10^5, a slight decrease of the peak of the bottom profile. This decrease is greater in the case of solutions of second order, as can be seen in Fig. 4.3 for $\tilde{u} = 1.04$. Solution is stable and well matches first order solution until $CFL = 10^4$, with DEC=1. For $CFL = 10^5$, the solution accuracy significantly decreases: the code is not able to calculate this case for GR2, and for GR2 a higher peak is found. Also, for GR1, a different slope at threshold condition is found. The number of DEC iteration is increased for $CFL = 10^5$ and results are shown in Fig. 4.5 for $\tilde{u} = 1.04$, without relevant results. In terms of computational resources, Tab. (4.2) shows the CPU time for weak interaction. Implicit scheme have a more efficient solution and, compared to the result obtained with Grass model, the maximum CFL allowed to obtain an accurate solution is increased of one order of magnitude.

Method	$\theta_{cr} = 0.047$		$\theta_{cr} = 0$	
	100 el.	250 el.	100 el.	250 el.
Explicit 1^{st} CFL= 0.8	33.61 s	214.537 s	35.43 s	224.83 s
Explicit 2^{nd} CFL= 0.8	74.22 s	467.55 s	79.14 s	514.02 s
Implicit 1^{st} CFL= 10^4	< 0.001 s	0.004 s	0.02 s	0.12 s
Implicit 2^{nd} CFL= 10^4 DEC 1	0.02 s	0.116 s	0.02 s	0.124 s

Table 4.2: *Simulation time for MPM model,* $\tilde{A} = 10^{-3}$*,* $\tilde{u} = 1.04$ *m/s.*

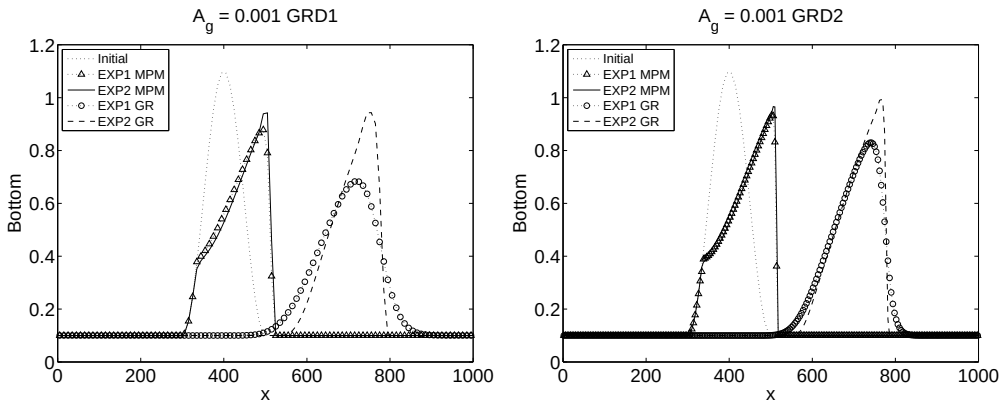

Figure 4.2: *Differences between initial condition, Grass model and MPM model for* $\tilde{A} = 0.001$*, GR1 and GR2. Explicit case CFL*= 0.8*,* $\tilde{u} = 1.04$ *m/s.*

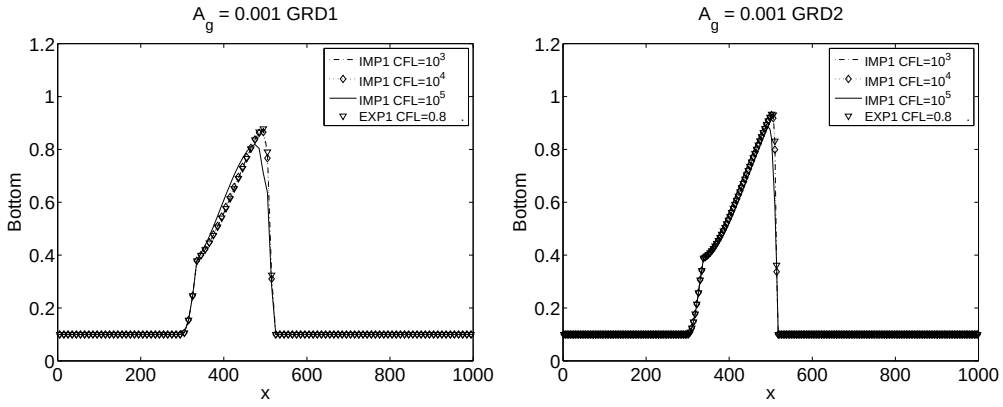

Figure 4.3: *Implicit case for MPM model for* $\tilde{A} = 0.001$ *compared to explicit solution, CFL*=0.8*. First order solution, CFL varies from* 10^3 *to* 10^5*, with* $\tilde{u} = 1.04$ *m/s.*

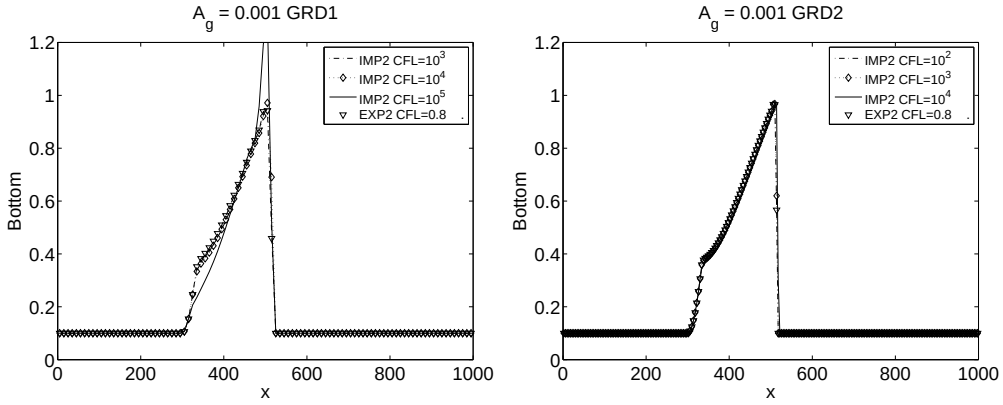

Figure 4.4: *Implicit case for MPM model for* $\tilde{A} = 0.001$ *compared to explicit solution, CFL*=0.8*. Second order solution, CFL varies from* 10^3 *to* 10^5*, with* $\tilde{u} = 1.04$ *m/s.*

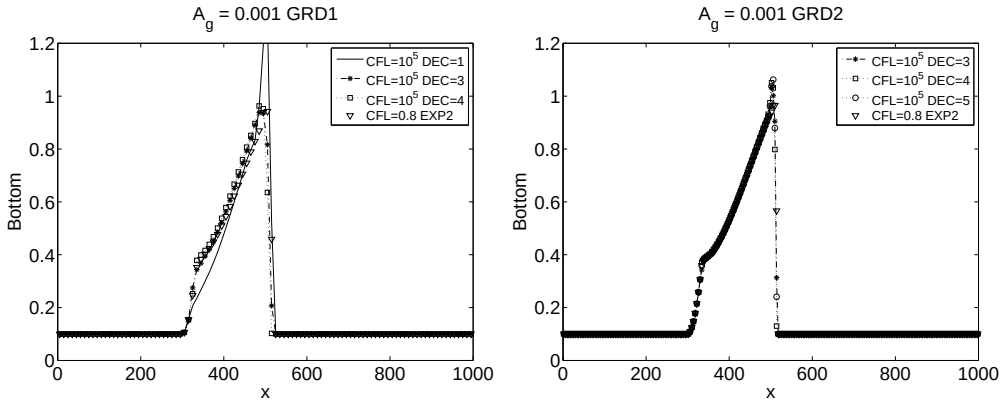

Figure 4.5: *Second order implicit case for MPM model for* $\tilde{A} = 0.001$*, effects of the number of DEC iterations for CFL*=10^5*,* $\tilde{u} = 1.04$ *m/s.*

4.2.2 Weak/intermediate interaction

Increasing A_g value, weak/intermediate interaction between bedload and water flow are considered. As presented for weak interaction, the bottom slope is smaller, as it is possible to see for first and second order of explicit solution, compared to Grass results, in Fig. 4.6 for $\tilde{u} = 1.04$. The presence of the threshold is evident, especially for the fact that it is linked to the velocity profile, constraining the bottom slope to the initial one. Implicit first order solutions are compared with explicit first order, in Fig. 4.7 for $\tilde{u} = 1.04$. In terms of accuracy resolution, an order of CFL is gained also for weak/intermediate interactions,with respect to Grass solution. Implicit second order solutions are compared with explicit second order in Fig. (4.7) for $\tilde{u} = 1.04$. Solution is stable and well matches second order solution until $CFL = 10^3$, with $DEC = 1$. After that, a peak for GR1 is found, and for GR2 the solution is not stable, as for weak interaction. Further increasing the DEC iteration is increased for $CFL = 10^4$ and results are shown in Fig. (4.9) for $\tilde{u} = 1.04$. Moreover, for DEC=2, unphysical oscillation are observed for GR2. Solution seems to lose accuracy also for DEC=3, with an higher peak. As for weak interaction, implicit scheme allows to gain one order degree in CFL condition but an increment of DEC correction does not reach a larger value. Finally, Tab. (4.3) shows the CPU time for weak/intermediate interaction. As for weak interaction, DEC=1 assures the best ratio accuracy-time calculation.

Method	$\theta_{cr} = 0.047$		$\theta_{cr} = 0$	
	100 el.	250 el.	100 el.	250 el.
Explicit 1^{st} CFL= 0.8	3.38 s	21.43 s	3.63 s	22.54 s
Explicit 2^{nd} CFL= 0.8	7.39 s	46.85 s	7.97 s	50.07 s
Implicit 1^{st} CFL= 10^3	0.02 s	0.116 s	0.02 s	0.12 s
Implicit 2^{nd} CFL= 10^3 DEC 1	0.02 s	0.116 s	0.094 s	0.016 s

Table 4.3: *Simulation time for* $\tilde{A} = 10^{-2}$, $\tilde{u} = 1.04$ *m/s.*

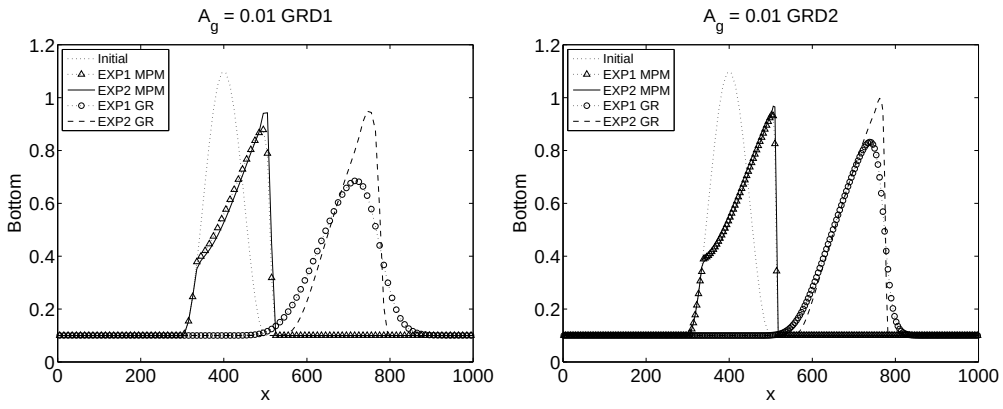

Figure 4.6: *Differences between initial condition, Grass model and MPM model for* $\tilde{A} = 0.01$*, GR1 and GR2. Explicit case CFL*= 0.8, $\tilde{u} = 1.04$ *m/s.*

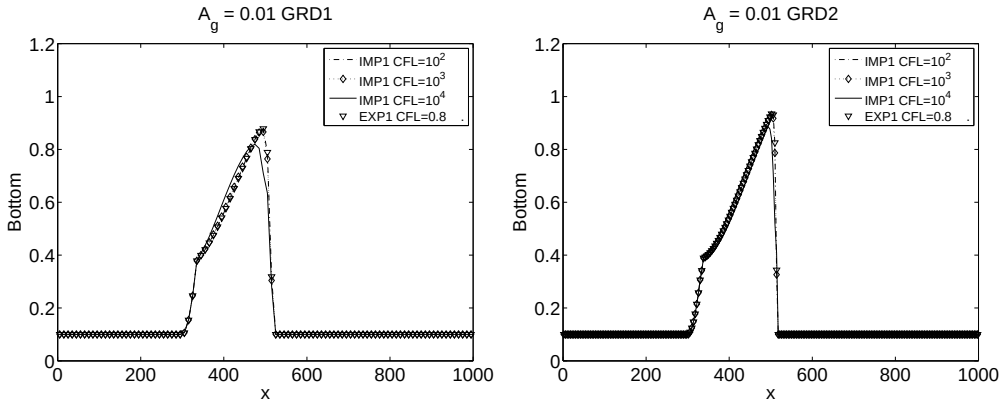

Figure 4.7: *Implicit case for MPM model for* $\tilde{A} = 0.01$ *compared to explicit solution, CFL*=0.8*. First order solution, CFL varies from* 10^2 *to* 10^4*, with* $\tilde{u} = 1.04$ *m/s.*

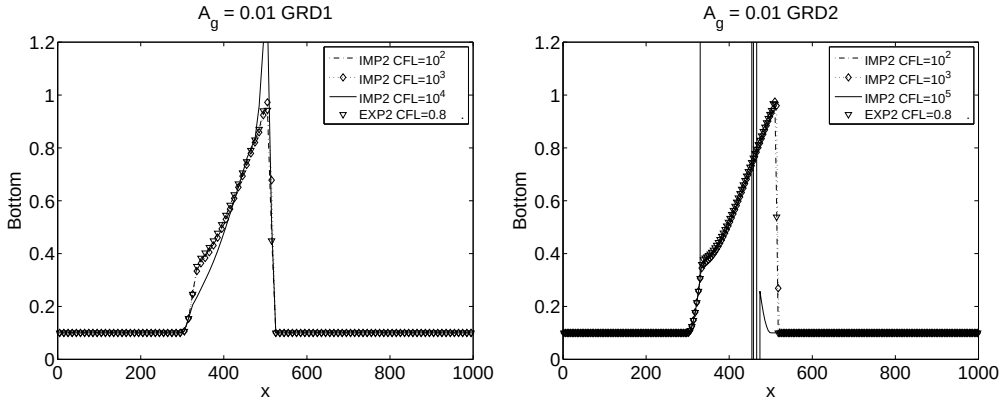

Figure 4.8: *Implicit case for MPM model for* $\tilde{A} = 0.01$ *compared to explicit solution, CFL*=0.8*. Second order solution, CFL varies from* 10^2 *to* 10^5*, with* $\tilde{u} = 1.04$ *m/s. For GR2, CFL*=10^4*, the code gives no results.*

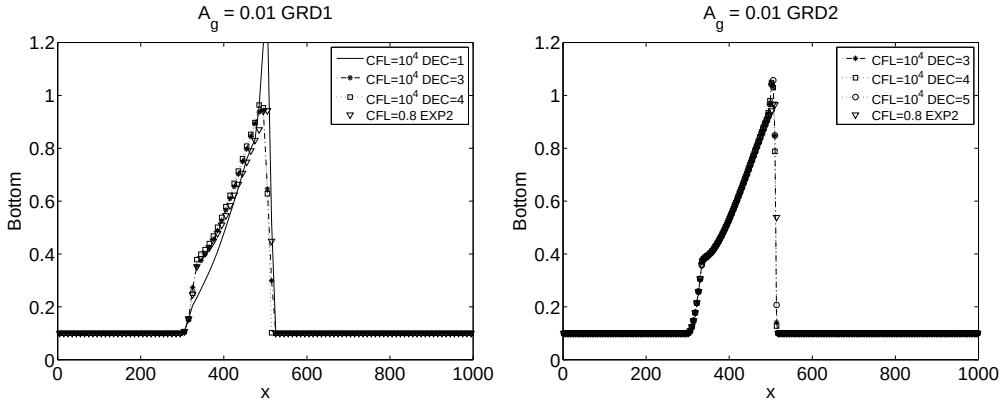

Figure 4.9: *Second order Implicit case for MPM model for* $\tilde{A} = 0.01$*, effects of the number of DEC iterations for CFL*=10^4*,* $\tilde{u} = 1.04$ *m/s.*

4.2.3 Strong/intermediate interaction

The value of Grass constant $\tilde{A} = 0.1$ corresponds to intermediate/strong interactions between sediment transport and fluid. Also in this case, as shown for weak interactions, the solution with MPM model is bound by the threshold, appearing more stable. First and second order of explicit solution, compared to Grass results, are shown in Fig. 4.10 for $\tilde{u} = 1.04$. Even for weak interactions, for implicit first order solutions, an order degree on CFL value is gained, as Fig. 4.11 shows. For $CFL = 10^3$, the solution near the threshold presents a lower peak, and some oscillations of second order. The same happens for implicit second order scheme, compared with explicit second order in Fig. 4.21 for $\tilde{u} = 1.04$.Solution is stable and well matches second order solution until CFL= 10^3, with DEC= 1. For CFL= 10^3, solution it is unstable, with an higher peak for GR1.For GR2 the code is not able to calculate the solution, and for CFL= 10^5 significant oscillation were found. Moreover, increasing DEC iteration for $CFL = 10^3$ and, as it possible to see in Fig. 4.13, the scheme is almost unstable, with an higher peak. Solution with DEC correction couldn't be considered valid. In this case, increasing DEC iteration is recommended to find a better ratio accuracy-computational time only for Grass model. Finally, as presented in Tab. (4.4), which shows the CPU time for strong/intermediate interaction.

Method	$\theta_{cr} = 0.047$		$\theta_{cr} = 0$	
	100 el.	250 el.	100 el.	250 el.
Explicit 1^{st} CFL= 0.8	0.47 s	2.98 s	0.52 s	3.254 s
Explicit 2^{nd} CFL= 0.8	1.06 s	6.55 s	1.15 s	7.26 s
Implicit 1^{st} CFL= 10^2	0.18 s	1.09 s	0.028 s	0.168 s
Implicit 2^{nd} CFL= 10^2 DEC 1	0.028 s	0.16 s	0.010 s	0.11 s

Table 4.4: *Simulation time for for MPM model,* $\tilde{A} = 10^{-1}$*,* $\tilde{u} = 1.04$ *m/s.*

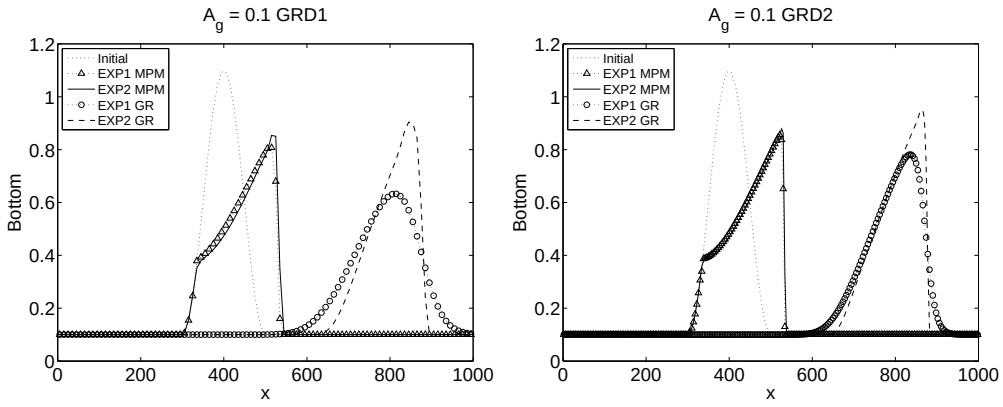

Figure 4.10: *Differences between initial condition, Grass model and MPM model for* $\tilde{A} = 0.1$*, GR1 and GR2. Explicit case CFL*= 0.8*,* $\tilde{u} = 1.04$ *m/s.*

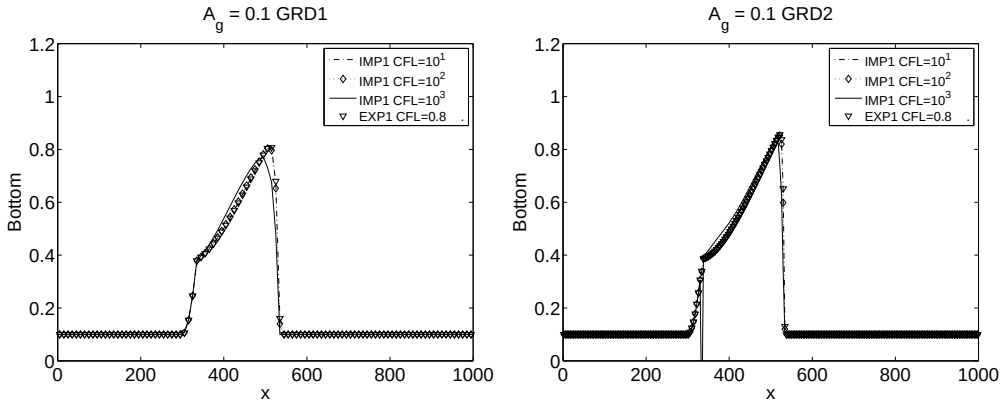

Figure 4.11: *Implicit case for MPM model for* $\tilde{A} = 0.1$ *compared to explicit solution, CFL*=0.8*. First order solution, CFL varies from* 10^1 *to* 10^3*, with* $\tilde{u} = 1.04$ *m/s.*

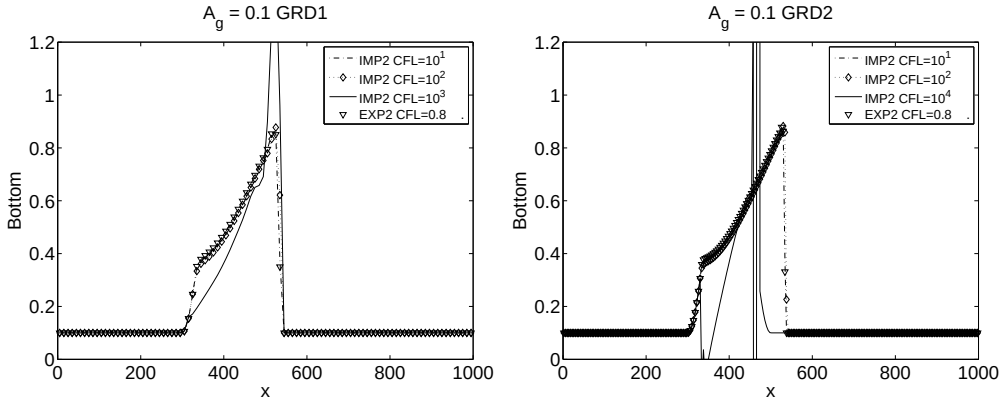

Figure 4.12: *Implicit case for MPM model for* $\tilde{A} = 0.1$ *compared to explicit solution, CFL*=0.8*. Second order solution, CFL varies from* 10^1 *to* 10^3 *for GR1 and from* 10^1 *to* 10^4 *for GR2, with* $\tilde{u} = 1.04$ *m/s.*

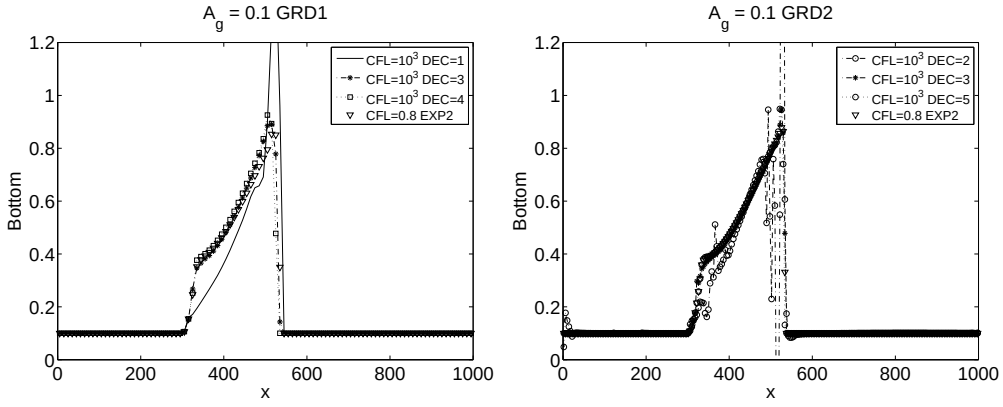

Figure 4.13: *Second order Implicit case for MPM model for* $\tilde{A} = 0.1$*, effects of the number of DEC iterations for CFL*=10^3*,* $\tilde{u} = 1.04$ *m/s.*

4.2.4 Strong interaction

IN order to compare the different solution between obtained with Grass and MPM models, first and second order of explicit solution, for $\tilde{A} = 1$ are presented in Fig. 4.14. For strong interaction, the quality of the results imposes a maximum CFL number equal to 1 for first order and second order scheme but, for GR2, a god accuracy is found also for $CFL = 10^2$, as it possible to see in in Fig. 4.15. Implicit second order solutions are compared with explicit second order in Fig. 4.15 for $\tilde{u} = 1.04$. Solution is stable and well matches first order scheme until $CFL = 10^1$, with DEC=1. The number of DEC iterations is increased for $CFL = 10^2$ and results are shown in Fig. (4.17) for $\tilde{u} = 1.04$. With 4 or 5 DEC iterations, good accuracy is recovered, although only small oscillation are present near the peak on GR2. Finally, Table (4.5) shows the CPU time for strong interaction. In this case, explicit solution do not present large differences in time than implicit one, so it is possible to use it without losing efficiency. In CFL condition, also in this case one order degree is gained with DEC=1

Method	$\theta_{cr} = 0.047$		$\theta_{cr} = 0$	
	100 el.	250 el.	100 el.	250 el.
Explicit 1^{st} CFL= 0.8	0.55 s	0.32 s	0.6 s	0.384 s
Explicit 2^{nd} CFL= 0.8	0.116 s	0.7 s	1.36 s	0.85 s
Implicit 1^{st} CFL= 10^1	0.028 s	0.164 s	0.18 s	0.2 s
Implicit 2^{nd} CFL= 10^1 DEC 1	0.028 s	0.172 s	0.036 s	0.204 s

Table 4.5: *Simulation time for for MPM model,* $\tilde{A} = 1$, $\tilde{u} = 1.04$ *m/s.*

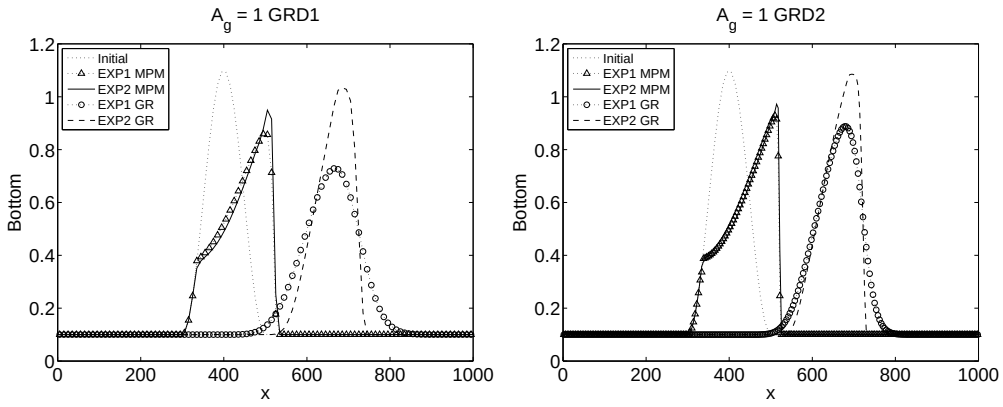

Figure 4.14: *Differences between initial condition, Grass model and MPM model for* $\tilde{A} = 1$*, GR1 and GR2. Explicit case CFL*= 0.8*,* $\tilde{u} = 1.04$ *m/s.*

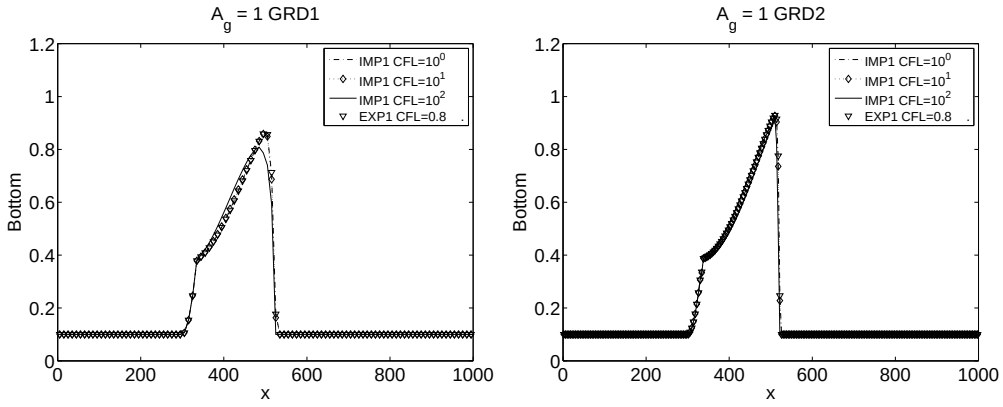

Figure 4.15: *Implicit case for MPM model for* $\tilde{A} = 1$ *compared to explicit solution, CFL*=0.8*. First order solution, CFL varies from* 10^0 *to* 10^2*, with* $\tilde{u} = 1.04$ *m/s.*

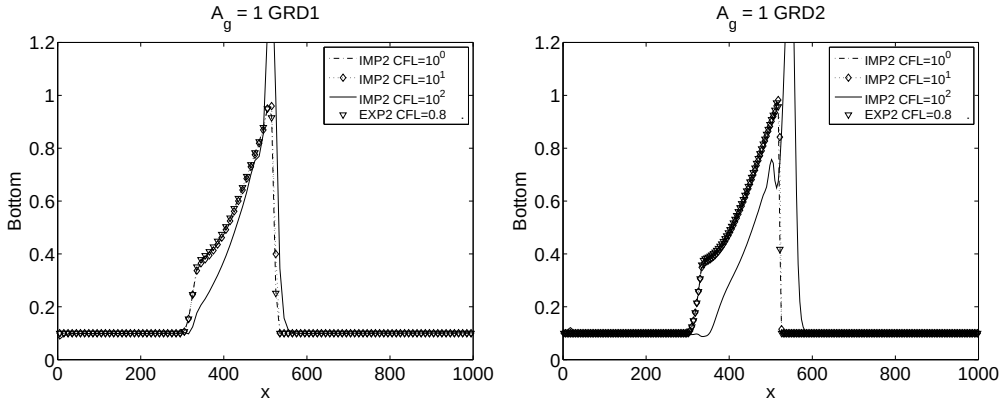

Figure 4.16: *Implicit case for MPM model for* $\tilde{A} = 1$ *compared to explicit solution, CFL*=0.8*. Second order solution, CFL varies from* 10^0 *to* 10^2*, with* $\tilde{u} = 1.04$ *m/s.*

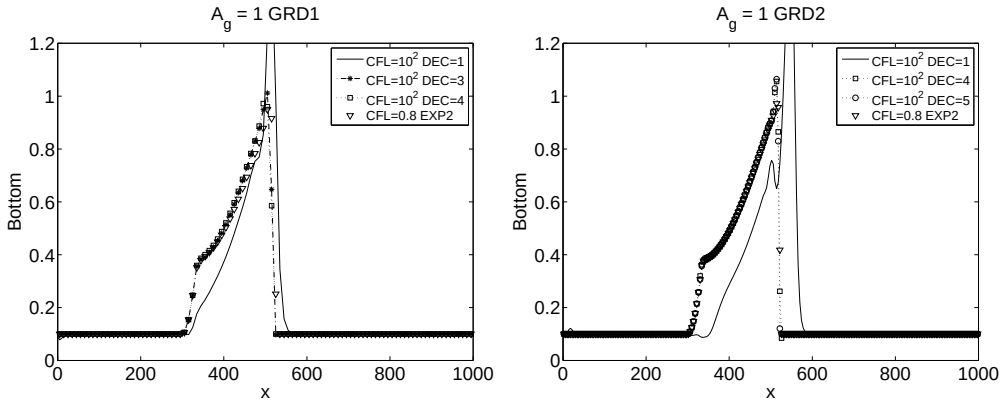

Figure 4.17: *Second order Implicit case for MPM model for* $\tilde{A} = 1$*, effects of the number of DEC iterations for CFL*=10^2*,* $\tilde{u} = 1.04$ *m/s.*

4.2.5 Concluding remarks for MPM model

The results obtained with MPM model presents an increasing in the CFL condition, considering only 1 DEC iteration. So, considering only one DEC iteration, the time scale of the problem is proportional to:

$$CFL \backsimeq \frac{10}{A_g} \tag{4.3}$$

which is the best ratio obtained with Grass model, but with DEC=3. For the MPM model, the solution doesn't shows a better trend with DEC= 3 at 2^{nd}-order scheme, and the maximum CFL can't be further increased by carrying out more DEC iterations. The computational efficiency is compared in Fig 4.18, in which the best solution for bot model is presented, with the solution obtained with only one DEC for Grass model. It is important to note how MPM model allows the same computational efficiency of Grass model with only one DEC. Especially for weak and weak/intermediate solution, a larger gain is obtained in CPU time using implicit scheme.

It is important to note, observing Tab. (4.1), that the values of the physical parameters imposed for $\tilde{A} = 10^{-3}$ hasn't got a valid meaning. The constant $\tilde{A}$ is too high and the particle diameter is not congruent with the displacement of the problem. For $\tilde{A} = 10^{-3}$, values of the physical parameters imposed has got a valid meaning. The corresponding value of G and C are typically used in sandy areas. The mean diameter is a bit high, but this is in agreement with Grass model, which is developed for sandy areas. For low values of the density ratio G, transport is present if the particle diameter has a considerable dimension, according to eq. (2.45). In sandy areas, G and d_{50} are small and transport is still present. To introduce the threshold, a larger value of mean diameter is required, as it is shown Tab. (4.1). The case analyzed is more suitable for sediment transport in rocky rivers, for which MPM equation is developed.

4.3 Threshold influence on MPM model

The principal effect of the threshold is to reduce the sediment discharge. In order to fully understand its influence on simulation performed, an analysis varying the threshold value was performed. Two additional values for $\tilde{u}$ have been analyzed.

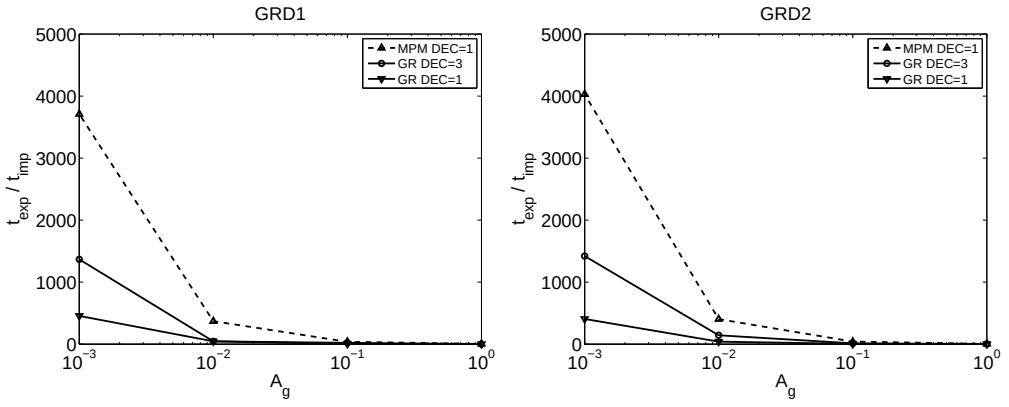

Figure 4.18: *Time ratio between second order implicit and explicit scheme, for MPM model (DEC= 1) and Grass model (DEC= 3) model for all the interaction analyzed.*

Interaction	$G = \frac{\rho_s}{\rho}$	C	$\tilde{u}$ $[m/s]$	d_{50} $[m]$
$A_g = 1$	1.8155	1	1.02	2.767
			1.04	2.876
			1.06	2.9883
$A_g = 0.1$	9.1549	1	1.02	0.2767
			1.04	0.2877
			1.06	0.2988
$A_g = 0.01$	1.08155	0.01	1.02	0.2767
			1.04	0.287
			1.06	0.2988
$A_g = 0.001$	1.8155	0.01	1.02	0.0277
			1.04	0.0288
			1.06	0.02988

Table 4.6: *Values imposed in eq. (2.44) and (2.45) to obtain weak interaction for MPM model.*

4.3.1 CFL influence

The presence of the threshold leads to a different bottom evolution with respect to the one obtained with the Grass model. This bottom slope could influence, in particular, the value of CFL for which the solution might be considered accurate. At this matter, two additional thresholds are considered for the MPM model. As mentioned in Chap. 4 for MPM model, varying only the parameter d_{50} it is possible to set the threshold, as reported in Tab 4.6. As it possible to see in Fig. 4.19, for GR2, the threshold position influence the bottom slope. As expected, the bottom movement is reduced increasing the threshold magnitude. The threshold constrains the location of the bottom at the initial one, so it is expected an influence on the peak of the bottom slope. So, it is expected also an influence on the behavior of the implicit scheme with varying CFL. As it possible to see in Fig. 4.20 and Fig. 4.21, a different trend is found for different threshold magnitude. For $\tilde{u} = 1.02$ m/s, solution losses accuracy at the same CFL for $\tilde{u} = 1.04$ m/s. The solution is still accurate for CFL=10^3. This trend confirm the influence of the threshold on the instability mode. However, also if with a higher

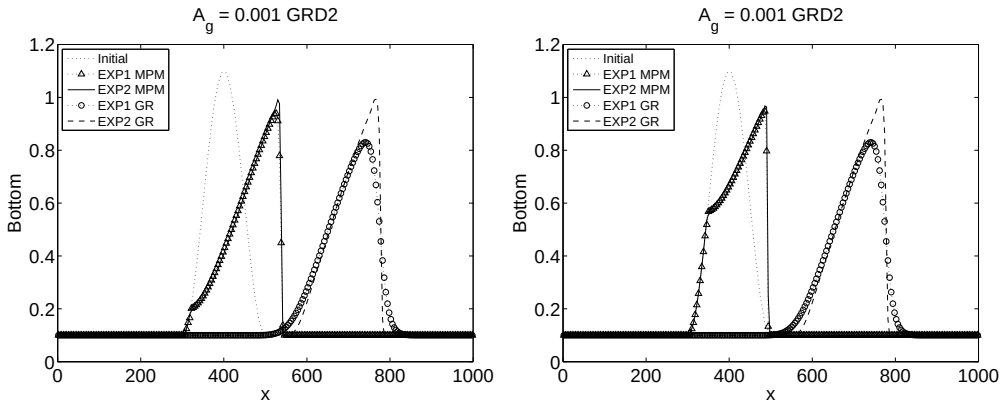

Figure 4.19: *Differences between initial condition, Grass model and MPM model for* $\tilde{A} = 0.001$*, GR2. Explicit case CFL*$= 0.8$*,* $\tilde{u} = 1.02$ *m/s (right) and* $\tilde{u} = 1.06$ *m/s (left).*

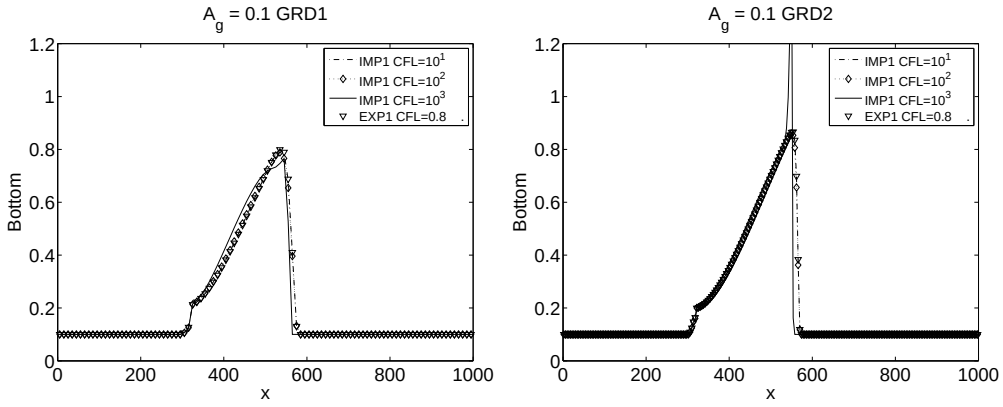

Figure 4.20: *Implicit case for MPM model for* $\tilde{A} = 0.1$ *compared to explicit solution, CFL*=0.8*. First order solution, CFL varies from* 10^1 *to* 10^3*, with* $\tilde{u} = 1.02$ *m/s.*

value of the threshold the solution seems to be stable, the scheme had to produce a valid solution for all case. The solution is considered valid for CFL= 10^2, strong/weak interaction, first order solution. For the others interaction, first order implicit scheme, a similar trend is found so results obtained for MPM model with $\tilde{u} = 1.04$ m/s. The

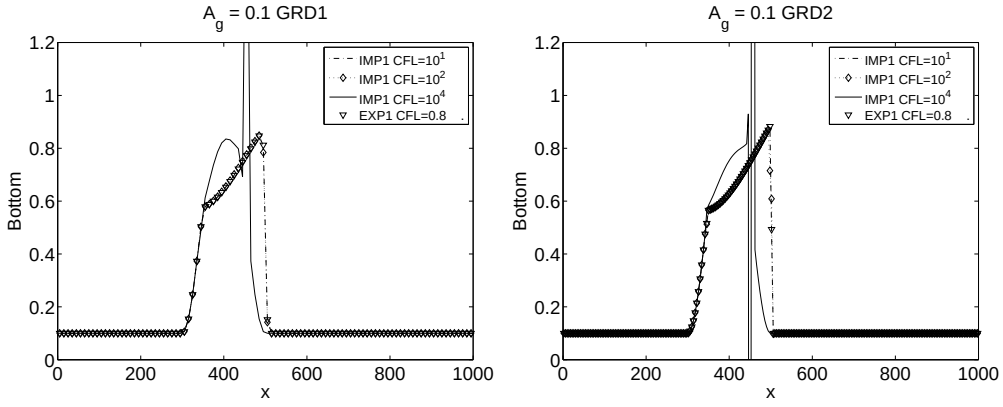

Figure 4.21: *Implicit case for MPM model for* $\tilde{A} = 0.1$ *compared to explicit solution, CFL*=0.8*. First order solution, CFL varies from* 10^1 *to* 10^3*, with* $\tilde{u} = 1.06$ *m/s.*

effect on implicit second order scheme is now considered. To investigate the threshold effect in CFL and DEC condition in second order implicit scheme, considering both threshold, are presented for strong speed interaction in Fig. 4.22 and Fig. (4.23. For strong interaction, the threshold position does not influence the CFL condition: also further oscillations were found for $\tilde{u} = 1.04$ m/s. Increasing the DEC iteration does not allow a larger value of CFL. Moreover, the same condition were found for weak interaction, as presented for both threshold in Fig. 4.24 and Fig. 4.25. The second order implicit solution gives the same results for all threshold value considered. It is possible to affirm that the time scale is the same considered in eq. (5.1) and, in all case analyzed, increasing the DEC iteration number does not allow a larger CFL value.

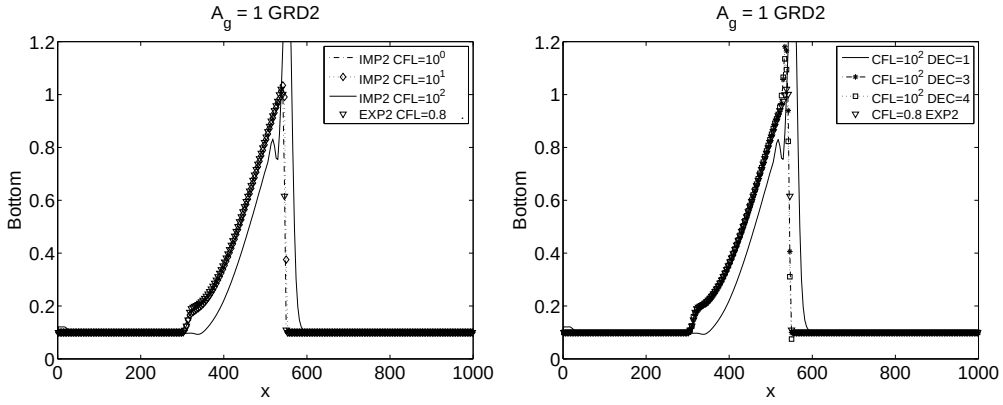

Figure 4.22: *Implicit case for MPM model for* $\tilde{A} = 1$ *compared to explicit solution, CFL*=0.8*, with* $\tilde{u} = 1.02$ *m/s. Second order solution, CFL varies from* 10^0 *to* 10^2 *and DEC iteration is visualized for CFL*= 10^2*.*

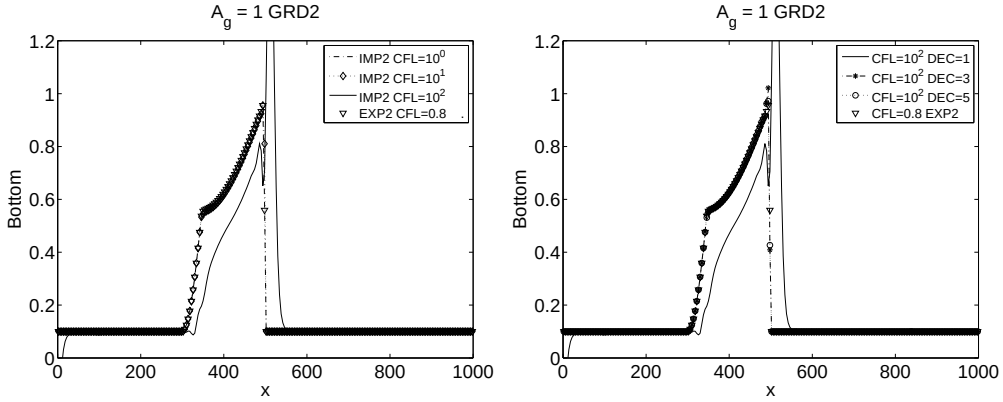

Figure 4.23: *Implicit case for MPM model for* $\tilde{A} = 1$ *compared to explicit solution, CFL*=0.8*, with* $\tilde{u} = 1.06$ *m/s. Second order solution, CFL varies from* 10^0 *to* 10^2 *and DEC iteration is visualized for CFL*= 10^2*.*

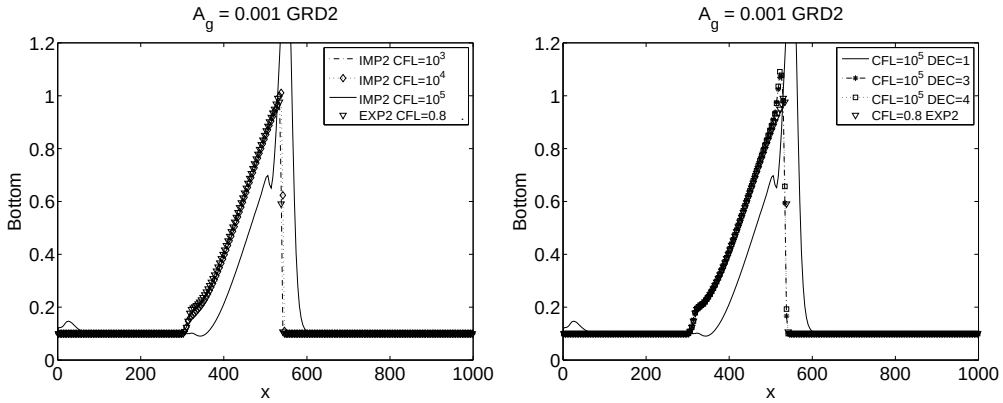

Figure 4.24: *Implicit case for MPM model for* $\tilde{A} = 0.001$ *compared to explicit solution, CFL*=0.8*, with* $\tilde{u} = 1.02$ *m/s. Second order solution, CFL varies from* 10^0 *to* 10^2 *and DEC iteration is visualized for CFL*= 10^2*.*

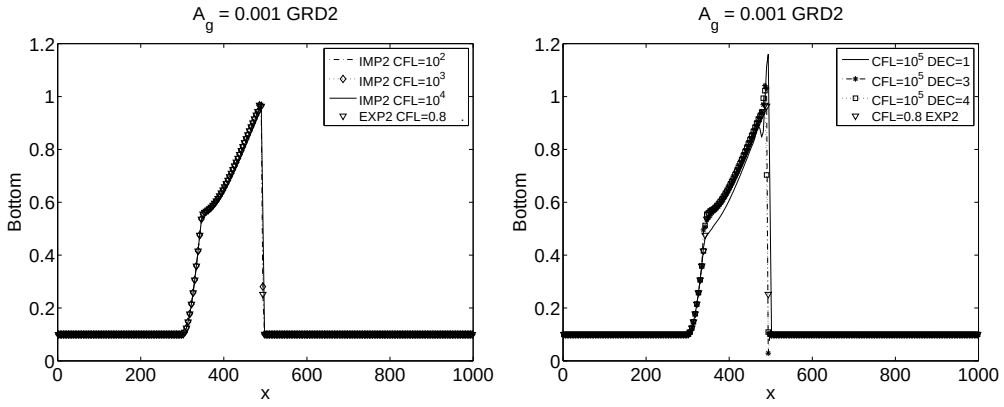

Figure 4.25: *Implicit case for MPM model for* $\tilde{A} = 0.001$ *compared to explicit solution, CFL*=0.8*, with* $\tilde{u} = 1.06$ *m/s. Second order solution, CFL varies from* 10^2 *to* 10^4 *and DEC iteration is visualized for CFL*= 10^5.

4.3.2 Final time: influence on the steady state

As observed, threshold condition modifies the steady shape of the bottom. The total time imposed is the same used in [28] to convergence as a steady solution for Grass model, to well compare different solution. At this matter, it important to study if the situation proposed is a steady condition and how the model reaches it. A series of different simulations, changing the final time, are executed. The objective is to understand if the threshold introduce or not a delay in the sediment discharge. At this matter, each simulation is advanced in 3 different steps, each of these 2% of the total time previously used, taken as initial reference. Indeed, as noted in previous chapters, the main effect of the threshold is to reduce the sediment discharge and, consequently, a solution is reached in less time than steady. As further confirmation, tests are performed reducing the overall time. Three backwards steps are considered, each of these 2% of the total time taken as initial reference. The considered simulation times are presented in Tab. (4.7) and in Tab. (4.8). To well understand the influence of the threshold, different geometrical characteristic of the sediment slope are analyzed.

Interaction	Time step [s]	T_0 [s]	T_1 [s]	T_2 [s]	T_3 [s]
$A_g = 1$	14	700	714	728	742
$A_g = 0.1$	140	7000	7140	7280	7420
$A_g = 0.01$	1000	50000	51000	52000	53000
$A_g = 0.001$	10000	500000	510000	520000	530000

Table 4.7: *Threshold influence, final time analysis. Total time upwards steps for each interaction value used for MPM and Grass models. The time step considered is the* 2% *of the total time used in the previous simulation.*

All the geometrical characteristic are made dimensionless with the occurred at the reference time T_0. First of all, the bedload geometrical coordinate x and z (G_x and G_z) are calculated for all interaction value. G_x indicates how the sediment slope moves along the x direction, G_z indicate the behavior of the sediment along the z direction. Together they gives an idea of the movement of the sediment, so it is possible to check what happens in the presence of threshold for the MPM model compared to the Grass one. For this purpose, it should be remembered as the model without MPM threshold

Interaction	Time step [s]	T_0 [s]	T_1 [s]	T_2 [s]	T_3 [s]
$A_g = 1$	14	700	686	672	658
$A_g = 0.1$	140	7000	6860	6720	6580
$A_g = 0.01$	1000	50000	49000	48000	47000
$A_g = 0.001$	10000	500000	490000	480000	470000

Table 4.8: *Threshold influence, final time analysis. Total time backwards steps for each interaction value used for MPM and Grass models. The time step considered is the* 2% *of the total time used in the previous simulation.*

coincides with Grass model, as observed in Chapter 4. As it possible to see in Fig. 4.26,

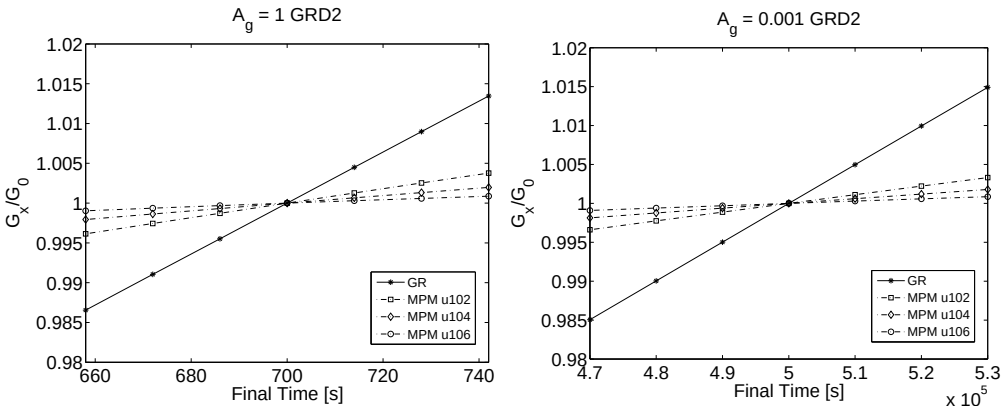

Figure 4.26: *Threshold influence on the center of gravity on x direction, for weak and strong interaction, GR2. Explicit second order scheme with CFL*= 0.8.

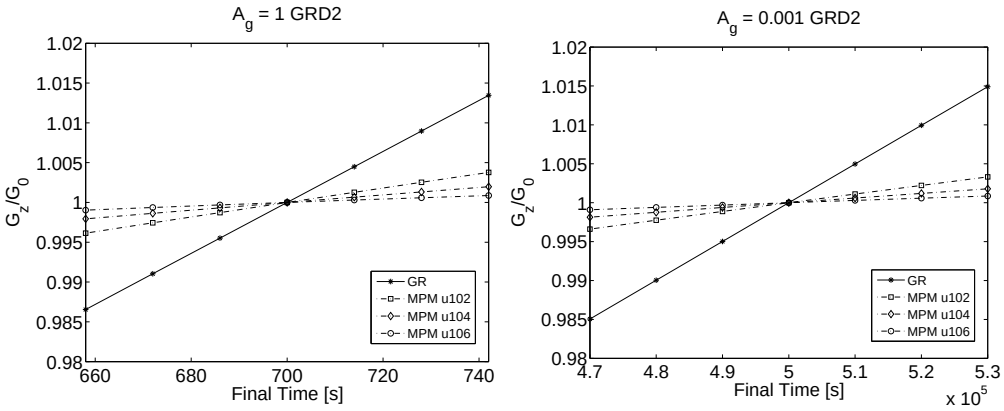

Figure 4.27: *Threshold influence on the center of gravity on z direction, for weak and strong interaction, GR2. Explicit second order scheme with CFL*= 0.8.

the presence of the threshold reduces the movement of the sediment in the x direction. A linear trend is found for all interactions. The movement reduction is larger as higher is the threshold value. Interesting is the trend in the z direction, presented in Fig. 4.27. The shape of the sediment moves along x and elongates, increasing its height. This justifies what observed for the correction of the Grass model. The sediment transport,

function of the speed, increases more than fluid velocity is high. As consequence of this, the shape of the sediment is more stretched and more shifted towards the bottom of the field. The correction of the model becomes necessary as a continuous shift with strain is not expected physically and goes against the idea of bedload, a phenomenon for which the model was developed for. Therefore, it is important to understand how the movement of sediment occurs. For this purpose, in Fig 4.28 the average displacement Z_{mean} along z is shown and, in Fig 4.29, the relative value of the peak Z_{max}. The thing

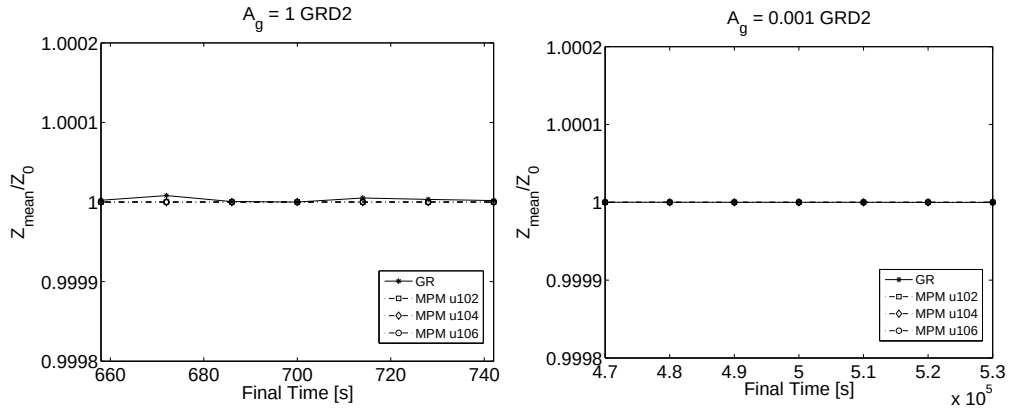

Figure 4.28: *Threshold influence on mean height of the bottom slope, for weak and strong interaction, GR2. Explicit second order scheme with CFL*= 0.8.

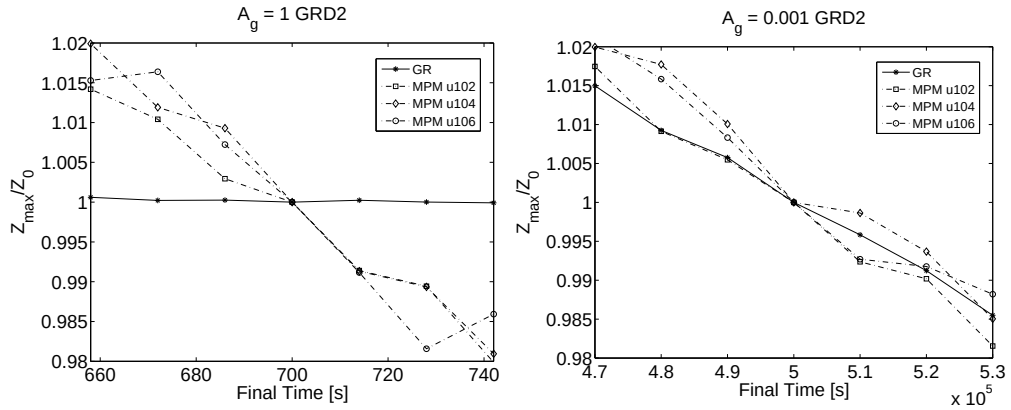

Figure 4.29: *Threshold influence on the maximum height of the bottom slope, for weak and strong interaction, GR2. Explicit second order scheme with CFL*= 0.8.

that should be immediately observed is that the average displacement Z_{mean} remains almost constant for both models, with minor fluctuations for the model of Grass, for strong interactions. The maximum displacement, however, tends to decrease with a non-regular pattern, if not for the Grass model for weak interactions. This means that for strong interactions, the model of Grass, the sediment has found an almost stable shape, which tends to move along x. For weak speed interaction, instead of to disperse itself, the sediment becomes more compact. It is important to observe that, for the Grass model, the variation of G_x and G_z are in the order of a thousandth of the initial displacement at T_3. The presence of the threshold reduces to one-tenth the displacement

respect to the Grass model. The variation of the peak instead remains, for both models, in the same order. This means that the threshold has an influence on the displacement along x and y along, while on its peak is reduced. The average displacement remains constant for both models. Therefore, the stability for the MPM model at higher values of CFL with only one iteration DEC can thus be linked to a large reduction of the displacement. The MPM model, consequently, owes its stability to its smoothness of sediment discharge.

4.3.3 Computational costs

No significant differences for MPM model, were found in computational time, changing the threshold value, as Fig. (4.30) shows. CPU time is similar for each case, and the time gain observed for $\tilde{u} = 1.04$ m/s is the same for all threshold values. The different discharge caused by different thresholds do not influence computational costs.

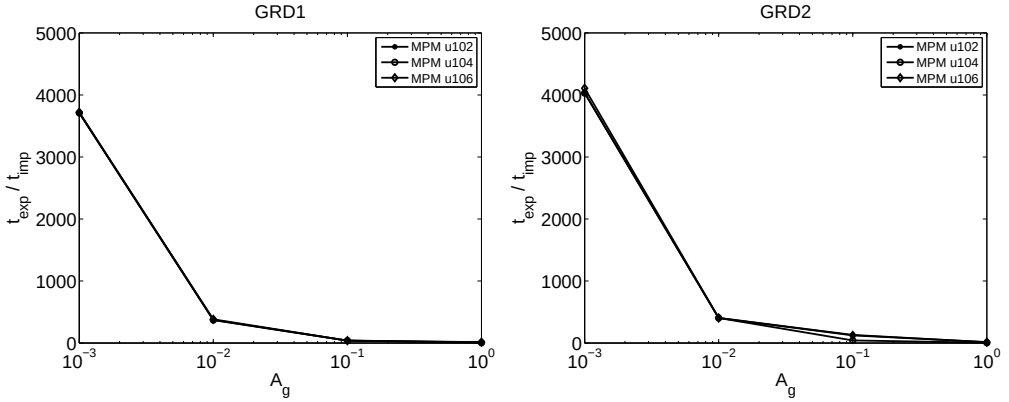

Figure 4.30: *Ratio between implicit and explicit time, second order scheme, for MPM model. Comparison between different threshold values for all the interaction analyzed.*

4.4 Modified MPM model simulations with $\tilde{u} = 1.04$

Finally, the MPM model is corrected as Grass model. In this case, the constant which is correct is $\tilde{A}$, eq. (2.47), which has the same meaning of the sediment constant A_g. Test are conducted setting $\tilde{A}$ as shows Tab. (4.10): with this values, the higher value of the sediment constant is near the interaction required. As done for MPM model, it is important to well define the various parameter which define $\tilde{A}$, expressed by eq. (2.44) Table (4.9) resumes the constant value imposed in input to reach all fluid interaction. As for MPM model, the threshold condition is imposed at $\tilde{u} = 1.04$ m/s.

Interaction	$G = \frac{\rho_s}{\rho}$	C	$\tilde{u}$ $[m/s]$	d_{50} $[m]$
$\tilde{A}_d = 0.1$	9.1549	1	1.04	0.2876
$\tilde{A}_d = 0.01$	82.5494	1	1.04	0.0288
$\tilde{A}_d = 0.001$	1.8155	0.01	1.04	0.0288
$\tilde{A}_d = 0.0001$	9.1549	0.01	1.04	0.0029

Table 4.9: *Values imposed as input constant to obtain each fluid interaction.*

$\tilde{A}$	1	0.1	0.01	0.001
$\tilde{A}_d$	0.1	0.01	0.001	0.0001

Table 4.10: *Values imposed in input constant to obtain each fluid interaction.*

4.4.1 Weak interaction

Weak interaction are obtained setting $\tilde{A}_d = 0.0001$. The maximum value of the sediment constant is at the bottom, and it coincides with the value imposed for Grass model. First of all, explicit solution for MPM and MPMH are compared in Fig. 5.1. As it found for GRH and GR models, a reduction int discharge is found for the modified model. The solution introducing the threshold is similar at MPM model, with a clear hump near the threshold condition. First order implicit scheme is presented Fig. 4.32. This solution is stable until CFL= 10^4, and presents a similar instability trend of MPM model. For the second order implicit scheme, instabilities were found for CFL= 10^5, as shows Fig. 4.33, and DEC iteration for this value are presented in Fig. 4.34. The solution doesn't present a stability also increasing the DEC iterations. The instability mode is also different from MPM solution. However, the same increase trend in CFL condition found for the MPM model of CFL has been found. Finally, computational time required are presented in Tab. (4.11). For weak interaction, solution is considered valid for CFL=10^4 with DEC= 1. A little increasing in computational time it is observed in the solution without threshold, maybe caused by the increasing of the discharge.

Method	$\theta_{cr} = 0.047$		$\theta_{cr} = 0$	
	100 el.	250 el.	100 el.	250 el.
Explicit 1^{st} CFL= 0.8	33.54 s	205.945 s	34.79 s	214.24 s
Explicit 2^{nd} CFL= 0.8	76.60 s	470.43 s	80.30 s	498.20 s
Implicit 1^{st} CFL= 10^4	0.002 s	0.116 s	0.02 s	0.12 s
Implicit 2^{nd} CFL= 10^4 DEC 1	0.002 s	0.12 s	0.02 s	0.12 s

Table 4.11: *Simulation time for modified MPM model, $\tilde{A} = 0.0001$, $\tilde{u} = 1.04$ m/s.*

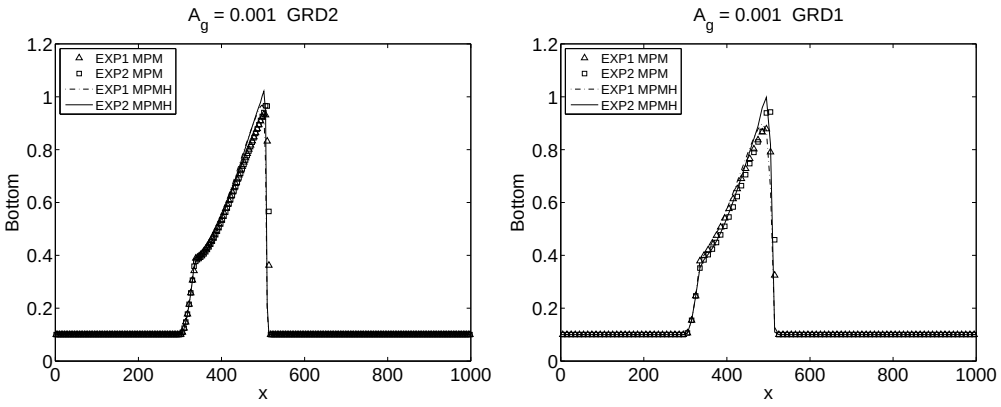

Figure 4.31: *Differences between initial condition, MPM model and modified MPM model for strong interaction, GR1 and GR2. First and second order explicit scheme.*

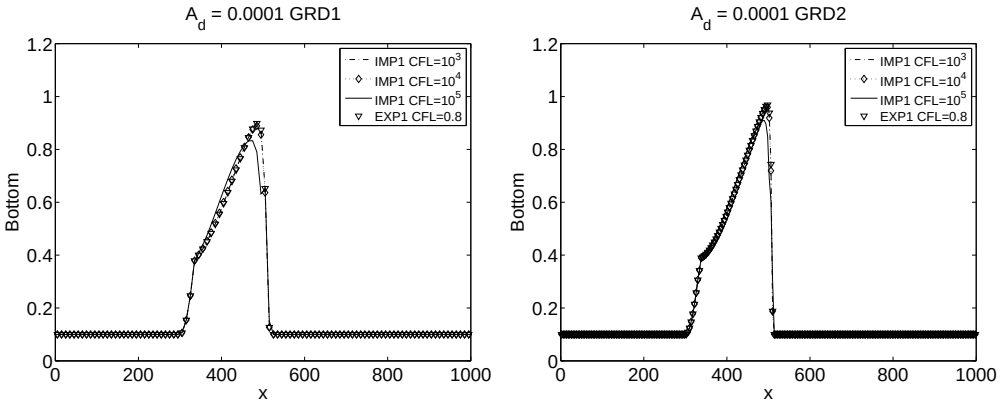

Figure 4.32: *Implicit case for modified MPM model for* $A_d = 0.0001$ *compared to explicit solution, CFL*$= 0.8$*. First order solution, CFL varies from* 10^3 *to* 10^5*.*

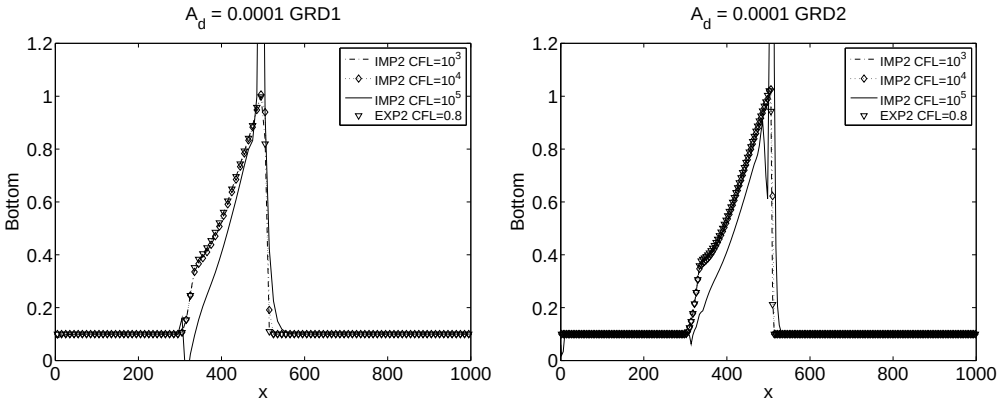

Figure 4.33: *Implicit case for modified MPM model for* $A_d = 0.0001$ *compared to explicit solution, CFL*$= 0.8$*. Second order solution, CFL varies from* 10^3 *to* 10^5*.*

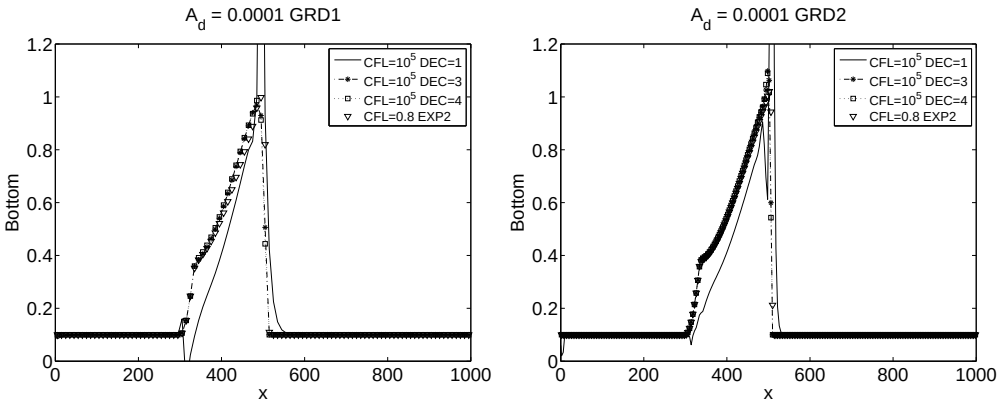

Figure 4.34: *Second order implicit case for modified MPM model for* $A_d = 0.0001$*, effects of the number of DEC iterations for CFL*$=10^5$*.*

4.4.2 Weak/intermediate interaction

Weak/interaction are obtained setting $\tilde{A}_d = 0.001$. The comparison between explicit solution for modified MPM and MPM model are presented in Fig. 4.35. A global reduction of the sediment discharge is found. Moreover, to investigate the effect in the implicit scheme of the correction implemented, the solutio for first order implicit scheme is presented Fig. 4.36 shows. In this case, the implicit scheme is stable until CFL= 10^3. The instability mode is similar to the one found for MPM model. Moreover, for second order implicit scheme, instabilities appears for CFL= 10^4, as it possible to see in Fig. 4.37. Increasing the value of DEC iteration does not assure a larger value of CFL, as Fig. 4.38 shows. Also with DEC= 3 the solution present an high peak and some unphysical oscillation in the first part of the field. Finally, computational time required are presented in Tab. (4.12). For second order implicit scheme, solution is considered valid for CFL=10^1, with DEC= 1, which represent the best ratio between accuracy and computational cost.

Method	$\theta_{cr} = 0.047$		$\theta_{cr} = 0$	
	100 el.	250 el.	100 el.	250 el.
Explicit 1^{st} CFL= 0.8	3.352 s	20.62 s	3.484 s	21.45 s
Explicit 2^{nd} CFL= 0.8	7.676 s	47.127 s	8.056 s	49.847 s
Implicit 1^{st} CFL= 10^3	0.016 s	0.116 s	0.02 s	0.12 s
Implicit 2^{nd} CFL= 10^3 DEC 1	0.02 s	0.116 s	0.016 s	0.124 s

Table 4.12: *Simulation time for modified MPM model,* $\tilde{A}_d = 0.001$*,* $\tilde{u} = 1.04$ *m/s.*

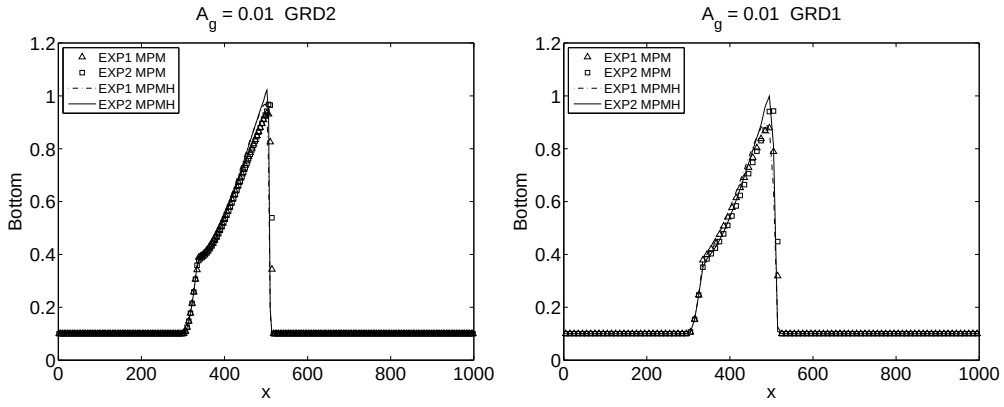

Figure 4.35: *Differences between initial condition, MPM model and modified MPM model for strong/intermediate interaction, GR1 and GR2. First and second order explicit scheme.*

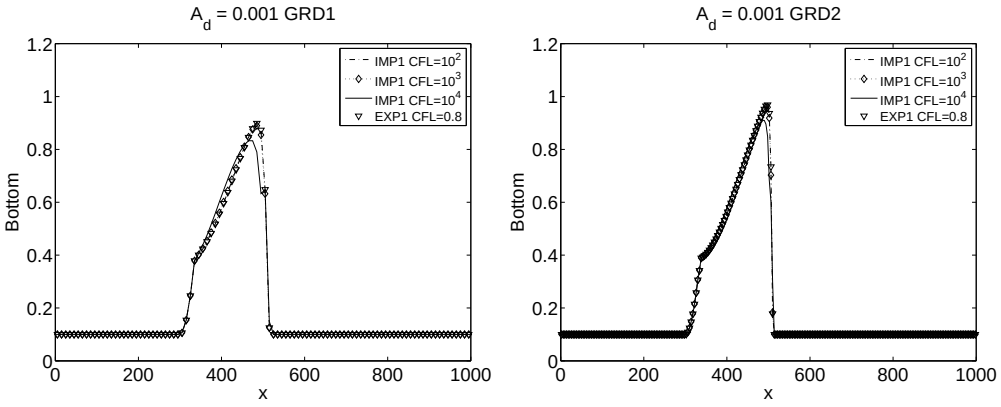

Figure 4.36: *Implicit case for modified MPM model for* $A_d = 0.001$ *compared to explicit solution, CFL*$= 0.8$*. First order solution, CFL varies from* 10^2 *to* 10^4*.*

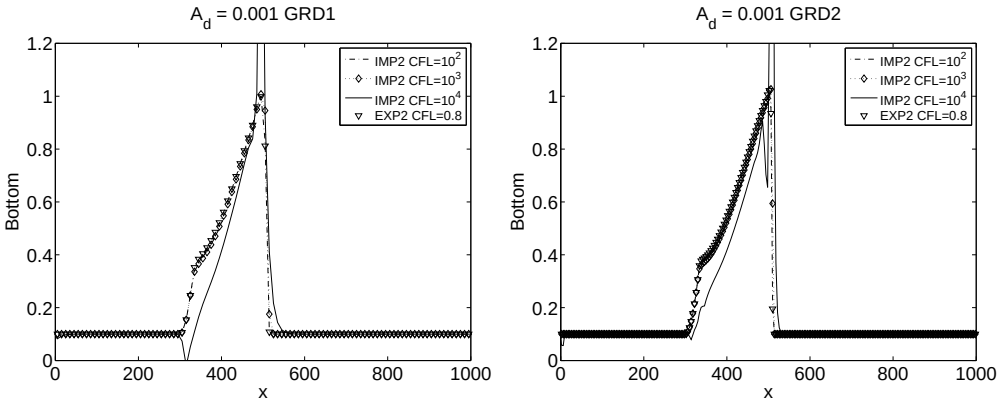

Figure 4.37: *Implicit case for modified MPM model for* $A_d = 0.001$ *compared to explicit solution, CFL*$= 0.8$*. Second order solution, CFL varies from* 10^2 *to* 10^4*.*

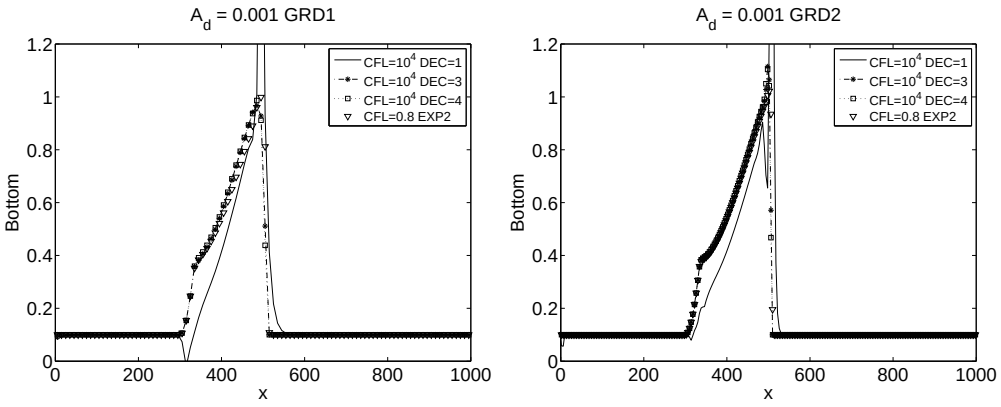

Figure 4.38: *Second order implicit case for modified MPM model for* $A_d = 0.001$*, effects of the number of DEC iterations for CFL*$= 10^4$*.*

4.4.3 Strong/intermediate interaction

Also for $\tilde{A}_d = 0.01$ a similar shape were found to MPM model, as Fig. 4.39 shows. A global reduction of the sediment discharge is found, obviously, with similarities on the displacement on what happened for weak and weak/intermediate interaction. Solution without threshold seems to be more stable than Grass and modified Grass models. For first order implicit scheme, Fig. 4.40, the solution is stable until CFL=10^3. An instability mode similar to MPM model is found, with a different lower peak. Instead of, for MPM model second order implicit scheme, unphysical oscillation are higher for strong/intermediate interaction. In this case, as Fig. 4.41 and Fig. 4.42 shows, oscillation were reduced but are still presents. DEC iteration for second order implicit scheme are increased for CFL=10^3. A large number of DEC correction does not provide a good approximation of the results. For DEC= 4, solution present a higher peak than explicit solution. For GR2, unphysical oscillation were found near the threshold condition, as found for MPM model. Computational time required are presented in Tab. (4.12). For second order implicit scheme, solution is considered valid for CFL=10^2, with DEC= 1, which represent the best ratio accuracy and computational cost.

Method	$\theta_{cr} = 0.047$		$\theta_{cr} = 0$	
	100 el.	250 el.	100 el.	250 el.
Explicit 1^{st} CFL= 0.8	0.468 s	2.884 s	0.5 s	3.084 s
Explicit 2^{nd} CFL= 0.8	1.076 s	6.688 s	1.148 s	7.216 s
Implicit 1^{st} CFL= 10^2	0.028 s	0.168 s	0.024 s	0.172 s
Implicit 2^{nd} CFL= 10^2 DEC 1	0.032 s	0.164 s	0.028 s	0.172 s

Table 4.13: *Simulation time for modified MPM model,* $\tilde{A}_d = 0.01$*,* $\tilde{u} = 1.04$ *m/s.*

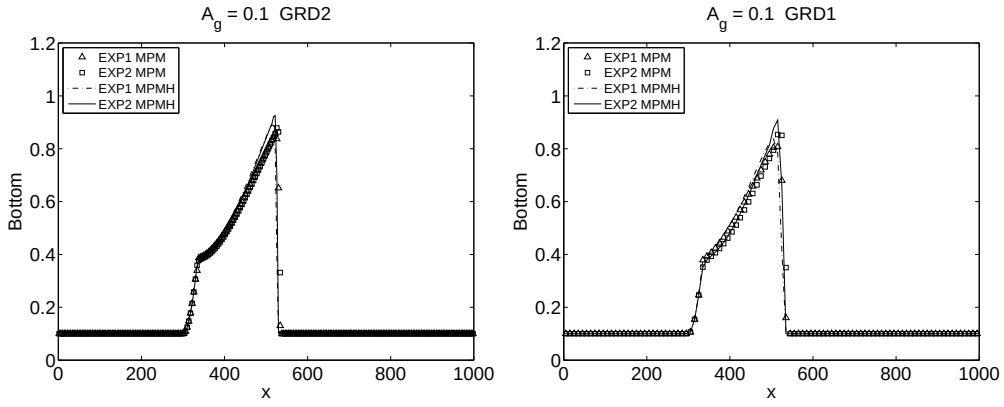

Figure 4.39: *Differences between initial condition, MPM model and modified MPM model for strong/intermediate interaction, GR1 and GR2. First and second order explicit scheme.*

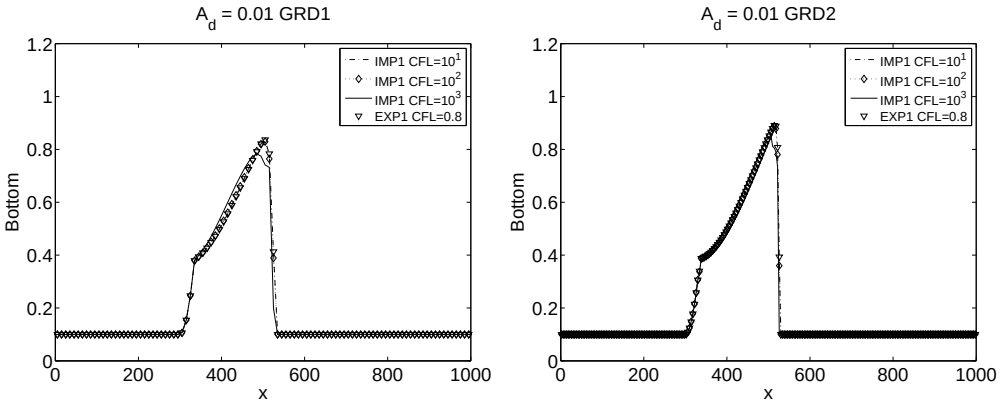

Figure 4.40: *Implicit case for modified MPM model for* $A_d = 0.01$ *compared to explicit solution, CFL*$= 0.8$*. First order solution, CFL varies from* 10^1 *to* 10^3*.*

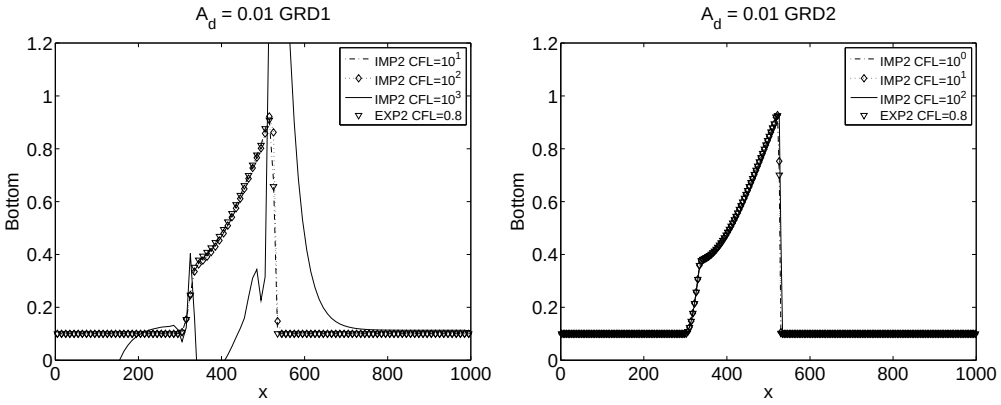

Figure 4.41: *Implicit case for modified MPM model for* $A_d = 0.01$ *compared to explicit solution, CFL*$= 0.8$*. Second order solution, CFL varies from* 10^1 *to* 10^3 *for GR1 and from* 10^1 *to* 10^4 *for GR2. For GR2, the code isn't able to write the solution for CFL*$=10^3$*.*

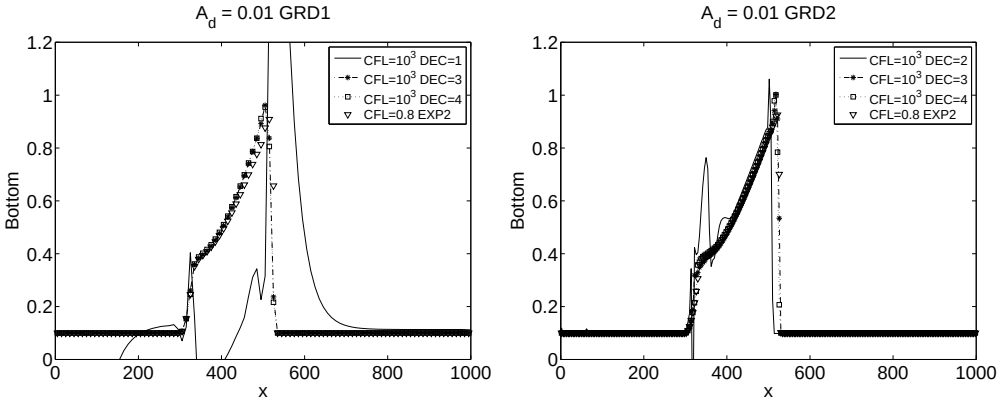

Figure 4.42: *Second order implicit case for modified MPM model for* $A_d = 0.01$*, effects of the number of DEC iterations for CFL*$=10^3$*.*

4.4.4 Strong interaction

Strong interaction, for which $\tilde{A}_d = 0.1$, presents the same trend for explicit solution found for other interaction, but with a lower total time. This trend is observable in Fig. (5.2), in which modified MPM model and MPM model are compared. The solution is similar, only a little reduction of the discharge were found. Also in this case, the steady state for explicit solution without threshold is similar to modified Grass model. First order implicit scheme, which is shown in Fig. (4.44), presents an unphysical oscillation at the peak for CFL= 10^2, using GR1. Instead of, for GR2, the code isn't able to write the solution. For the same value of CFL, unphysical oscillation were found for second order implicit scheme, as Fig. (4.45) shows. Also with DEC iteration, Fig. (4.46), solution for GR2 don't match explicit scheme, losing solution accuracy. Computational time required for strong interaction are presented in Tab. 4.12. For second order implicit scheme, solution is considered valid for CFL=10^1, with DEC= 1, which represent the best ratio accuracy and computational cost.

Method	$\theta_{cr} = 0.047$		$\theta_{cr} = 0$	
	100 el.	250 el.	100 el.	250 el.
Explicit 1^{st} CFL= 0.8	0.056 s	0.308 s	0.06 s	0.36 s
Explicit 2^{nd} CFL= 0.8	0.108 s	0.696 s	0.132 s	0.828 s
Implicit 1^{st} CFL= 10^1	0.024 s	0.164 s	0.028 s	0.2 s
Implicit 2^{nd} CFL= 10^1 DEC 1	0.028 s	0.176 s	0.036 s	0.2 s

Table 4.14: *Simulation time for modified MPM model,* $\tilde{A}_d = 0.1$*,* $\tilde{u} = 1.04$ *m/s.*

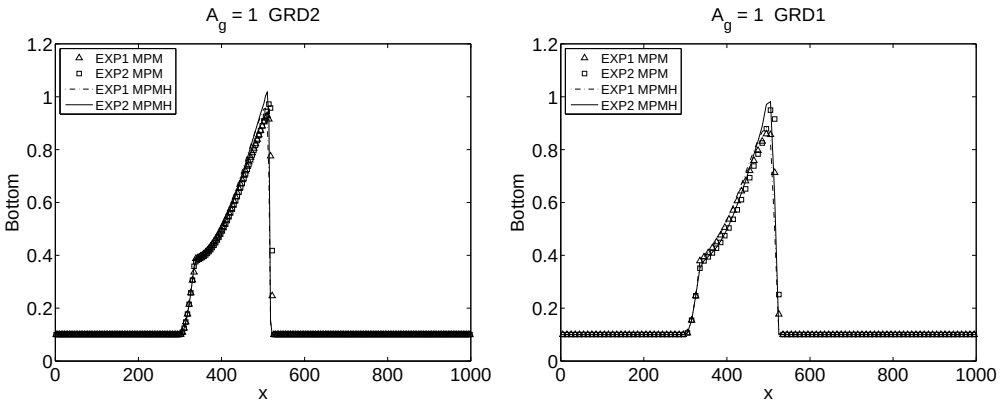

Figure 4.43: *Differences between initial condition, MPM model and modified MPM model for weak interaction, GR1 and GR2. First and second order explicit scheme.*

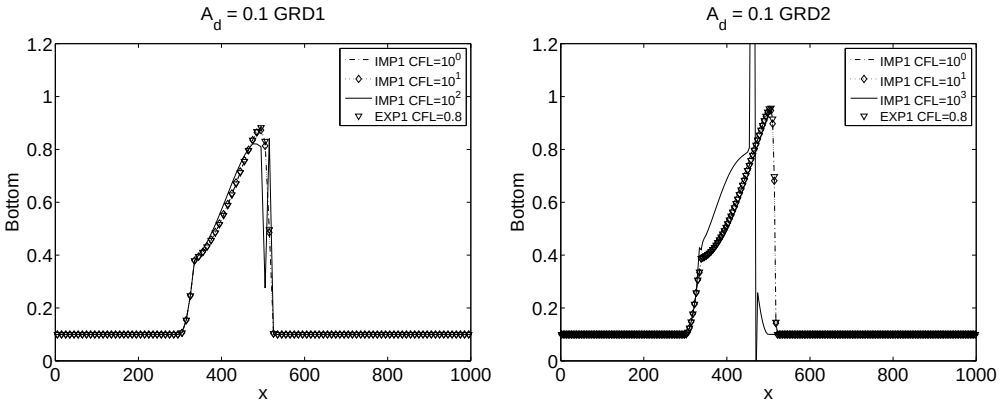

Figure 4.44: *Implicit case for modified MPM model for* $A_d = 0.1$ *compared to explicit solution, CFL*$= 0.8$*. First order solution,CFL varies from* 10^0 *to* 10^2*. For GR1, the code does not provide a solution.*

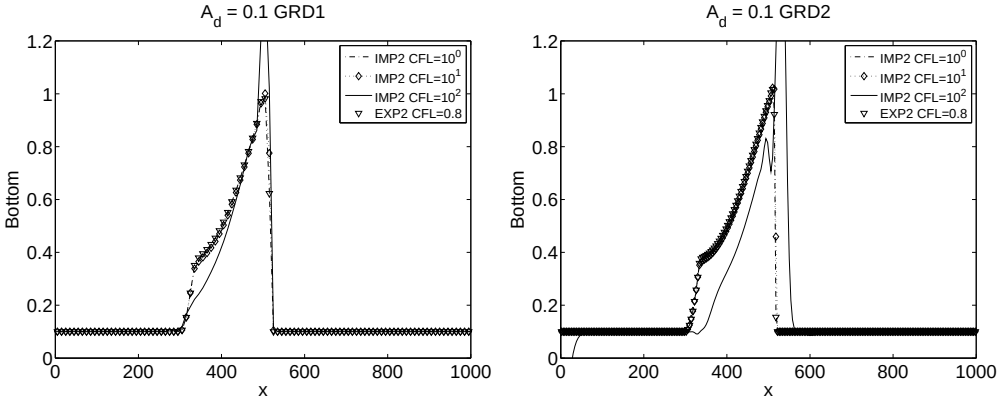

Figure 4.45: *Implicit case for modified MPM model for* $A_d = 0.1$ *compared to explicit solution, CFL*$= 0.8$*. Second order solution,CFL varies from* 10^0 *to* 10^2*.*

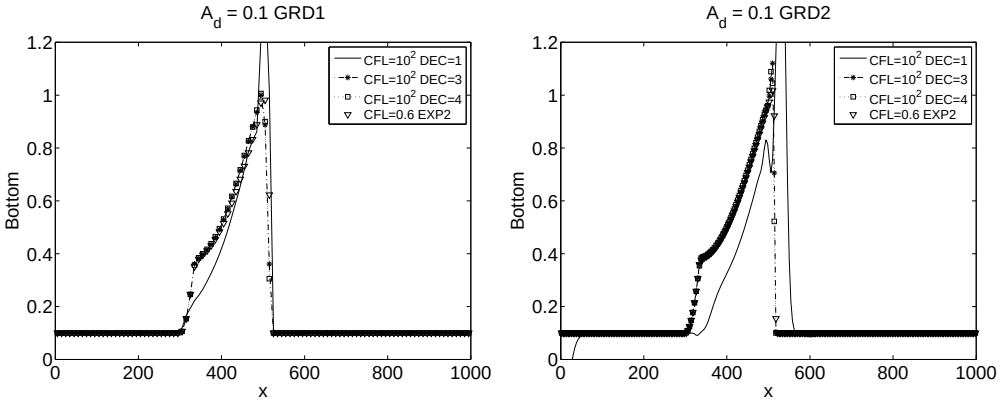

Figure 4.46: *Second order implicit case for modified MPM model for* $A_d = 0.1$*, effects of the number of DEC iterations for CFL*$=10^2$*.*

4.4.5 Concluding remarks for modified MPM model

As found for MPM model, increasing DEC iteration for second order scheme does not assure a better accuracy of the solution, considering all speed interactions. So, for modified MPM model the time scale is connected to the interaction as:

$$CFL \backsimeq \frac{10}{A_g} \tag{4.4}$$

for second order implicit scheme, only with a DEC iteration. A larger value of DEC iteration does not give a valid approximation of the solution. In conclusion, observing Fig. 4.47, it is important to note how MPMH guarantee the same computational efficiency with respect to Grass model, but with only one DEC iteration. A larger computational gain is found for weak/weak intermediate solution.

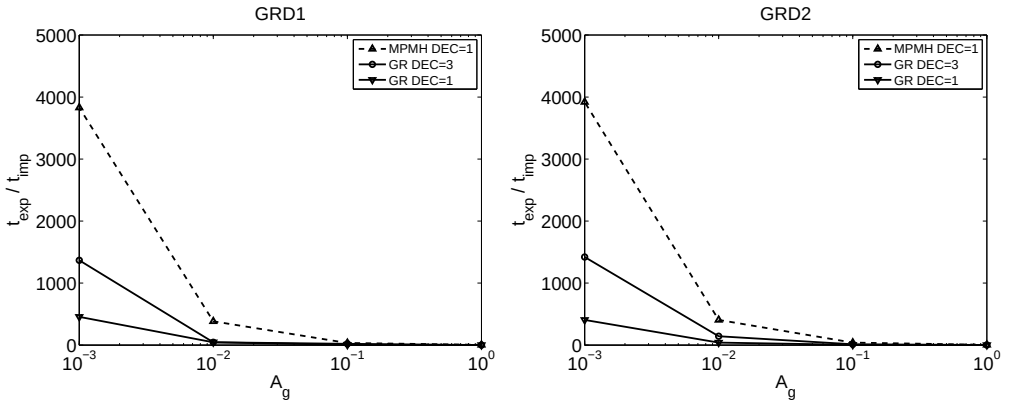

Figure 4.47: *Ratio between implicit with DEC= 1 and explicit time, second order scheme, for modified MPM and Grass model for all the interaction analyzed.*

4.5 Threshold influence on MPMH model

Even for the model of MPM is performed an analysis to the variation of the module of the threshold. This will help you understand the effect of the threshold in motion and as a further reduction of the motion changes the results and the computational time required.

4.5.1 CFL influence

The analysis at threshold for the modified MPM model produces results similar to those obtained for MPM. The value imposed for all constant were presented in Tab. (4.15). First, an overall reduction of the transport is obtained, presented in Fig. 4.48 were compared. In that figure, all the models with two different values of threshold for MPM and modified MPM. The difference in threshold magnitude is observable with a different position of the classical hump found also for MPM model. For first order scheme, solution found its instability as MPM model. As presented in Fig. 4.49, the influence on the bottom peak is more evident for first order scheme. Relevant unphysical oscillation were also found for second order scheme, for all value of interaction with $\tilde{u} = 1.06$ m/s. Therefore, for strong interaction Therefore, for strong interaction oscillation were found near the peak for CFL=10^2. Results for varying CFL and DEC iteration for

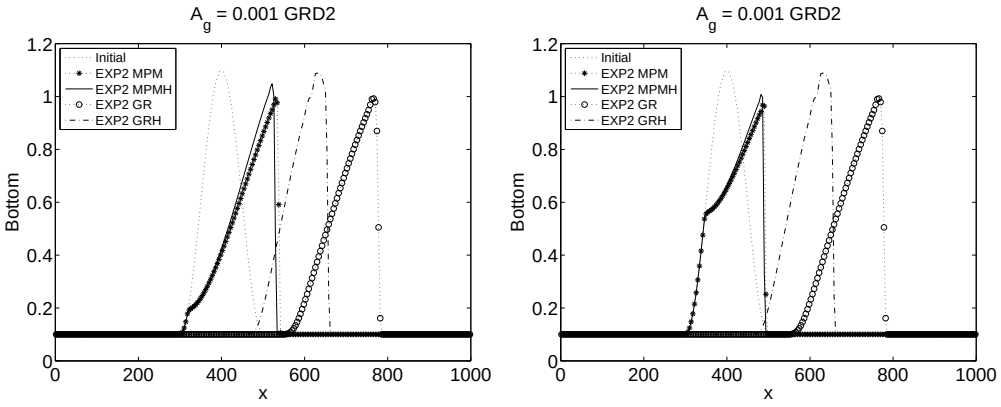

Figure 4.48: *Model comparison for two different threshold condition, weak interaction, GR2. Explicit solution scheme.*

strong interaction are presented in Fig. 4.50, with $\tilde{u} = 1.06$ m/s. Solution isn't stable also increasing DEC iteration. The same instability is found for $\tilde{u} = 1.02$ m/s, but oscillation are reduced as it possible to see in Fig. 4.50. Moreover, other oscillation were found in the first part of the field, also found for weak interaction. For $\tilde{u} = 1.06$ m/s, a first instability appears in the first part of the field, as Fig. 4.53 shows. Instead of, for $\tilde{u} = 1.02$ m/s, a reduction of unphysical oscillation is found. Also near the peak oscillation were reduced. The presence of a threshold seems to not give different result in computational time and instability. Maybe oscillation were reduced but the value of CFL for which they appears remains the same than MPM. A larger CFL value it is obtained with only one DEC iteration with respect to the Grass model.

4.5.2 Final time: influence on the steady state.

Also for modified MPM model, a similar trend is found in threshold analysis, The global discharge is reduced increasing the threshold magnitude, as it possible to see in

Interaction	$G = \frac{\rho_s}{\rho}$	C	$\tilde{u}$ $[m/s]$	d_{50} $[m]$
$A_g = 1$	1.8155	1	1.02	0.2767
			1.04	0.2877
			1.06	0.2988
$A_g = 0.1$	9.1549	1	1.02	0.0277
			1.04	0.0288
			1.06	0.0299
$A_g = 0.01$	1.08155	0.01	1.02	0.0277
			1.04	0.0288
			1.06	0.0299
$A_g = 0.001$	1.8155	0.01	1.02	0.0028
			1.04	0.0029
			1.06	0.03

Table 4.15: *Values imposed in eq. (2.44) and (2.45) to obtain weak interaction for modified MPM model.*

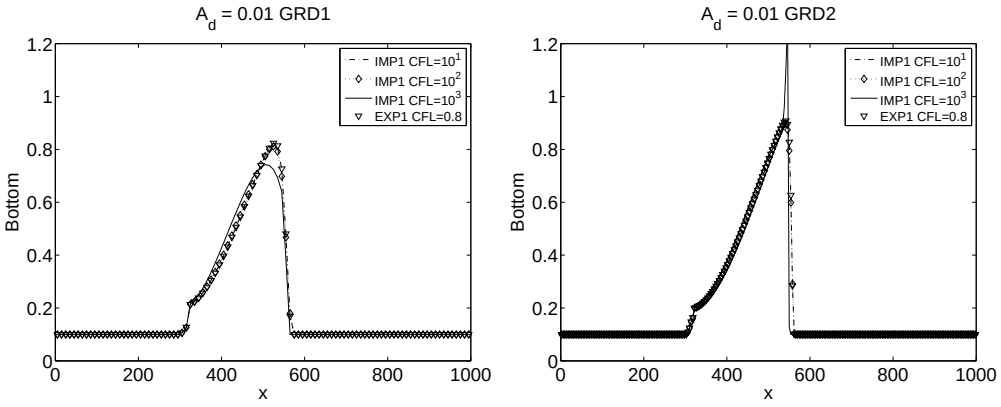

Figure 4.49: *Model comparison for two different threshold condition, weak interaction, GR2. Explicit solution scheme.*

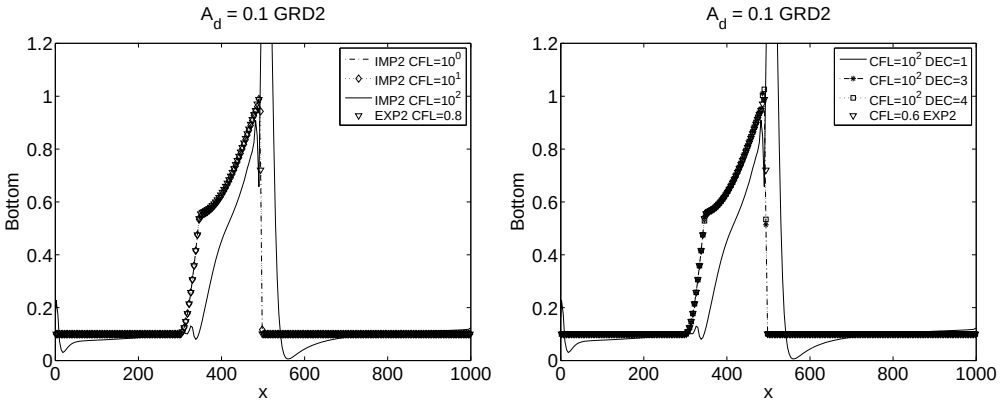

Figure 4.50: *Second order implicit case for modified MPM model for $A_d = 0.1$, GR2, second order scheme for $\tilde{u} = 1.06$ m/s. effects of the number of DEC iterations is executed for CFL= 10^2, without relevant results.*

Fig. (4.54) and Fig. (4.55). The displacement on x direction is reduced increasing the threshold and little variation on z variation were found. Also in the variation of the peak and average height, the variations are small and subject to the same speeches made for MPM model. Only the variation of the peak, in Fig. (4.56), appears slightly reduced compared to the case of MPM: this is an effect of the reduction of transport along the z axis in modified MPM model. However, also the average displacement, presented in Fig. (4.57), does not undergo large variations. *Zmean* is strictly constant, and the solution could be considered in a steady state.

4.5.3 Computational cost

No significant difference in computational efficiency were found changing the threshold for MPMH. The time ratio remains almost the same, as it is possible to see in Fig. 4.58.

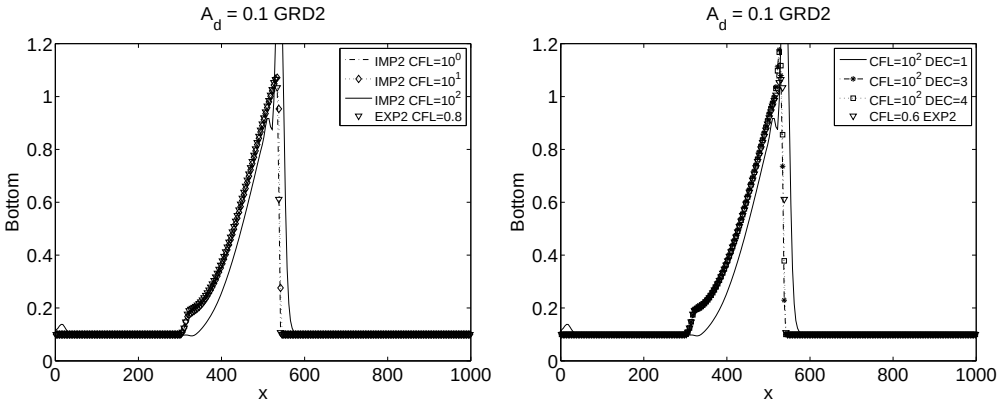

Figure 4.51: *Second order implicit case for modified MPM model for* $A_d = 0.1$*, GR2, second order scheme for* $\tilde{u} = 1.02$ *m/s. effects of the number of DEC iterations is executed for CFL*$= 10^2$*, without relevant results.*

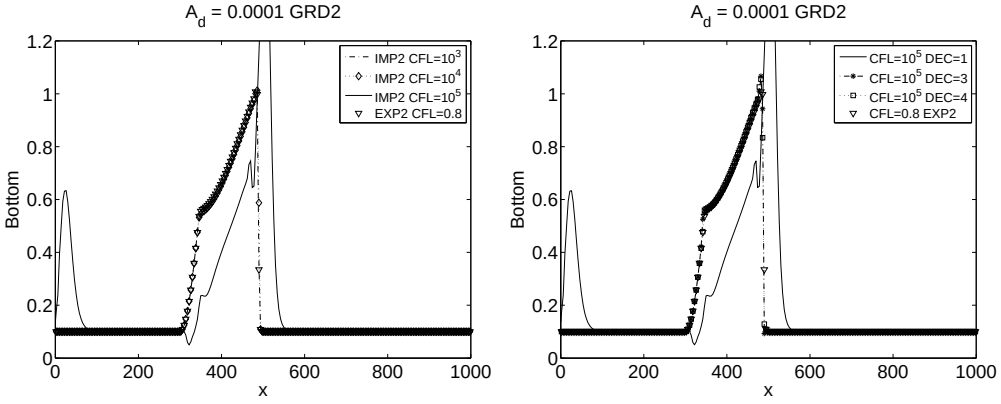

Figure 4.52: *Second order implicit case for modified MPM model for* $A_d = 0.0001$*, effects of the number of DEC iterations for CFL*$= 10^5$*.*

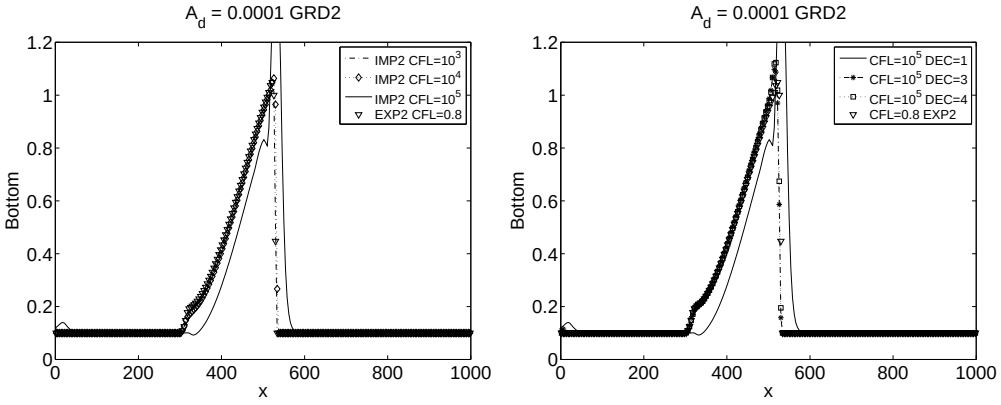

Figure 4.53: *Second order implicit case for modified MPM model for* $A_d = 0.0001$*, effects of the number of DEC iterations for CFL*$= 10^5$*.*

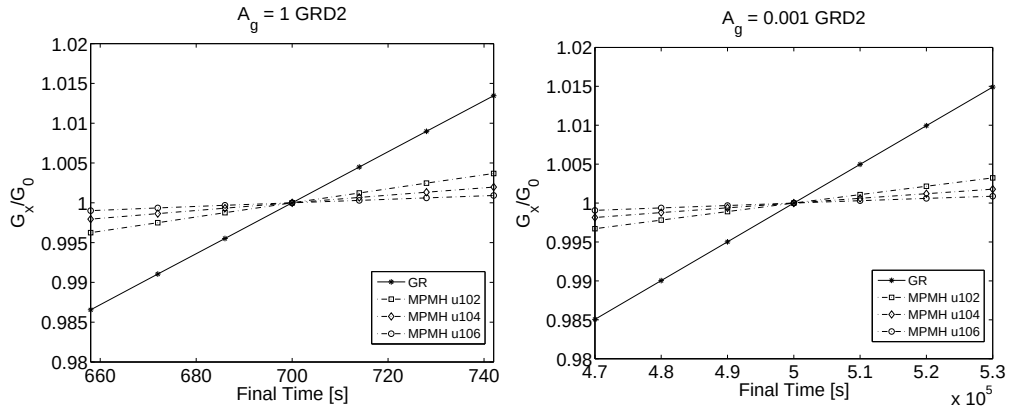

Figure 4.54: *Geometrical center G_x variation for modified MPM model for strong (right) and weak (left) interaction.*

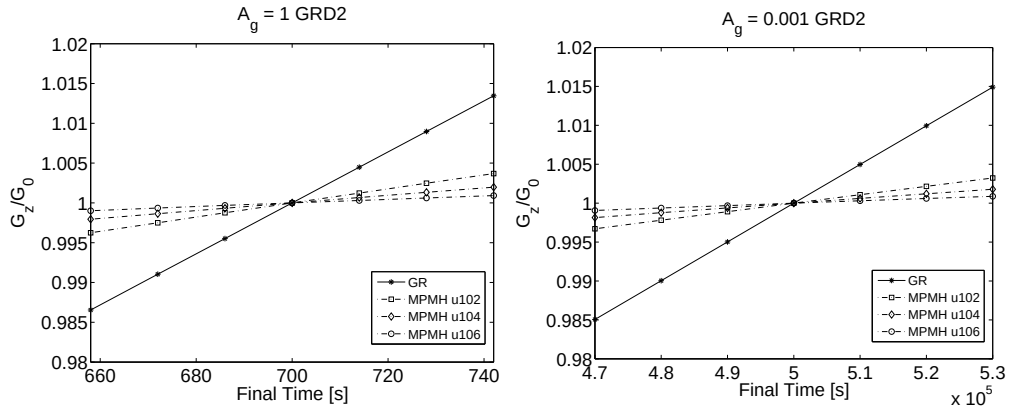

Figure 4.55: *Geometrical center G_z variation for modified MPM model for strong (right) and weak (left) interaction.*

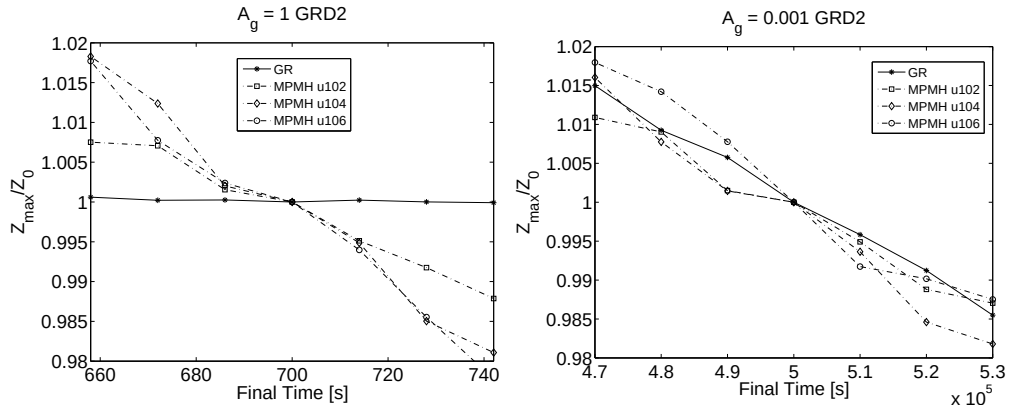

Figure 4.56: *Maximum height Z_x variation for modified MPM model for strong (right) and weak (left) interaction.*

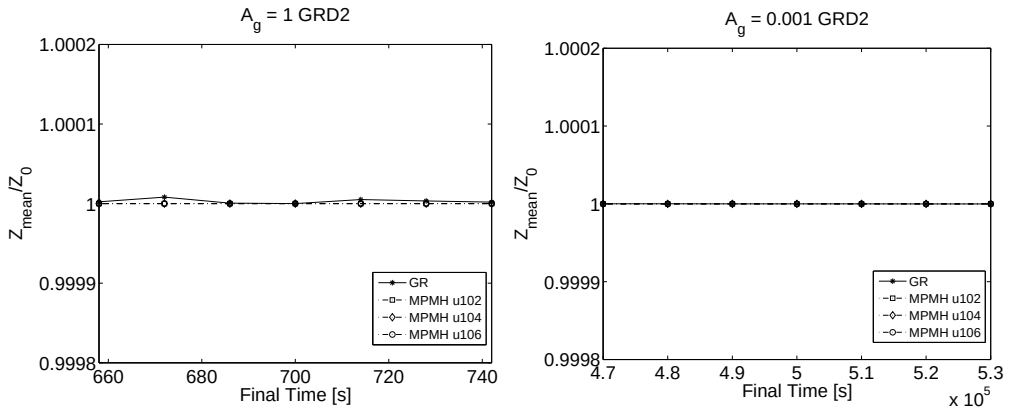

Figure 4.57: *Mean height Z_{mean} variation for modified MPM model for strong (right) and weak (left) interaction.*

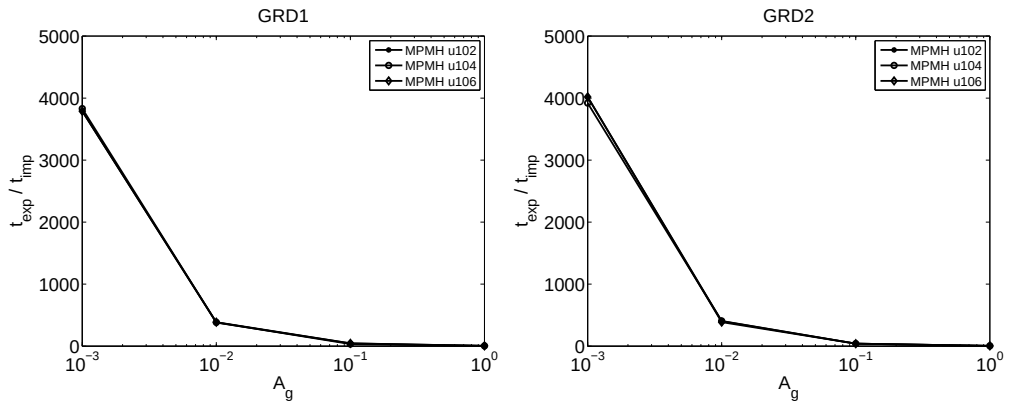

Figure 4.58: *Ratio between implicit and explicit time, second order scheme, for modified MPM model at different threshold condition, all the interaction analyzed.*

Chapter 5

Comparison and concluding remarks

Four different models for sediment transport are analyzed to understand the influence in shallow water problems. The analysis was carried out for different types of interaction speed. For weak interactions, the four models are presented in Fig. 5.1 second-order explicit scheme. Obviously, it is possible to observe that there is a discrepancy between the transport models with threshold (MPM and MPMH) and those without a threshold. The presence of the threshold reduces the global discharge, so MPM model presents a reduction on x displacement of the bottom slope. In addition, the effect of the correction with the introduction of the state h is more pronounced in the case of Grass, where there is a reduction of the global discharge. Since the MPM model has a clearly smaller displacement, the effect of the correction is reduced. For weak/intermediate interaction, the comparison is not presented for the sake of brevity. Also in this case, the same remarks as for weak interaction can be made. For strong/intermediate and strong interactions the effect of transports reduction is more pronounced, due to an increase of interaction strength. For strong interactions, presented in Fig. 4.35, it is possible to observe as modified Grass model seems to reduce the movement of the sediment slope, keeping the shape unchanged. This is not observable for others interactions, with a higher peak. From the computational point of view, the CFL values that represents

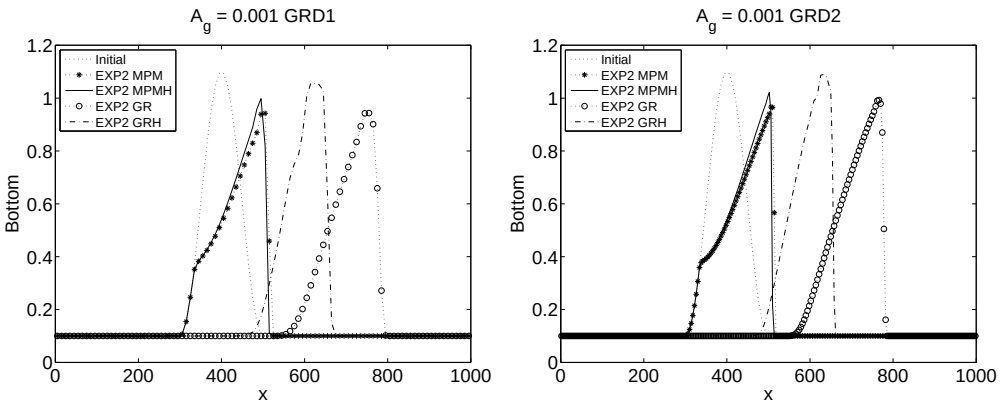

Figure 5.1: *Differences between initial condition and all model analyzed for for strong interaction, GR1 and GR2. Second order explicit scheme.*

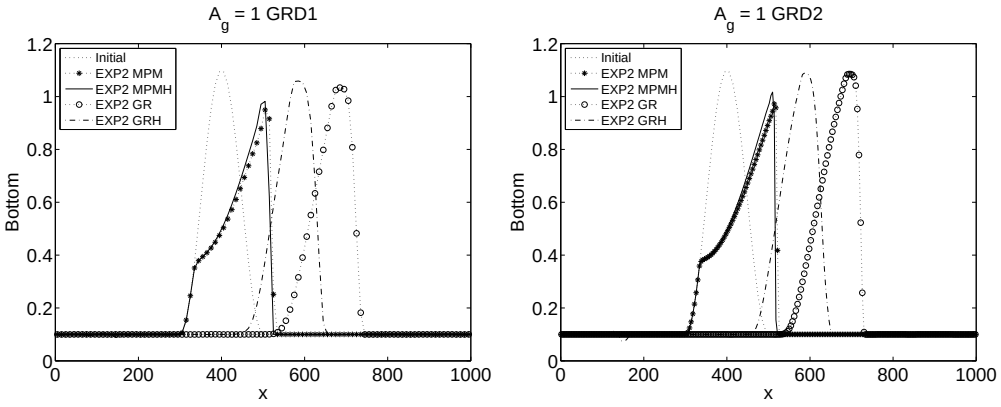

Figure 5.2: *Differences between initial condition and all model analyzed for for weak interaction, GR1 and GR2. Second order explicit scheme.*

the best value for accuracy/costs are presented in Tab. (5.1) for modified Grass model, in Tab. (5.2) for MPM model, in Tab. (5.3) for modified MPM model. It is possible to observe that, for implicit scheme, an order degree of magnitude of CFL is gained. However, introducing a large number of DEC correction, helps to improve the solution accuracy only for Grass and modified Grass models. Therefore, for MPM and MPMH, the time scale is defined with:

$$CFL \backsimeq \frac{10}{A_g} \tag{5.1}$$

for only 1 DEC iteration. This is the same ratio found for Grass and modified Grass, but with 3 DEC iterations. At this manner, the best computational efficiency is presented in Fig. 5.3 for all the model investigated. The same computational efficiency is found for Grass, MPM and modified MPM, considering the DEC condition which allows the larger CFL value. Only modified Grass model seems to have a bad explicit/implicit time ratio. For all model, it is possible to observe that the implicit scheme has a better efficiency for weak and weak/intermediate interaction speed.

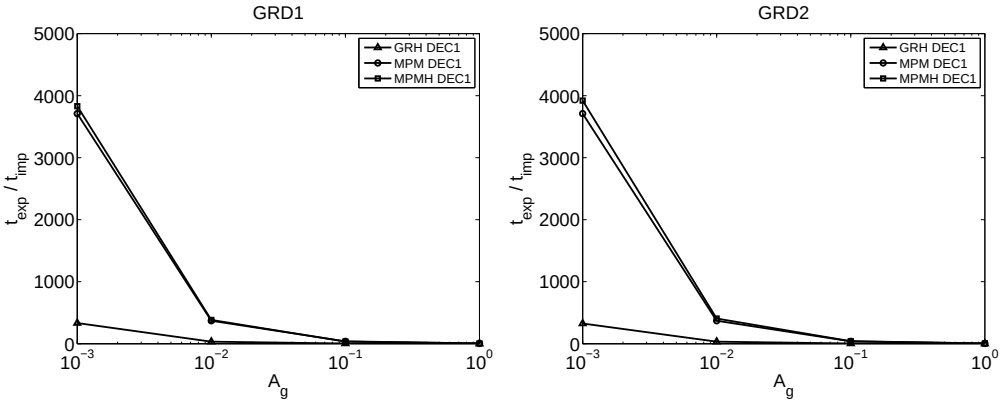

Figure 5.3: *Ratio between implicit and explicit time, second order scheme, for GRH and MPM model for all the interaction analyzed.*

Modified Grass				
Method	A_g			
	1	0.1	0.01	0.001
Explicit 1^{st}	0.6	0.8	0.8	0.8
Explicit 2^{nd}	0.6	0.8	0.8	0.8
Implicit 1^{st}	10^0	10^1	10^2	10^3
Implicit 2^{nd} DEC 1	10^0	10^1	10^2	10^3
Implicit 2^{nd} DEC 3	10^1	10^2	10^3	10^4

Table 5.1: *Best values of CFL for modified Grass model.*

Meyer – Peter Muller				
Method	A_g			
	1	0.1	0.01	0.001
Explicit 1^{st}	0.8	0.8	0.8	0.8
Explicit 2^{nd}	0.8	0.8	0.8	0.8
Implicit 1^{st}	10^1	10^2	10^3	10^4
Implicit 2^{nd} DEC 1	10^1	10^2	10^3	10^4
Implicit 2^{nd} DEC 3	n.v.	n.v.	n.v.	n.v.

Table 5.2: *Best values of CFL for modified MPM model.*

Modified Meyer – Peter Muller				
Method	A_g			
	1	0.1	0.01	0.001
Explicit 1^{st}	0.8	0.8	0.8	0.8
Explicit 2^{nd}	0.8	0.8	0.8	0.8
Implicit 1^{st}	10^1	10^2	10^3	10^4
Implicit 2^{nd} DEC 1	10^1	10^2	10^3	10^4
Implicit 2^{nd} DEC 3	n.v.	n.v.	n.v.	n.v.

Table 5.3: *Best values of CFL for modified MPM model.*

Part III

2D Simulations

Chapter 6

Simulation for Tunis Lake

This investigation is part of the Medlagoon project,and it is partly carried out during a stage at LIM, Ecole Polytechnique de Tunisie (18/03/2012-04/04/2012). The objective is to study the Tunis lake, which is very shallow and suitable to the application of the previously developed numerical methods and models.

6.1 Tunis Lake

Tunis is the capital of both the Tunisian Republic and the Tunis Governorate. Behind the Lake of Tunis and the port of La Goulette (Halq al Wadi), the city extends along the coastal plain and the hills that surround it. At the centre of more modern development (from the colonial era and later) lies the old medina. Beyond this district lie the suburbs of Carthage, La Marsa, and Sidi Bou Said. The Lake of Tunis is a natural lagoon located between the Tunisian capital city of Tunis and the Gulf of Tunis (Mediterranean Sea). The lake covers a total of $37km^2$, in contrast to its size its depth is very shallow (average depth estimated around 0.9 meters). It was once the natural harbor of Tunis. The Lac Nord is 9620 meters long, and 4589 meters large. The Lac Nord is bigger than the Lac Sud, which is 6516 meters long, and 1881 meters large.

6.1.1 Historical notes

Situated on a large Mediterranean Sea gulf (the Gulf of Tunis), Tunis is located in north-eastern Tunisia on the Lake of Tunis, and is connected to the Mediterranean sea by a canal which terminates at the port of La Goulette / Halq al Wadi. The ancient city of Carthage is located just north of Tunis, along the coastal part. The city of Tunis is built on a hill slope down to the lake of Tunis. These hills contain the places, Notre-Dame de Tunis, Ras Tabia, La Rabta, La Kasbah, Montfleury and La Manoubia which altitudes beyond just 50 meters. The isthmus between them is what geologists call the "Tunis dome", which includes hills of limestone and sediments. It forms a natural bridge and since ancient times several major roads linking to Egypt and elsewhere in Tunisia have branched out from. The Tunis-Carthage connection was very important to the Romans, as it meant control over the fertile hinterland. The Romans therefore built a dam through the lake. The dam is used today as an expressway for automobiles and railway connecting Tunis to the harbor, La Goulette, and the coastal cities of Carthage, Sidi Bou Said, and La Marsa. The northern lake includes the island

of Chikly, once home to a Spanish stronghold, and now (since 1993) a nature reserve. Due to the lake's continuing aggradation during the 19^{th} century, the French colonial forces traversed the lake with a 10 km long, 450 m wide, and 6 m deep canal. In those days, there was a small port in Tunis, developed between 1778 and 1814. The port was small, the lagoon not too deep sea trade was unaffected. In 1888 a modern port was developed, which required a connection to La Goulette. So, they built the canal that is currently used to reach the Mediterranean sea, seen in Fig (6.2). The channel is 9 km long, 45 m wide and about 8 meters deep. After this work of rebuilding, the division between North and South Lake has been scored. In addition, also changed the perimeter shape of the lagoon, due to the presence of dams erected for the development of this channel. Approximately 120.000 m^2 are changed by this work. In 1893 was inaugurated the new port of Tunis, with the construction of engines for purification, and irrigation in some areas used to grow. In 1980 another important change was made to North Lake, performed by SIDA (Swedish International Development Cooperation Agency). The North lake, after this intervention, suffered only a few adjustments while the southern lake, which has suffered a new and profound intervention between 1993 and 2002. Recently, the Tunisian government and Sama Dubai of the UAE (led by Dubai Governor Mohammed bin Rashid Al Maktoum) have joint-ventured an investment agreement to develop the southern shore of the lake into a new commercial, residential and touristic center in Tunisia and the Mediterranean. Total costs of the investment, considered the biggest in Tunisia's history, will be around 18 billion USD. The project should be ready in the next 10 to 15 years. The intervention is located on the Nord, and is in the zone.

6.1.2 SIDA intervention on Nord Lac

The city of Tunis had long suffered from the bad breath of the polluted lake. Until the 1970s the stench was most repelling close to the population center, and it was there

Figure 6.1: *Satellite view of the Lac Tunis, where it is possible to recognize the Lac Nord, the Lac Sud and the third channel which connect the port to the sea.*

that the Tunisian authorities wanted to create an attractive environment. The planning of the Lake of Tunis restoration project was in 1972 organized and sponsored by the Tunisian Government in cooperation with the Swedish International Development Authority (SIDA) and the Institute of Limnology at Lund. The City of Tunis is surrounded by very shallow, highly saline lakes. As the Lake of Tunis is connected with the Mediterranean, it does not dry up as the other lakes do. The water level, however, is dependent upon that in the sea. Although the self-purification capacity of Lac Nord was very high during most of the year, the ecosystem of the whole lake collapsed periodically (oxygen depletion, fish-kills). Furthermore, during nearly the whole year the odor of sewage and hydrogen sulphide from the permanently highly overloaded western part was a most unpleasant environmental embarrassment in the environs of the City of Tunis. The area bordering the lake was really a no-man's-land impossible to use for human habitation. Instead it was used for the unregulated deposition of rubbish and, generally speaking, was in a deplorable state of degradation. The fish catches from the overloaded, periodically collapsing lagoon ecosystem were successively reduced. This had economic consequences and the smell after severe fish-kills aggravated the odor problems. The bad smell from the lake could even be noticed at the Tunis international airport, Carthage, thus discouraging tourists from visiting the capital area. In the early 1970s the situation was so bad that it was decided to make efforts immediately to alleviate the worst problems consequent on the pollution. The first phase of the restoration had to be carried out during a period when the sewerage system and the existing primitive treatment plant were being put in order. Although the self-purification capacity of the lagoon was very high, Lac de Tunis should not be used as a receiver of sewage and industrial waste water. Instead the capital, built on the shore of the lagoon, should have access to a water aesthetically attractive and enjoyable. Lac de Tunis had already in the early 1970s been included in the CW-list, i.e. selected for protection as a lake/wetland of utmost value for waterfowl (CW is the abbreviation of Conservation of Wetlands). The goals for the

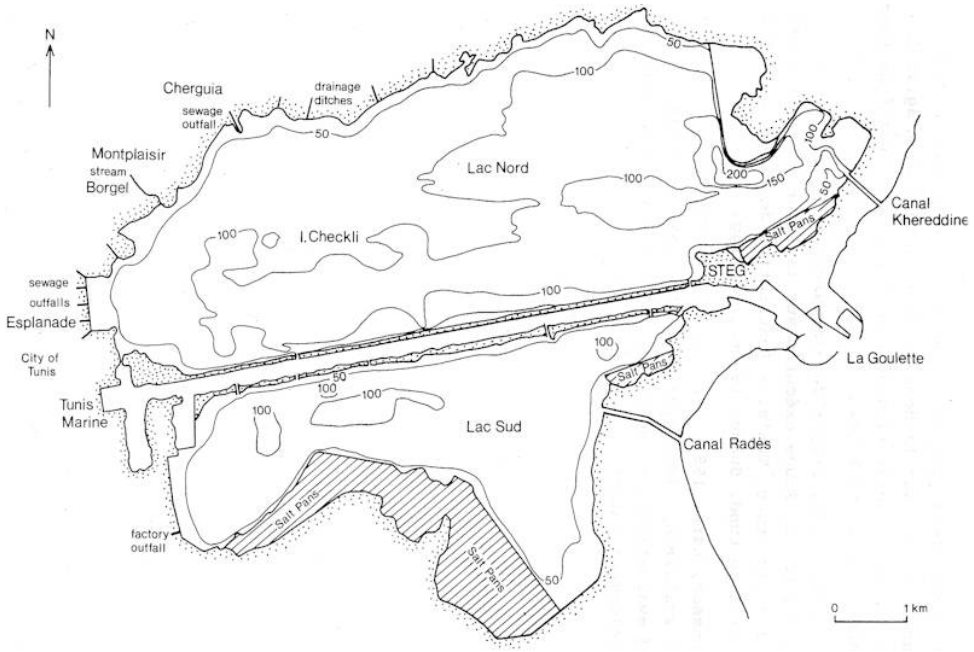

Figure 6.2: *Lac Tunis after the restoration works done by SIDA in 1972-1980.*

measures to be taken immediately in Lac Nord were mainly to:

- avoid the nasty smell
- improve the lagoon's efficiency as a receiver of sewage during the years it still had to be utilized as such
- avoid fish-kills

constitute phase one in a systematically realized plan for a definitive restoration of Lac de Tunis. Thereby prerequisites should be created partly for an attractive environment and close contact with the water in the westernmost part closest to the capital, partly to ensure the high value of the lagoon as a fish-producing water. The methods recommended were:

1. suction dredging of sewage sludge sediments
2. construction of settling ponds for temporary treatment of sewage
3. removal of floating big algae
4. aeration
5. direction and control of water flow through the lagoon
6. restoration of the littoral zone (deposition sites for solid waste etc)

all interventions are primarily aimed at local water purification. Instead, with the participation number 4, we try to foster a self-purification of the lake. It necessary that the current should be directed in such a way that nutrient-rich water be transported from the lagoon and replaced by nutrient-poor water from the Mediterranean Sea. Only in-flow should be allowed at Khereddine and only out-flow through other connections between Lac Nord and the harbor Tunis Marine by way of the navigation canal. The connections closest to La Goulette should be closed. Canal Khereddine should be widened from its present 24 m to at least 40 and preferably 45 m. The depth should be kept at 1.5 m. Considering the small depth of the lake no greater depth is necessary in the connection with the Mediterranean Sea. Automatic water gates were installed in the inlet for sea water at Khereddine and at the outlet for lagoon water at Tunis Marine. By these arrangements a very important renewal of nutrient-poor water will be secured. As the wind is the main driving force for the water level fluctuations made use of in this system, the renewal is brought about in the cheapest possible way. However, it is of utmost importance that the water gates are carefully maintained in order to function properly also with minor changes in the water level. The arrangement should not be looked upon as a simple hydromechanical measure. Instead it is a means of creating a suitable nutrient budget in order to control the productivity of the lagoon ecosystem.

6.1.3 SPLT intervention

The intervention on Lac Sud are developed by SPLT (Societe de Promotion du Lac de Tunis). In recent years the work of maintenance upgrade of the lake have been developed by the SPLT. The major tasks are related to the maintenance of the North Lake, especially in the Khereddine dredging at the channel entrance. This to ensure a continuous flow of water to encourage a continuous cleaning of industrial contaminants. In addition, controls are designed to continue the water, with a reorganization of some areas of the Lake Contour Controls continues on flora and fauna are provided. With

regard to the South Lake, substantial work on the beach along the Lake have been performed. Also they worked to facilitate the cultivation of marine salt and other crops . Have less information about South Lake because of a greater economic interest to the North Lake. More information could be found in the SPLT website.

6.1.4 The water

The supply of surface water and sewage from the area of the City of Tunis reduced the salinity in the westernmost part of Lac Nord. Heavy rains caused flooding in the city and an intensified supply of solid material which settled in the lake. The massive discharge of sewage resulted in very high concentrations of nutrients in Lac Nord. However, the extremely good self purification capacity of the water body was illustrated in the steep nutrient gradients from east to west. Wind induced water currents in alternating directions occur regularly in the connections with the Mediterranean Sea and the Navigation canal. Thereby sea water very poor in nutrients moved back and forth through the Khereddinde Canal as did heavily polluted water through the Tunis Marine connection between the harbor and the lake. The lake shores were besmeared by oil emanating from the city area, the harbor and the power plant STEG.

6.1.5 The sediment

The natural, characteristic bottom substrate is clayey and sandy soils and shell fragments. Outside the outlets of sewage in the western part of Lac Nord concentrated deposits of sewage sludge had accumulated. Also in calm water areas, as among the reefs of Mercierella a top sediment rich in organic matter occurred. However, in relation to the total bottom area the distribution of sewage sediments was small. The concentrations of nitrogen and phosphorus were very high in the sewage sediment and the concentration of ammonia extremely high in the interstitial water. As to the organic top sediment layer, several substances showed steep concentration gradients from west to east. The exchange of substances between sediment and water was investigated by SIDA under aerobic and anaerobic conditions (laboratory experiments). The studies revealed that very large quantities of ammonia and phosphate were released from the top sediment to the water. Thus, it was estimated that $500-900$ mg NH4-N and $25-30$ mg PO4-P were added to the lake water per day from a sediment area of 1 m^2. As to the oxygen concentration in the water, the heavy release from the sediment of phosphate took place under anaerobic as well as under aerobic conditions. Under prevailing high pH conditions and intensive formation of sulphide in the sediment, iron did not play any role for either the precipitation or the release of phosphate. In the thick deposits of organic matter in the western part of Lac de Tunis there were, with respect to the release of phosphate, considerable differences between the top layer and layers deeper down. Thus, from the superficial layer twice as much was released as from the layers at $100-150$ and $150-200$ cm. It is characteristic for recipients which gradually become overloaded that the concentrations of nutrients and other substances increase upwards in the sediment. Through the intensive gas ebullition the concentrations of nutrients in the water increased still more as interstitial water was mixed with lake water.

6.2 Mesh generation

The first step of the analysis is to build a realistic mesh of both lakes. The Code developed in [28] uses the Grass model for sediment transport, and discretizes the system with MR scheme. The mesh file request is an *.amdba* file, which is composed as follow:

first line *a b* (where *a* is the number of the nodes and *b* the number of the triangles)

***a* lines** node table (number of the node - x coordinate - y coordinate - label)

***b* lines** connectivity table (number of the triangle - node 1 - node 2 - node 3 - label)

The label indicates where the vertex is located:

0 for a point in the fluid-dynamic field

1 for a point on the wall

2 for a point on the outlet line

3 for a point on the inlet line

Thus, it is necessary to create the mesh and to assign to each node the corresponding label. The mesh file is obtained with MATLAB ®, using the function *pdepoly*. The lakes are reconstructed point-by-point, using GOOGLE MAPS ®to well fix the contours. For each point, longitude and latitude are detected, as shows Fig. (6.3). After that, the shape is rebuilt in meters with an homothety. Finally, the mesh is created and exported in the connectivity table and the node table. So, using a graphical interface, developed in MATLAB ®, the *.amdba* file is created. Table (6.1) resumes the mesh characteristic for each Lac and the node distribution is shown in Fig. (6.4) and in Fig. (6.5).

Lac	Contour Points	Nodes	Triangles
Nord	88+135	8014	14968
Sud	344	2559	4498

Table 6.1: Mesh Characteristic

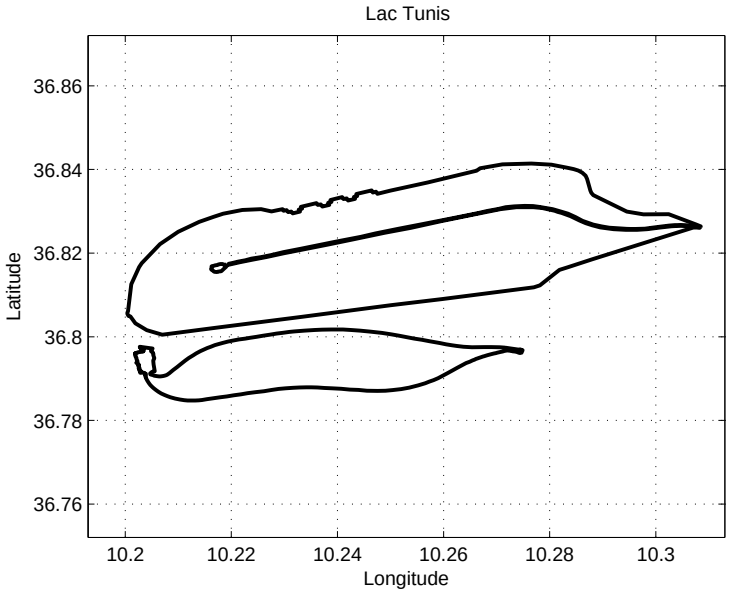

Figure 6.3: *Coordinates for the Lac Nord and the Lac Sud.*

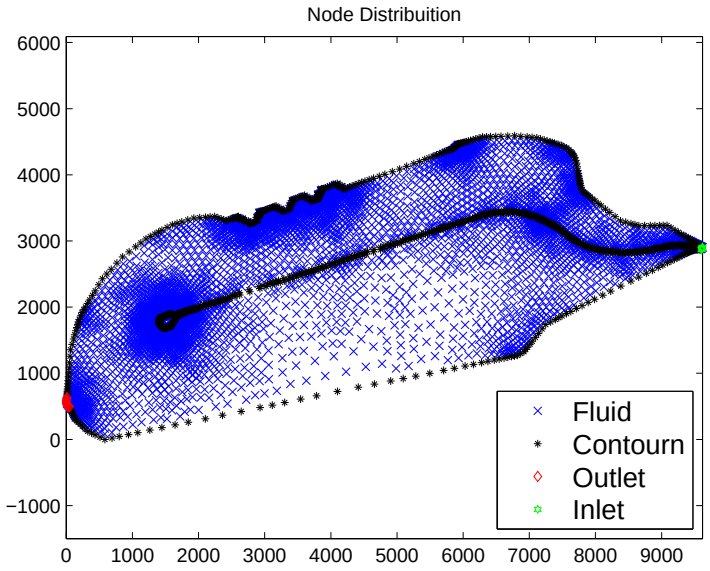

Figure 6.4: *Node distribution for the Lac Nord. It is possible to recognize the inlet and the outlet line.*

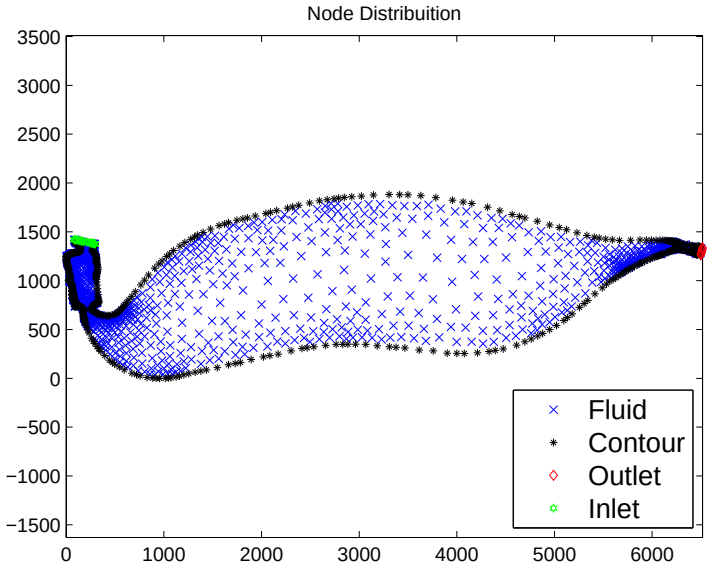

Figure 6.5: *Node distribution for the Lac Sud. It is possible to recognize the inlet and the outlet line.*

6.3 Bathymetry

The bathymetry is imposed point by point. The code set the initial condition with a pre-definite function. Therefore, it has been modified so that it is possible to insert

the bathymetry through an external file, point by point. The bathymetry should be calculated as a finite function or a table of points. Those points are interpolated to reconstruct the shape of the lake, using MATLAB ®. So it is possible to give at each node of the internal mesh, the corresponding value of bathymetry H. The bathymetry is obtained from the data proposed in Appendix A and Appendix B and it is presented in Fig. (6.6) for Lac Nord and in Fig. (6.7) for Lac Sud.

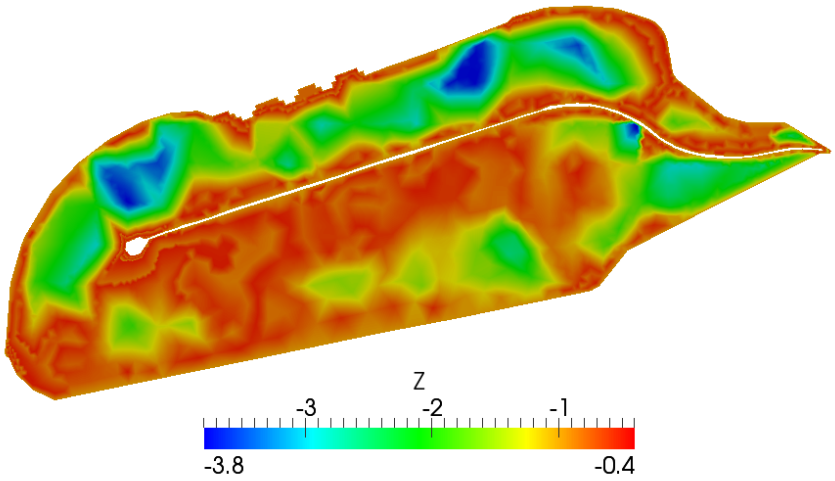

Figure 6.6: *Lac North Bathymetry visualized with Paraview.*

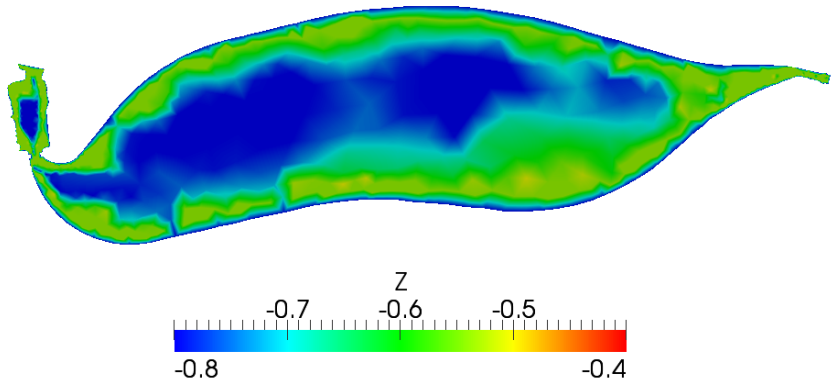

Figure 6.7: *Lac Sud Bathymetry visualized with Paraview.*

Chapter 7

Lac Nord

In this chapter the simulations carried for Lac Nord are presented. Three different fluid interactions are tested, for the same total time, in Tab. (7.1).

7.1 Lac Nord simulation

The Lac Nord presents a particular composition of the water. As previously observed, the Canal Khereddine is used to introduce clean water in the lake. At this matter, several interventions are done each year at the entrance of the Lake by SPLT. This interventions want to reduce the sediment accumulation at the entrance, to guarantee a regular water flow in the lake. To analyze the flux of the water and the bathymetric variation, a real value of sediment transport constant is calculated, according to eq. (2.44), developed for MPM model. The code uses the Grass model to solve Exner equation. The interaction constant A_g is calculating precisely by exploiting the similarities between the two implemented models presented for 1D simulations. The model chosen for the shear stress the one is proposed by Chezy (C):

$$\tau = Cu^2 \tag{7.1}$$

where the constant C is expressed by the Chezy constant $\mathcal{C}$, which is related to the Manning roughness coefficient η as:

$$C = \frac{g}{\mathcal{C}^2} = \frac{g\eta^2}{(R_h^{\frac{1}{6}})} \tag{7.2}$$

Introducing this simplification in the expression of constant $\tilde{A}$ (2.44), the sediment constant could be expressed as follow:

$$A_g = \frac{8}{(G-1)g}\eta^3\sqrt{\frac{g}{RH}} \tag{7.3}$$

It is necessary to set properly the values of each constant to have a good approximation of the problem. The Manning roughness constant is set as $\eta = 0.07$, according to Tab. (C.1), which correspond to a scattered brush with many weeds or medium to dense brush. This value is chosen according to the observation done for the Tunis Lake. The water, due to the pollution produced from industries near the Lac, has a high

amount of polluting material. Consequently, the constant G, which describes precisely the relationship between density of the sediment and water, is chosen equal to 3. Instead, the hydraulic diameter RH, in the case of large water surfaces, is to be considered equal to the average height of bathymetry. The Lake of Tunis is very shallow, with an average depth of 0.9 meters. Thus, a good approximation of the constant of Grass is equal to:

$$A_g = 0.0045 \tag{7.4}$$

which might describe the real environment of Nord lake. This value is near weak interaction and weak/intermediate interaction between water velocity and sediment discharge previously investigated in the 1D case. Simulations are executed also for this two values, for 10 hours (360000 seconds). Therefore, according to what found by Bilanceri in [28], only implicit solutions were considered because the assure good results without high computational costs. Tab. (7.1) resumes the simulation executed for Lac Nord.

Interaction	*Weak*	*Weak/intermediate*	*Real*
A_g	0.001	0.01	0.0045
Total Time [s]	360000	360000	360000

Table 7.1: *Numerical simulation for Lac Nord: water interaction and total time.*

7.1.1 Initial condition

As observe in subsection 6.1.2, the Lac Nord, is connected to the sea with the Canal Khereddine, which must be considered as an input. This channel introduces nutrient-poor water to purify the lake. The port of Tunis is considered as an outlet. The water exit from Lac Nord through Lac Sud. A small channel connect both Lac and the navigation channel. The inlet-outlet condition are imposed following those considerations. The inlet velocity of the water is considered studying the marine charts of Mediterranean sea. At the inlet a velocity normal to the boundary and having a modulus of 1 knot (0.514 m/s) is assumed. In the middle of the field, the velocity is taken as zero and the height of the water column h is equal to the bathymetry. Tab. (7.2) resumes the initial conditions for all simulations.

NORD	*Inlet*	*Outlet*	*Field*
u [m/s]	-0.2715	/	0
v [m/s]	0.4364	/	0
h [m]	1	1	-H
H [m]	1	1	Fig. 6.6

Table 7.2: *Initial conditions for Lac Nord.*

7.2 Weak/intermediate interaction

For weak/intermediate interaction, the same large CFL values found for 1D case for Grass model were used. In order to compare those different solution, implicit second order solutions with CFL=10^2 with only one DEC iteration and with CFL=10^3 with DEC= 3 are presented in Fig 7.1. The bed evolution is practically the same, without significant changes. To confirm the results obtained, also the velocity field is presented

in Fig. 7.2, in which the velocity component in x direction is considered. No significant difference were found. The water diffuses in the lake according to what done by SPTL, especially in the nord part near the Arabian zone. The effect of DEC correction it is observable from Tab. (7.3). A considerable gain it is found with implicit second order solution with CFL=10^3 with DEC= 3. The computational gain is roughly one hour with respect to implicit second order solutions with CFL=10^2, DEC=1. Moreover, to invenstigate two of the hot-spot in Tunis lake according to what observed by SPLT, solution near Chikly island and at the inlet Kerredine channel are presented in Fig. 7.3. The Chikly island present a considerable sediment accumulation in the nord part, near the deepest zone of Lac Nord. Maybe this is due to a strong variation of the depth, which favors the accumulation of sediment. For the inlet channel, the results confirm what is expected based on the work performed by SPLT, with a strong accumulation of the sediment and an area in which the water mass flow digs. This area is constantly supervised by SPLT with weekly/monthly processes of dredging, to encourage the inflow of clean water from the Mediterranean Sea. Therefore, the results obtained are in accordance with what found by the SPLT.

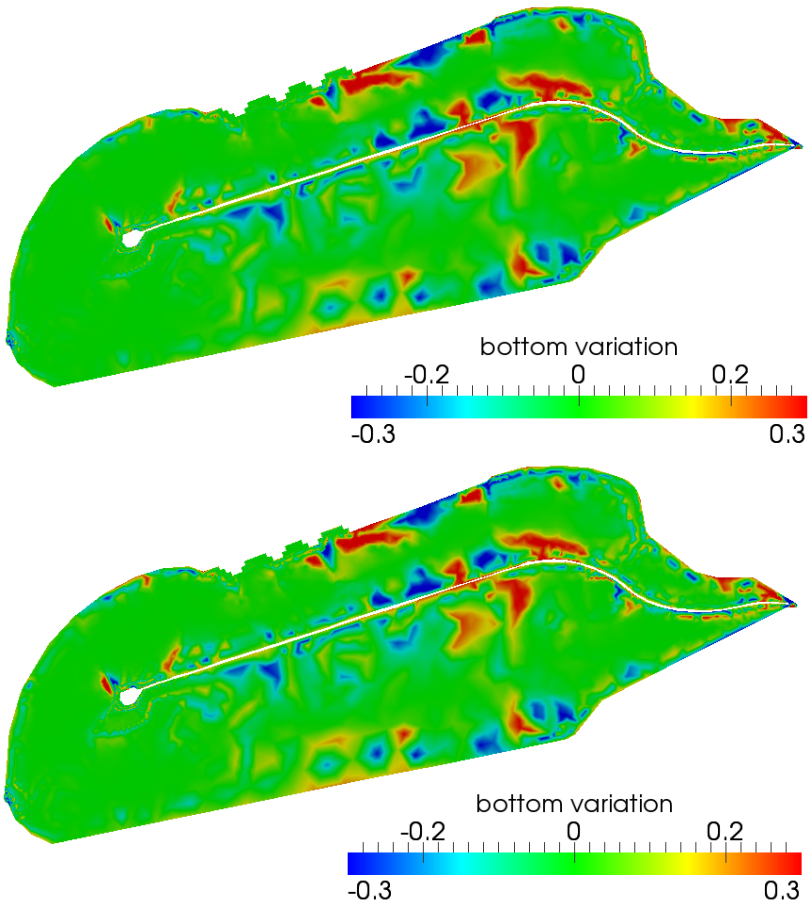

Figure 7.1: *Bottom variation for Tunis Nord Lake, weak/intermediate interaction: implicit second order scheme CFL=10^3, with DEC=1 (up) and DEC=3 (down).*

Scheme	*CPU time* [s]
IMP CFL=10^2 DEC=1	22595.718
IMP CFL=10^3 DEC=3	19298.442

Table 7.3: *Simulation times for Lac Nord for weak/intermediate interaction.*

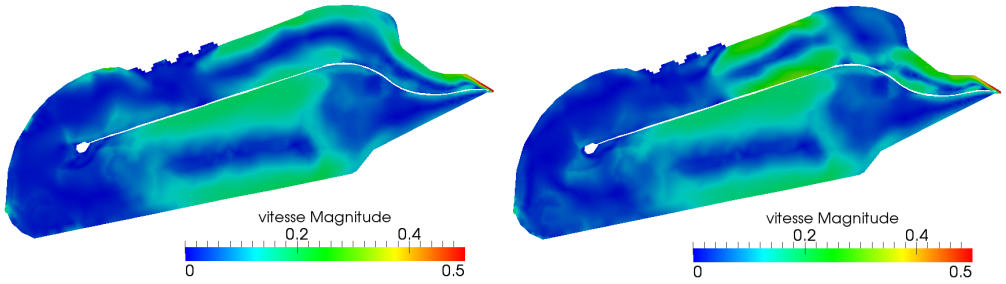

Figure 7.2: *Velocity field [m/s] for Tunis Nord Lake, weak/intermediate interaction: implicit second order scheme CFL=10^3, with DEC=1 (left) and DEC=3 (right).*

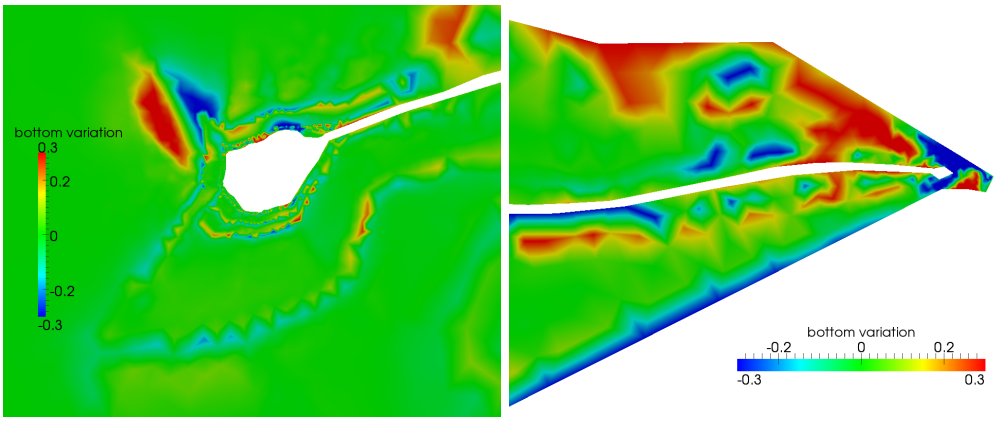

Figure 7.3: *Bottom Variation for Tunis Lake near Chikly island and Kherredine channels, weak/intermediate interaction. Implicit second order scheme with CFL=10^3 and DEC=3.*

7.3 Weak interaction

In this section weak interaction was considered. In this case, simulations were carried out for implicit second order scheme with CFL=10^3, DEC=1 and with CFL=10^4, DEC=3. In order to compare the CFL effect, the bathymetry variation for both cases are presented in Fig. 7.4. The sediment discharge is practically the same in all the field, except in the nord part of the lake, near the Arabian zone, where for implicit second order with CFL=10^3, DEC=3, the sediment transport is about zero. To evaluate if this reduction is present in the rest of the lake, comparison between both solution near Chikly island is presented in Fig. 7.5. Near the island, a global reduction of sediment discharge it is found for implicit second order scheme with CFL=10^3, DEC=1. Moreover, this reduction it is also found at the inlet channel, as it possible to see in Fig. 7.6. Near the

Scheme	*CPU time* [s]
IMP CFL=10^3 DEC= 1	7276.320
IMP CFL=10^4 DEC= 3	4701.356

Table 7.4: *Simulation times for Lac Nord for weak interaction.*

Kherredine channel, the sediment discharge has a similar trend for both solutions, but a little decrease on sediment transport were found for CFL=10^3, DEC=1. In order to investigate the accuracy of the solution, another comparison is executed on the velocity field, in Fig. 7.7. Implicit second order solution with CFL=10^3, DEC=1, presents a reasonable velocity field. Thus is not the case for the solution with CFL=10^4, DEC=3. For this CFL condition, velocity presents, in the nord part of the lake, an higher value of magnitude which could not be observed in reality. Finally, computational time were presented in Tab. 7.4. A considerable reduction on computational time is obtained using DEC correction with CFL=10^4, but a deterioration on solution accuracy it is observed.

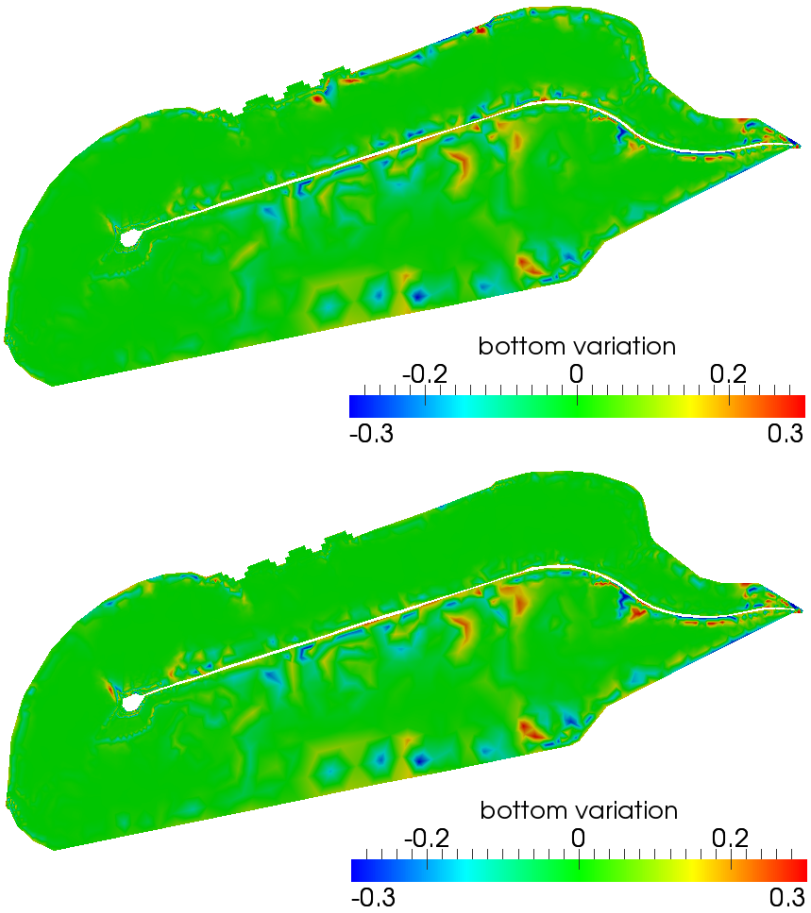

Figure 7.4: *Bottom variation for Tunis Nord Lake, weak interaction: implicit second order scheme CFL=10^3, with DEC=1 (left) and CFL=10^4, DEC=3 (right).*

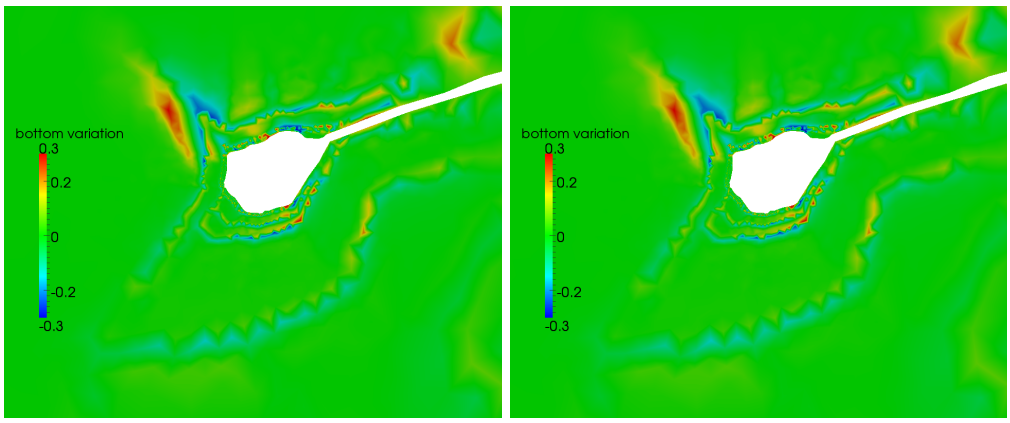

Figure 7.5: *Bottom Variation for Tunis Lake near Chikly island, weak interaction. Implicit second order scheme with CFL=10^3 with DEC=1 (left) and CFL=10^4, DEC=3 (right).*

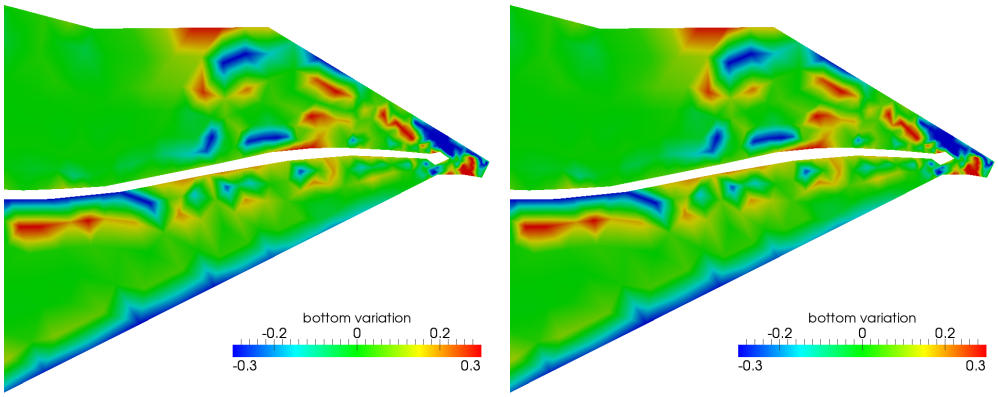

Figure 7.6: *Bottom Variation for Tunis Lake at Kherredine channels, weak interaction. Implicit second order scheme with CFL=10^3 with DEC=1 (left) and CFL=10^4, DEC=3 (right).*

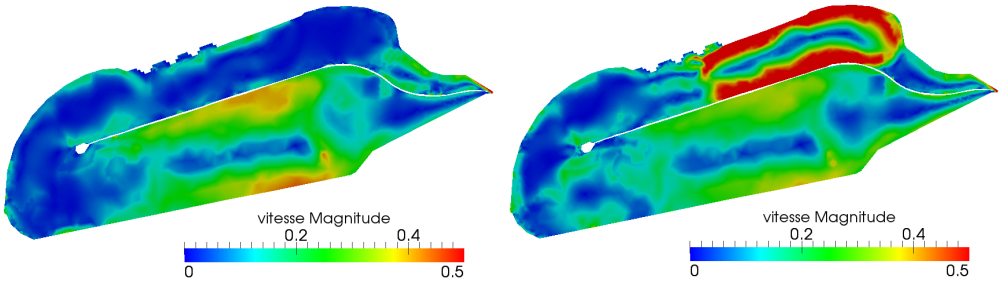

Figure 7.7: *Velocity field [m/s] for Tunis Nord Lake, weak interaction: implicit second order scheme CFL=10^3, with DEC=1 (left) and CFL=10^4, DEC=3 (right).*

7.4 Real interaction

Finally, real interaction conditions are imposed in the Grass model to have a better idea of the sediment discharge in Tunis Lake. According to the simplifications done, it is found that $A_g = 0.0045$, which could be considered as weak interaction. Therefore, simulation for second order implicit scheme with CFL=10^3, DEC=1, and with CFL=10^4, DEC=3, were carried out. Unfortunately, for CFL=10^4, the code is unstable and gives no results. In order to investigate if, for this interaction value, the most reasonable CFL condition is the same for weak/intermediate or for weak interaction, it was decided to impose the DEC iterations for CFL=10^3. A considerable difference is found in computational time, as Tab. (7.5) shows. Second order implicit scheme with CFL=10^3, DEC=3, has a computational time almost twice that obtained with only one DEC iteration. On the other hand, a deterioration of accuracy is found for the solution with only one DEC. At this matter, the velocity field it is presented in Fig 7.8 for both solutions, as done for weak interaction. As it possible to see, the solution with only one DEC iteration present value of speed which are not reasonable expected in reality. Therefore, the sediment discharge is analyzed taking into account only the solution with 3 DEC iterations. The bottom variation for Lac Nord it is presented in 7.9, for second order implicit scheme with CFL=10^3, DEC=3. The sediment discharge is more concentrated in the two hot spot found by SPLT, the Chikly island and the inlet at Kherredine channel. Other variations are observed along the south side of the lake, at the edge of a road that connects the city of Tunis and La Goulette. The sides of the road leading to the island of Chikly present some areas where there is a considerable flow of sediments. However, in the deeper area, in the north of Chikly, the sediment transport practically negligible. Moreover, the sediment discharge near Chikly island and at the inlet is presented in Fig. 7.10. The sediment discharge has the same trend found for weak and weak/intermediate interaction. The area in which the sediment discharge is more concentrated is at Kherredine channel: in this area, a critical zone in which the sediment accumulate and an other area in which the water digs the bottom are observed. Therefore, the mean value of bathymetry in this zone is about 0.7 meters and the bottom variation due at sediment accumulation is in the order to 0.08/0.09 for days. This results confirm the dredging plane done by SPLT, which provides weekly/monthly control and dredge plans. Consequently, the last hot spot in SPLT plane it is analyzed: the water currents il Lac Nord. The dredging plane are imposed to improve the inlet in the lake of fresh water from Mediterranean Sea, to favorite the water purification. At this matter, the velocity field and streamline are presented in Fig. 7.11. The water flow, coming from the Kherredine channel, crosses around the Chikly island, forming a large recirculation area. Other recirculation zons were found near the inlet and in the nord literal of the lake. Therefore, by observing the behavior of the currents, it can be affirmed that the water flow has a good diffusion throughout the lake.

Scheme	*CPU time* [s]
IMP CFL=10^3 DEC= 1	8204.116
IMP CFL=10^3 DEC= 3	17843.149

Table 7.5: *Simulation times for Lac Nord for real interaction.*

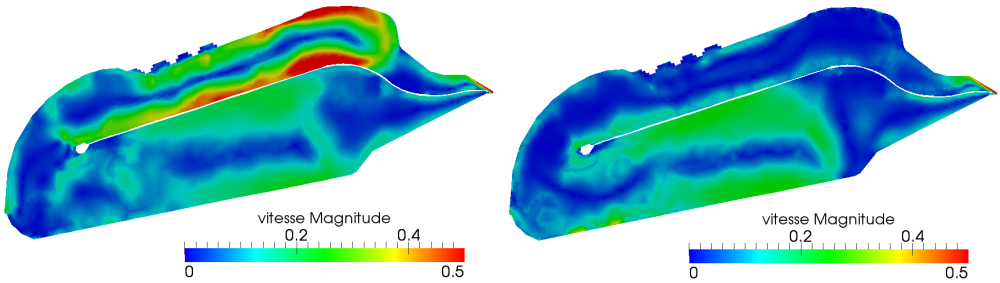

Figure 7.8: *Velocity field [m/s] in Tunis Lac Nord for second order implicit scheme CFL=10^3, with DEC=1 (left) and DEC=3 (right).*

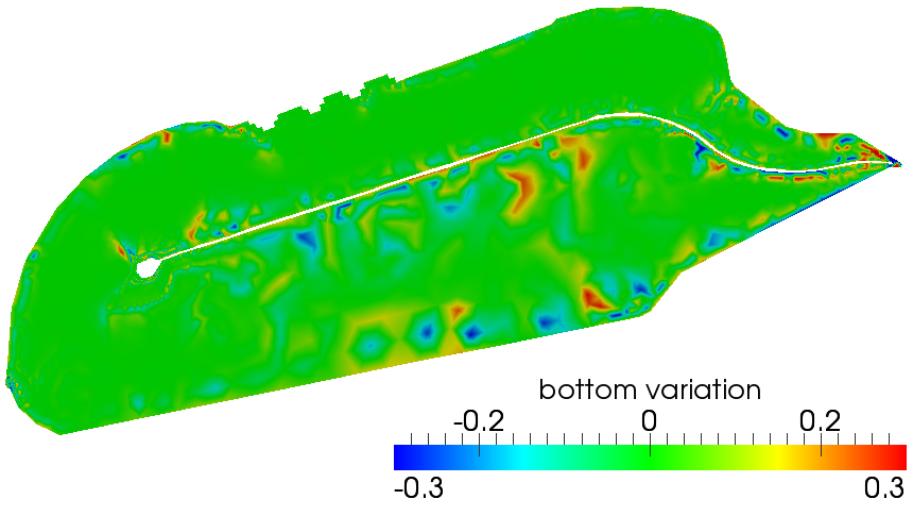

Figure 7.9: *Bottom Variation for Tunis Lake. Implicit scheme CFL=10^3 with DEC= 3.*

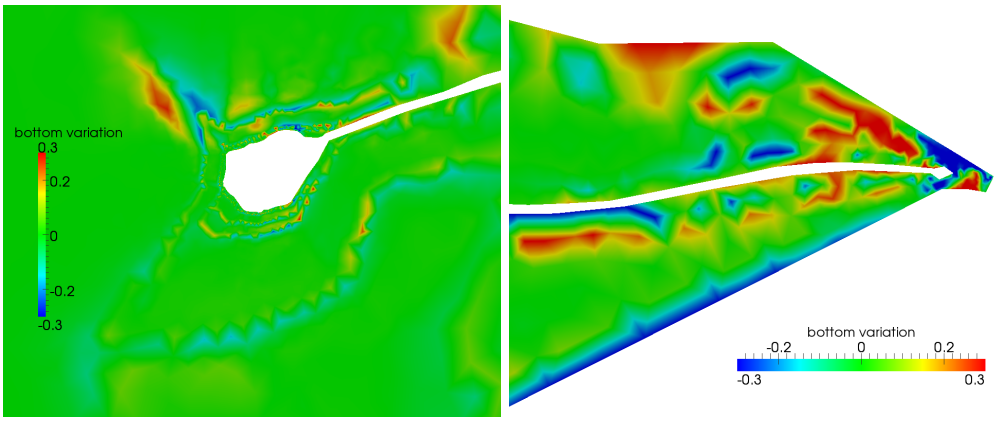

Figure 7.10: *Bottom Variation for Tunis Lake near Chikly island (left) and Kherredine channel (right). Implicit scheme CFL=10^3 with DEC= 3.*

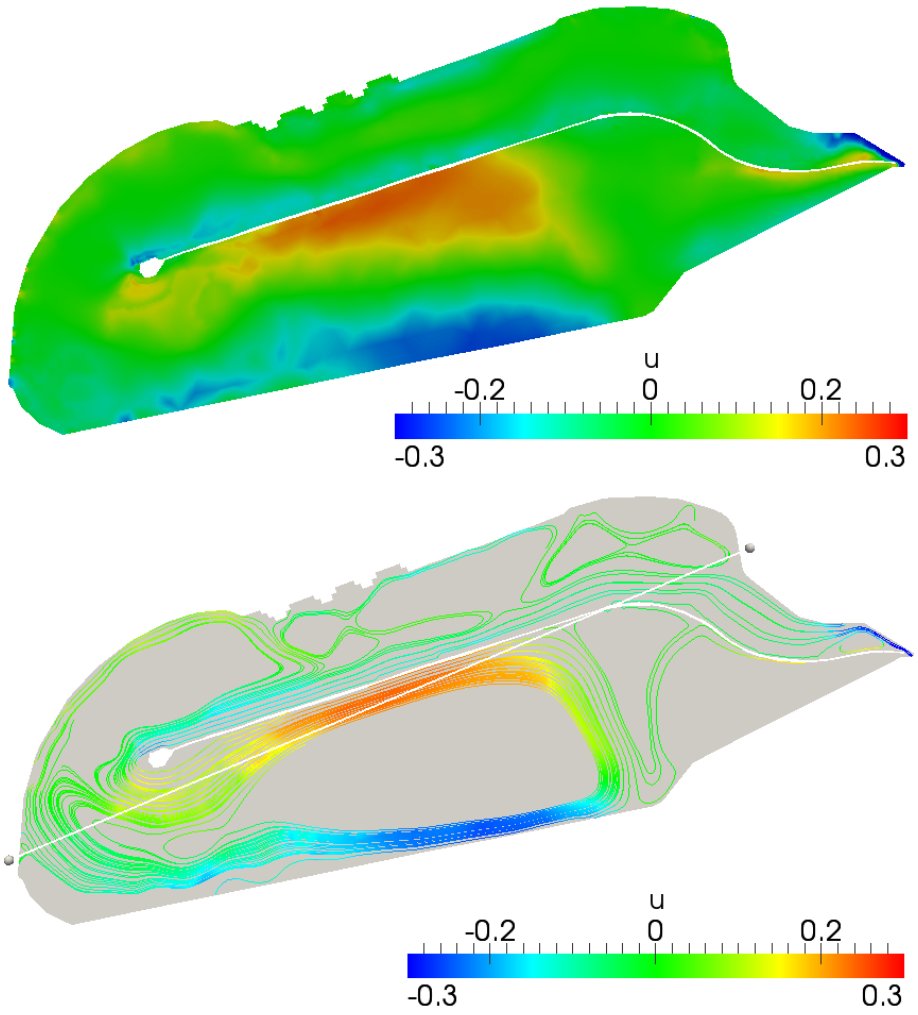

Figure 7.11: *Tunis lake, currents inside the Lake. Velocity field (u component) [m/s] and streamline starting from the inlet. Implicit scheme CFL=10^3 with DEC= 3.*

7.5 Concluding remarks for Lac Nord simulation

The simulations confirm what studied by SPLT, in terms of sediment discharge and water flow. For weak and weak/intermediate interaction the same dependence of the CFL with the interaction speed has been found. The largest value of CFL is roughly proportional of the inverse of sediment constant. For real interaction, the CFL condition is the same utilized for weak/intermediate interaction.

Chapter 8

Lac Sud

In this chapter the simulation carried out for Lac Sud are presented. Two different fluid interactions are tested, for the same total time, asin Tab. (7.1).

8.1 Sud Lac simulation

The Lac Sud has a different importance for Tunis than Lac Nord. It is used mostly to obtain salt or to grow plants, because it is small and shallow. The water is more clean, without industries which introduce pollution in the environment. So, constant G is set 2.8. Therefore, the medium value of the bathymetry is near 0.6 meters. The Manning roughness constant is set equal to 0.6, with a little decrease from the Lac Nord case, because the water is considered more clean due to the requirements cultivation in the lake. The realistic sediment constant is calculated as:

$$A_g = 0.0036 \tag{8.1}$$

Tab. (8.1) resumes the simulation carried out for Lac Sud.

$Interaction$	$Weak$	$Real$
A_g	0.001	0.0036
$Total\ Time$ [s]	360000	360000

Table 8.1: *Numerical Simulation for Lac Sud: water interaction and total time.*

8.1.1 Initial conditions

The initial conditions are imposed according with what was observed for the North Lake. The inlet condition is the connection with the port and the outlet is the channel which connect Lac Sud to the sea. At the inlet a velocity normal to the boundary and having a modulus of 1 knot (0.514 m/s) is assumed. In the computational domain, the velocity is taken as zero and the height of the water column h is equal to the bathymetry considerate. Tab. (8.2) summarizes the initial conditions for all simulations executed.

SUD	*Inlet*	*Outlet*	*Field*
u [m/s]	0.0808	/	0
v [m/s]	−0.5076	/	0
h [m]	0.8	0.8	-H
H [m]	0.8	0.8	Fig. 6.7

Table 8.2: *Initial condition for Lac Sud.*

8.2 Weak interaction

For weak interaction, the code presents two different computational behaviors. For the second order implicit solution, the code blows up. But it is possible to have an idea of sediment discharge few seconds before the final time imposed, at about 359996 seconds. Furthermore, for the solution with CFL=10^1, DEC=3, instabilities appear at about 306000 seconds. In this case, a different approach it is proposed: first of all, the instabilities mode are investigated, to evaluate for which condition they may occurs. To this aim, the velocity field, which is connected to the sediment discharge, is presented in Fig. 8.1 in various time istants. It is possible to observe how, after t=101551 s, the velocity magnitude reaches a steady condition. Therefore, the instability is not directly connected to u or v. The depth value Z $(-H)$is investigated in Fig. 8.2. A progressive

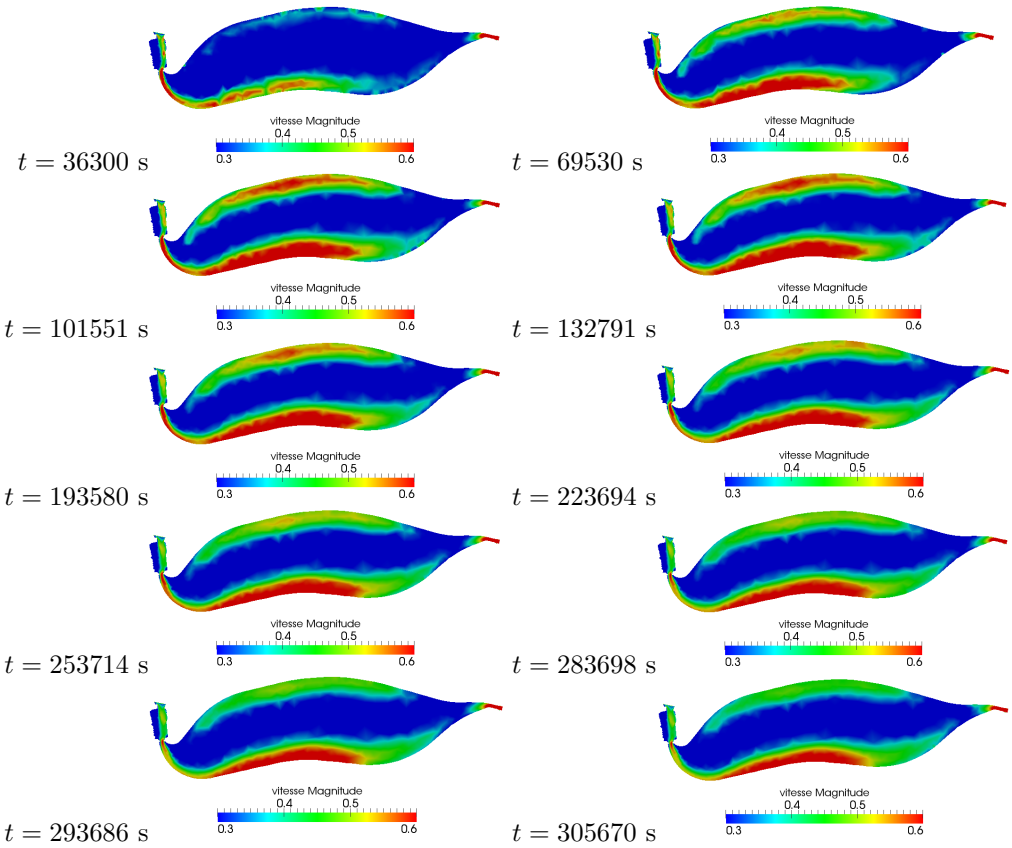

Figure 8.1: *Velocity field at different times, weak interaction, implicit second order scheme CFL=10^1, DEC=3.*

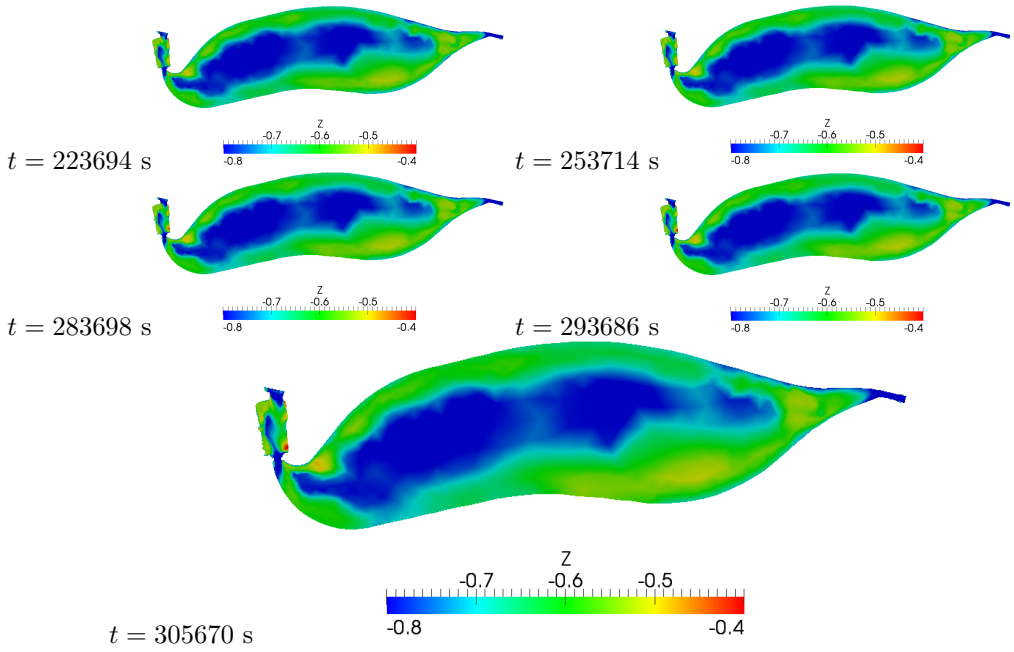

Figure 8.2: *Bathymetry values at different times, weak interaction, implicit second order scheme CFL=10^1, DEC=3.*

decrease of bathymetry it is found near the inlet of the Lac Sud, because of which the instability may occur. So, the bathymetry it is presented also for the solution with CFL=10^0, DEC=1, in Fig. 8.3. Moreover, the same bathymetry variation is found near the inlet and, to well understand this phenomenon, in Fig. 8.4, a zoom in that zone is proposed. It is possible to see how a big accumulation of sediment is present in both simulations, near the first part of the lake, with a mean value of depth, in the red zone, about of 0.2 meters. The same bathymetry trend is found, thus instability is expected also for the solution with CFL=10^0, DEC=1.

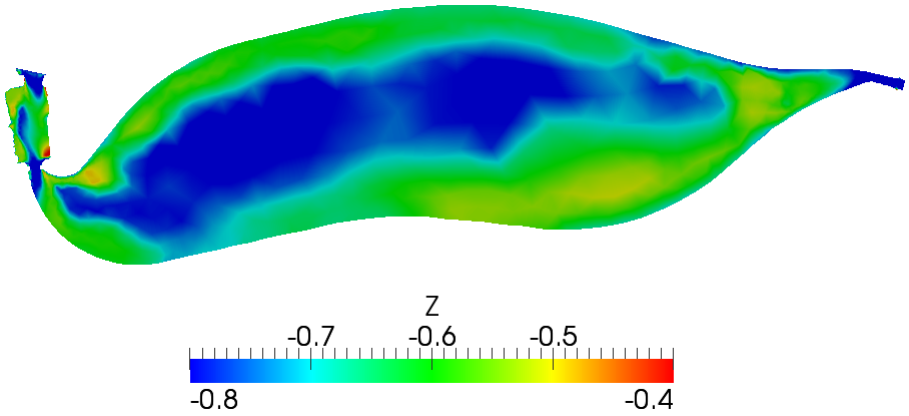

Figure 8.3: *Bathymetry values at different times, weak interaction, implicit second order scheme CFL=10^0, DEC=1.*

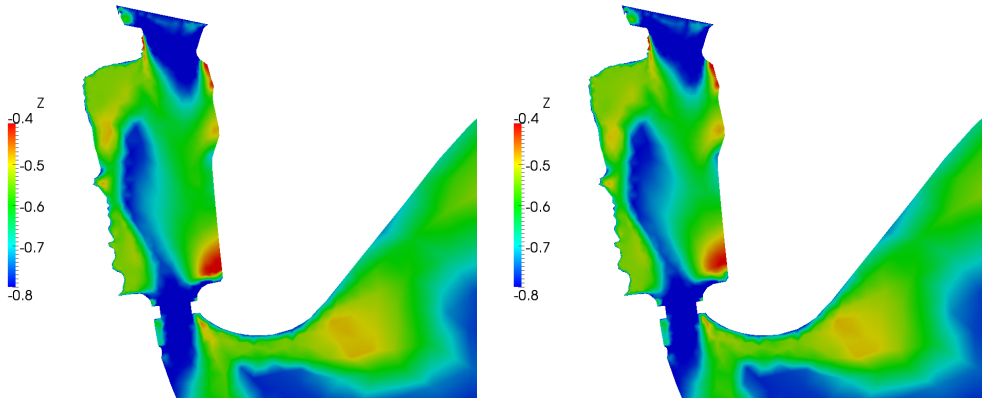

Figure 8.4: *Bathymetry values for weak interaction, implicit second order scheme CFL=10^0, DEC=1, near the final time, and CFL=10^1, DEC=3, t=305670 s.*

8.3 Real interaction

Also for realistic interaction a decrease in CFL is found. The code is unstable, and the largest value which allows to obtain a solution is CFL=1, with only one DEC iteration. However, the code isn't able to write the output file, so the solution at the final time imposed is not available. So, a solution near the final state it is analyzed, as done for weak interaction, to well understand the stability of the field. Moreover, the code become unstable for second order implicit scheme for CFL=10, DEC=3, after about90000 seconds. The reduction of the time for which the instability occurs, could be connected to the largest value of A_g, according to what found for weak interaction. To well understand if this connection is real, the bottom shape at the inlet it is presented for both solutions in Fig. 8.5. The bathymetry is reduced also in this case near the inlet of the lake, reaching values of $0.2 - 0.25$ meters. Also in this case, instability occurs and, before that, a bathymetry reduction is found in the inlet part of the Lac Sud. A further confirmation can be found in Fig. 8.6: the only area in which a consistent decrease of bathymetry value is near the inlet.

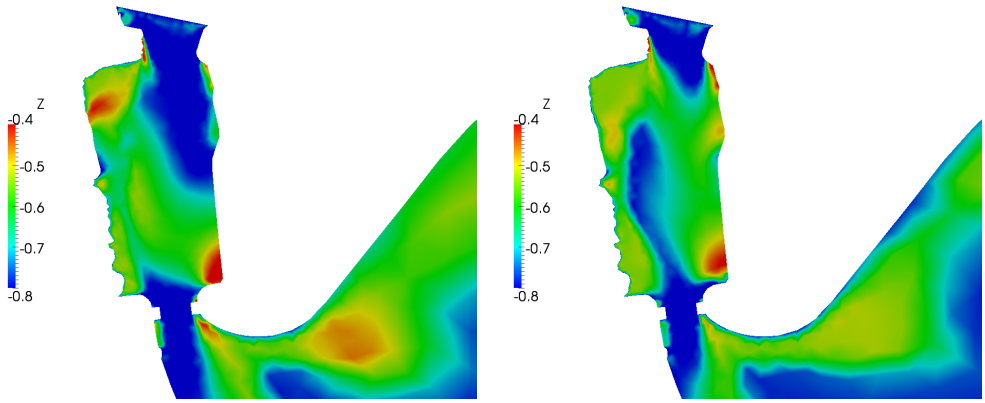

Figure 8.5: *Bathymetry values for real interaction, implicit second order scheme CFL=10^0, DEC=1, near the final time, and CFL=10^1, DEC=3, t=83176 s.*

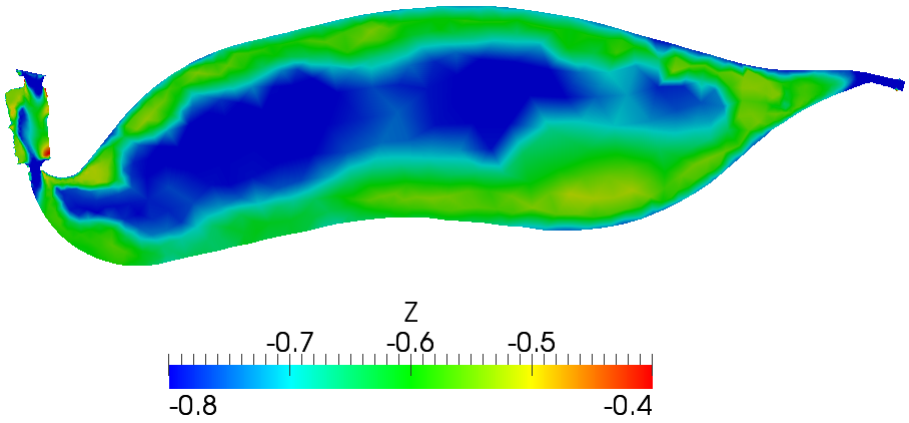

Figure 8.6: *Bathymetry values for real interaction, implicit second order scheme CFL=10[1], DEC=3, t=83176 s.*

8.4 Concluding remarks for Lac Sud

For Lac Sud a global reduction on CFL condition it is found and only non valid solution were found. An area after the inlet presents a large reduction in bathymetry value which may produce the instability in the code. Moreover, the velocity magnitude in all case oscillates around a value of 0.4 m/s, with the larger value of 0.75 m/s. These values could be expected in the physical reality in Lac Sud, according to the nautical charts and the morphodynamical characteristic of the lake.

Part IV

Conclusion

Chapter 9

Conclusion

The sediment transport model in shallow water problems has been considered, and the Exner equation has been used to describe the bed evolution. This equation need a model to represent the sediment discharge. In previous studies [28], the model chosen was the Grass one. The scheme to discretize the coupled system was the Modified Roe, together with the implicit and explicit time advancing. In the present work, three different models have been implemented to close the Exner equation: an amendment to Grass model, the Meyer-Peter Muller model and a modification of this, the same as for the Grass model.

Modified Grass model gives different bottom slope trend from Grass model, with a similar computational time. The correction implemented is in order to correct an intrinsical error of Grass model, in which the bedload is maximum near the water surface and not at the bottom. A linear dependence on water column in introduced. The global discharge is reduced and the bottom slope presents higher peak. The largest value of CFL which allows an accurate solution with implicit time advancing solution is the same of Grass model.

The Meyer Peter Muller model permit to take into account a very important physical issues: a threshold on motion condition. This condition is introduced in the code according to Shields theory, for which the movement of bedload is constant after a certain value of Reynolds at the bottom, typically 10^3. The introduction of the threshold influence the problem according to the model chosen for shear stress. In this work, a linear dependance between shear stress and the square of water speed it is imposed, according to Chezy theory. So, the threshold becomes a condition on the square of the critical velocity $\tilde{u}$. A different bottom slope with respect to the previous models it is found with a hump near the threshold condition. The largest value of CFL for the implicit scheme, with only one DEC iteration, presents a better trend than Grass model. The solution with only one DEC iteration gains one order of magnitude with respect to Grass and Modified Grass model. Therefore, However, DEC iterations does not eliminate the accuracy problems at larger CFL numbers. The computational efficiency is near the one found for Grass model with 3 DEC iterations. In order to investigate the threshold effects for implicit second order scheme, a set of three different critical velocity were carried out. The threshold magnitude does not influence computational efficiency. The smoothness of MPM model is analyzed taking into account some geometrical characteristic of the bottom slope changing the final time. The x and z position of the bedload geometrical center has a little displacement for MPM model, and this variation is lower with increasing threshold magnitude. This displacement reduction could explain the higher value of CFL obtained with MPM.

Finally, for 1D analysis, the same correction proposed for Grass model is applied at MPM model. In order to compare MPMH model with MPM, only a little reduction of the global discharge is found and the same hump appears near the threshold condition. Moreover, computational times are comparable and the same computational efficiency is found. Also in this case, the same threshold analysis done for MPM model were carried out. The threshold influence does not affect the largest CFL value and the computational efficiency also for MPMH model. Summarizing, it has been found that, as expected, the sediment transport model significantly affects the bedload evolution. On the other hand, implicit time advancing efficiency remains very effective for all the considered models for weak to intermediate speeds of interaction between bedload and water flow. As for possible development concerning sediment transport model, different shear stress theory, for example Manning one, which introduce different dependence on physical parameters may be considered.

Moreover, only models with the classical division of sediment transport (bedload, suspension load and saltation) were chosen in the present study. It could be interesting to chose a model based on Einstein theory, introducing the alveum concept, to analyze the efficiency of the MR scheme.

A realistic case is investigated for Tunis Lake by 2D simulations. The Tunis lake is divided in two part, Lac Nord and Lac Sud, and has a mean depth very shallow, about 0.8 meters. Both lakes, across the years, have undergone substantial changes, facilitated also by the small mean depth. Maintenance works have been carried out mainly in order to keep the lake clean from pollutants. The main objectives, during years, were to facilitate the circulation of clean water from the Mediterranean Sea and to avoid excessive sediment deposits in some hot spots. The results obtained with the model of Grass, confirmed what was done by maintenance works across the years. The same applies also for maintenance works weekly, in the points where the sediment tends to accumulate (for example at the entrance of the channel Kherredine). From the computational point of view, for Lac Nord the results have confirmed what that found for the 1D case. The highest value of CFL at which accurate solutions are obtained is approximately roughly proportional to the inverse of A_g. Instead, for the South Lake, a deterioration of numerical stability has been observed. This is due, according to observations made, to an excessive reduction of the bathymetry at a point in the first part of the lake, which can lead to instability. This issue, however, deserves further investigation.

Part V

Appendix

Appendix A

Lac Nord Tunis bathymetry

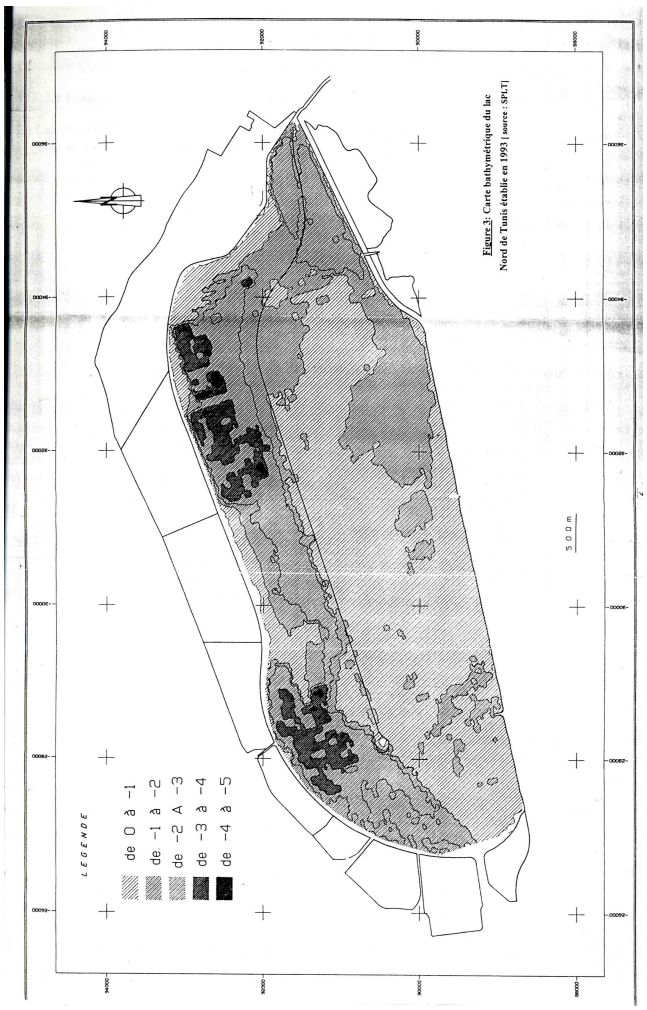

Figure A.1: *Lac Nord Tunis bathymetry*

Appendix B

Lac Sud Tunis bathymetry

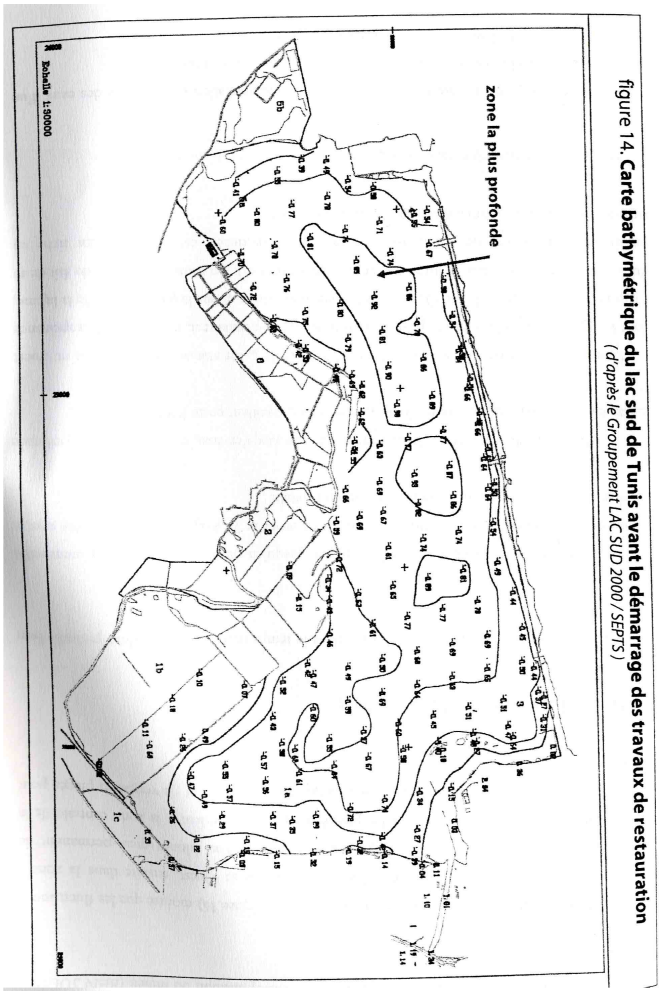

figure 14. **Carte bathymétrique du lac sud de Tunis avant le démarrage des travaux de restauration** *(d'après le Groupement LAC SUD 2000 / SEPTS)*

Figure B.1: *Lac Sud Tunis bathymetry*

Appendix C

Shear stress

To simplify the numerical system, for the shear stress *tau* the Chezy form is used. The shear stress are modeled as follows:

$$\tau = Cu^2 \tag{C.1}$$

The friction therm C is related to the roughness and the friction therm as the following relation:

$$C = \frac{g}{\mathcal{C}^2} \tag{C.2}$$

The formula is named after Antoine de Chezy, the French hydraulics engineer who devised it in 1775. This formula can also be used with Manning's Roughness Coefficient, instead of Chezy's coefficient.

C.1 Chezy Formula

Manning derived the following relation to C based upon experiments:

$$\mathcal{C} = \frac{R_h^{\frac{1}{6}}}{\eta} \tag{C.3}$$

where:

- is the Chezy coefficient $[m^{1/2}/s]$
- is the hydraulic radius ($\backsimeq$ water depth H) $[m]$
- Manning's roughness coefficient, Tab.(C.1)

Unlike the Manning equation, which is empirical, the Chezy equation is derived from hydrodynamics theory, studying steady, turbulent open channel flow near Paris.

C.2 Manning Formula

To express the Chezy constant C, Manning proposed the following

$$\mathcal{C} = \gamma R_H \left| SF \right| \tag{C.4}$$

γ is the unit weight, R_H is the hydraulic ratio, usually equal to the water column h, and the form factor is defined according to the Manning Theory:

$$SF = \frac{g\eta_0^2}{R_H^{\frac{4}{3}}} \tag{C.5}$$

The Gauckler Manning formula is used to estimate flow in open channel situations where it is not practical to construct a weir or flume to measure flow with greater accuracy. The friction coefficients across weirs and orifices are less subjective than n along a natural (earthen, stone or vegetated) channel reach. Cross sectional area, as well as n', will likely vary along a natural channel. Accordingly, more error is expected in predicting flow by assuming a Manning's n, than by measuring flow across a constructed weirs, flumes or orifices. The formula can be obtained by use of dimensional analysis. The Gauckler Manning coefficient, Tab.(C.1), often denoted as η, is an empirically derived coefficient, which is dependent on many factors, including surface roughness and sinuosity. When field inspection is not possible, the best method to determine η is to use photographs of river channels where n has been determined using Gauckler Manning's formula. In natural streams, η values vary greatly along its reach, and will even vary in a given reach of channel with different stages of flow. Most research shows that n will decrease with stage, at least up to bank-full. Overbank η values for a given reach will vary greatly depending on the time of year and the velocity of flow. Summer vegetation will typically have a significantly higher n value due to leaves and seasonal vegetation. Research has shown, however, that η values are lower for individual shrubs with leaves than for the shrubs without leaves. This is due to the ability of the plant's leaves to streamline and flex as the flow passes them thus lowering the resistance to flow. High velocity flows will cause some vegetation (such as grasses and forbs) to lay flat, where a lower velocity of flow through the same vegetation will not. Historically both the Chezy and the Gauckler Manning coefficients were expected to be constant and functions of the roughness only. But it is now well recognized that these coefficients are only constant for a range of flow rates. Most friction coefficients (except perhaps the Darcy Weisbach friction factor) are estimated 100% empirically and they apply only to fully rough turbulent water flows under steady flow conditions. One of the most important applications of the Manning equation is its use in sewer design. Sewers are often constructed as circular pipes. It has long been accepted that the value of n varies with the flow depth in partially filled circular pipes.

TABLE 2.1 Manning Roughness Coefficients of Natural Streams

Description of Stream	*Range of* n	*Normal* n
Small Streams (< 100-ft. width)		
Clean, straight, bankfull, no riffles or deep pools	0.025–0.033	0.030
Straight, no riffles or pools, no stones or vegetation	0.030–0.040	0.035
Clean, sinuous, some pools and riffles	0.033–0.045	0.040
Sinuous, some pools and riffles, some stones and vegetation	0.035–0.050	0.045
Sinuous, lower stages, more stones	0.045–0.060	0.050
Sluggish reaches, weedy, deep pools	0.050–0.080	0.070
Deep pools, very weedy, floodway with timber and brush	0.075–0.150	0.100
Major Streams (> 100-ft. width)		
No boulders or brush	0.025–0.060	
Irregular and rough reach	0.035–0.100	
Mountain Streams		
Clean channel, steep banks with vegetation on banks submerged at high flow, bed of gravel and cobbles	0.030–0.050	0.040
Same as above but with bed of cobbles and large boulders	0.040–0.070	0.050
Floodplains		
Pasture, no brush, short grass	0.025–0.035	0.030
Pasture, no brush, high grass	0.030–0.050	0.035
Scattered brush, many weeds	0.035–0.070	0.050
Medium to dense brush	0.045–0.160	0.070
Heavy stand of timber, little undergrowth, flood below branches	0.080–0.120	0.100
Heavy stand of timber, little undergrowth, flood reaching branches	0.100–0.160	0.120

SOURCE: Modified from Chow 1959.

Figure C.1: *Manning parameter η in different environment.*

Bibliography

[1] Hudson J. Damgaard J. Dodd N. Chesher T. Cooper A. Numerical approaches for 1d morphodynamic modelling. *Coastal Engineering*, 52:691–707, 2005.

[2] Kalinske A. Movemente of sediment as bed load in rivers. *American Geophysical Union*, 28(4):615–620, 1947.

[3] Postacchini M. Brocchini M. Corvaro S. Lorenzoni C. Mancinelli A. Comparative analysis of sea wave dissipation induced by three flow mechanisms. *Journal of Hydraulic Resources*, 49(4):554–561, 2011.

[4] Watanabe A. Total rate and distribution of longshore sand transport. In *Proceedings of the 23rd Coastal Engineering Conference*, pages 2528–2541, 1992.

[5] Junke Guo ad Julien Pierre Y. Efficient algorithm for computing einstein integrals. *Journal of Hydraulic Resources*, 130:1198–1201, 2004.

[6] Einstein Hans Albert. The bed load function for sediment trasport in open channel flows. *Coastal Engineering*, 52:691–707, 1950.

[7] Castro Diaz M.J. Fernandez-Nieto E.D. Ferreiro A.M. Sediment transport models in shallow water equations and numerical approach by high order finite volume methods. *Computers & Fluids*, 37:299–316, 2008.

[8] Castro Diaz M.J. Fernandez-Nieto E.D. Ferreiro A.M. Two-dimensional sediment transport models in shallow water equations. a second order finite volume approach on unstructured meshes. *Comput. Methods Appl. Mech. Engrg.*, 198:2520–2538, 2009.

[9] R. A. Bagnold. An approach to the sediment transport problem from general physics. *U.S. Geological Survey Professional Paper*, 422(I):73, 1966.

[10] Briganti R. Dodd N. Kelly D. Pokrajac D. An efficient and flexible solver for the simulation of morphodynamics of fast evolving flows on coarse sediments beachs. *International Journal for Numerical Methods in Fluids*, 2011. John Wiley and Sons, Ltd.

[11] Bailard J.A. Inman D.L. An energetics bedload model for plane sloping beach: local transport. *Journal of Geophysical Research*, 86(C3):2035–2043, 1981.

[12] Dietrich W. E. Settling velocity of natural particles. *Water Resources research*, 18(6):1615, 1982.

[13] Hans Albert Einstein. Formulas for the transportation of bed load. *Transactions of American Society of Civil Engineers*, 107(n.d.):561–573, 1949.

[14] Bijker E.W. Some considerations about scales for coastal models with movable bed. *Delft Hydraulics Laboratory*, (50), 1967.

[15] S. Gottlieb and C. W. Shu. Total variation diminishing runge-kutta schemes. *Mathematics of Computation*, 67:73–85, 1998.

[16] A.J. Grass. *Sediment transport by waves and currents.* SERC, London, report fl-29 edition, 1981.

[17] Bayram A. Larson M. Hanson H. A new formula for the total longshore sediment transport rate. *Coastal Engineering*, 54:700–710, 2007.

[18] Liu X. Garcia M. H. *Numerical Simulation of Local Scour with Free Surface and Automatic Mesh Deformation.* IAHR, In: Examining the Confluence of Environmental and Water Concerns, 2006.

[19] F.Benkhaldoun S.Daoudi I.Elmahi. Comparison of unstructured finite volume morphodynamic models in contracting channel flows. *Mathematics and Computers in Simulation*, (81):2087–2097, 2011.

[20] Engelund F. Fredsoe J. A sediment transport model for straight alluvial channels. *Nordic Hydrology*, 125(5):293–306, 1976.

[21] Zheng J. Hu J. Calculation of longshore sediment transport in shijui bay. In *International Conference on Estuaries and Coasts*, Hangzhou, China, November 9-11 2003. Research Institute of Coastal and Ocean Engineering, Hohai University.

[22] Barry J.J. Buffington J.M. King J.G. A general power equation for predicting bed load transport rates in gravel bed rivers. *Water Source Research*, 40, 2004.

[23] Kubatko E.J. Westerink J.J. Exact discontinuous solutions of exner bed evolution model: simple theory for sediment bores. *Journal of Hydraulic Engineering*, 133(3), March 2007.

[24] Van Rijn L.C. Bed load transport: Part 2. *Journal of Hydraulic Division*, 110(11):1613–1641, 1984.

[25] Van Rijn L.C. Sediment transport: Part 1. *Journal of Hydraulic Division*, 110(10):1431–1456, 1984.

[26] Van Rijn L.C. Suspended load transport: Part 3. *Journal of Hydraulic Division*, 110(12):1733–1754, 1984.

[27] Van Rijn L.C. Principles of sediment transport in rivers, estuaries and coastal seas. *Aqua Publication*, 1993. The Netherlands, Amsterdam.

[28] Bilanceri M. *Numerical Simulations of Barotropic Flows in Complex Geometries.* PhD thesis, Corso di Dottorato in Ingegneria Aerospaziale XXIII Ciclo, 2011.

[29] Camenen B. Larson M. A general formula for non cohesive suspended sediment transport. *Journal of Coastal Resource*, 24(3):615–627, 2008.

[30] Postacchini M. Brocchini M. Mancinelli A. Landon M. A multi-purpose, intra wave, shallow water hydro-morphodinamic solver. *Advanced in water Resource, in printing*, 38(I):13–26, 2012.

[31] Bilanceri M. Beux F. Elmahi I. Guillard H. Salvetti M.V. Implicit simulations of shallow water equations with mobile bed. In J. C. F. Pereira and A. Sequeira (Eds), editors, *ECCOMAS CFD 2010*, Lisbon, June 2010.

[32] Bayram A. Larson M. Miller H. C. Kraus N.C. Cross-shore distribution of longshore sediment transport: comparison between predictive formulas and field measurements. *Coastal Engineering*, 44:79–99, 2001.

[33] Camenen B. Larroudé P. Comparison of sediment transport formoulae for the coastal enviroment. *Coastal Engineer*, 48:111–132, 2003.

[34] Nielsen P. Coastal bottom boundary layers and sediment trasport. advanced series on ocean engineering. *World Scientific Publishing*, 4, 1992.

[35] Meyer-Peter E. Müller R. Formulas for bed-load transport. *Report on 2nd meeting on international associatio on hydraulic structures research.*, pages 39–64, Stockholm; 1948.

[36] M. Bilanceri F. Beux I. Elmahi H. Guillard M.V. Salvetti. Linearised implicit time advancing and defect correction applied to sediment transport simulation. *Computer Fluids, in press*, 2011.

[37] M. Bilanceri F. Beux I. Elmahi H. Guillard M.V. Salvetti. A comparison of two finite-volume methods combined with implicit time advancing in the simulation of sediment transport problems. *Mathematics and Computers in Simulation, submitted for publication*, 2012.

[38] USACE. *Shore Protection Manual*. Department of the Army, U.S. Corps of Engineers, Washington, DC 20314.

[39] Ackers P. White W.R. Sediment transport: new approach and analysis. *Journals of Hydraulics Division*, 99(1):2041–2060, 1973.

Acknowledgements

In primis, non voglio presentare dei ringraziamenti ma delle scuse formali. Scuse dovute al mio comportantamento durante questa lunga Tesi, rivolte principalmente alla Prof. Maria Vittoria Salvetti ed a Marco Bilanceri. Scuse perché la mia attenzione non è stata focalizzata su questo periodo in maniera constante, che non hanno che potuto influire negativamente anche nella parte finale dell'elaborato, portandomi a errori e distrazioni in una quantità tale che mi portano a dovervi delle scuse. Non è stata colpa mia, lo so, ma ve le devo. Passando ai ringraziamenti veri e propri, i primi vanno, senza ombra di dubbio, al Dott. Alberto Gramaglia. Senza ipocrisia, senza il suo aiuto la mia vita sarebbe stata ancora più difficile di quella che è stata finora, vuota, e non mi permetterebbe, adesso, di rivolgere i ringraziamenti alla Prof. Maria Vittoria Salvetti, per i consigli, la pazienza, le correzioni (sopratutto d'inglese) e l'umanità con cui delle volte si è rivolta nei miei confronti. Senza contare per la grande, grandissima, opportunità che mi ha dato nello Stage a Tunisi di partecipare e di parlare al lancio del MedLagoon Project, in cui ho potuto conoscere persone di una certa caratura tra cui Hervé Guillard, persona squisita e dalla grande voglia di fare, da prendere da esempio. Per lo stage a Tunisi, ringrazio Sondes, Slah e Lassaad per la cordialità e la premura con cui si sono rivolti verso di me. Marco. Non mi sono scordato di te. Grazie. Grazie per avermi introdotto nel mondo SWE, Fortran, per il tuo aiuto su Tapenade e per avermi sopportato quando ti rompevo cose che non possono essere scritte su una tesi di laurea. Grazie. Ringraziamenti vanno anche ad Andrea Fani (in particolare), ad Annabella e Alessandro Mariotti, ho condiviso per un pò il laboratorio con voi e siete bravissime persone, disponibili, destinate a grandi cose. In ultimo, per quanto riguarda l'ambito lavorativo, all'ultima persona che ho conosciuto e che mi ha stupito per osservazioni su particolari in cui non mi sarei mai aspettato domande e/o osservazioni, ma su cui avevo comunque perso tempo. Un grazie dunque a Francois Beux, per avermi insegnato come la puntigliosità e la precisione non sono ancora mercie rara, fortunatamente. Adesso tocca a voi, spina nel fianco. Antonio, Michela e Paola. Come farei senza di voi? Forse ho già risposto, che dite? Meglio sottolineare solo quanto bene voglia a Michela e quanto me ne volgia lei, solo a sopportarmi, e passare a ringraziare Isabella e Mariagrazia, la mia prima, seconda famiglia. Senza di voi non ce l'avrei fatta, sopratutto nell'ultimo, arduo ma tranquillo, periodo. Grazie per tutto quello che avete fatto nella mia vita, anche se, purtroppo, siete una juventina e l'altra interista. Non tutte le ciambelle riescono con il buco. Un ringraziamento anche a Matteo. Ma sopratutto a Franco, Francesco, e come ti chiami? Persona, quest'ultima, da cui è possibile imparare sia il buono della vita, che la sofferenza, che la voglia di non arrendersi mai. E adesso, passiamo alla mia seconda e terza, seconda famiglia. Si, perchè esperienze che ho passato con voi vi rendono una seconda famiglia per me. Sto parlando ovviamente del Milan e della sua tifoseria, grazie

di tutte le gioie che mi hai tolto e levato. Grazie. Oddio si, l'ho fatto. Siete cascati in uno dei miei classici scherzoni. Ovviamente, come seconda e terza famiglia sto parlando di due gruppi di amici, con cui ho stretto in ambiti diversi. Il primo, storico, è capitanato da Massimo e Veronica, seguito da Gabriele, Max, Annalaura e via dicendo da una parte, Simone e Nicola dal'altra. Lorenza, tu no. E poi no. E ancora... no. La terza, seconda famiglia, penso sia quella a cui devo di più, forse, ed è quella che mi odia, forse, di più. Per primi, ringraziamenti (d'ufficio, mica sentiti?) a Lucia ed ad Alberto. A quest'ultimo in particolare, mai e poi mai avrei pensato di riuscire a trovare una persona così lontana e vicina a me. Spero un giorno di poter lavorare con te o, comunque, frequentarti più assiduamente (povero a te). Poi nomino Francesco, Lorenzo e l'informatico di fiducia oramai, Alec. Nicoletta, Daniele, Nicolas, Daniele, Ernesto, Daniele, Ambra, Elena, Veronica, Roger, Lucia, Daniele, Daniele, Bianca, Daniele, Cristiano, il duo Lorenzo, Gufo, tutti i numeri da 0 a infinito e soprannominati/e varie. Grazie. Anche a quelli di cui mi sono scordato, a quelle persone che per poco sono entrate a far parte della mia vita e l'hanno resa migliore, e a quelli che non ho incluso e che ci vorrebbero essere, per non esserci. Chi mi conosce, sa cosa intendo. Un saluto ad un gruppo di simpatici nerd, conosciuto da poco ma a cui mi sono, purtroppo, un pò affezionato, con cui ho condiviso una passione su internet. Due scuse, per chiudere, come ho aperto, anche perché la stessa vita è ciclica, e non vorrei disobbedire alle leggi naturali. La prima, va ad una persona che ogni tanto mi torna in mente, con cui ho avuto un comportamento vigliacco, pauroso e infelice. Mi dispiace, effettivamente non dovrei azzardarmi neanche a scrivere queste cose, ma che dico, niente giustificazioni, zero scuse. In secondo luogo, a mio zio Angelino, per non averlo nominato nei ringraziamenti. Scusa, non l'ho fatto solo perchè sono sicuro che stai concludendo questo lavoro al mio fianco, come sempre farai, spero. Ne ho avuto riprova subito dopo che ti ho chiesto aiuto, non sono bastate neanche 24 ore. Ti voglio bene. Grazie. Grazie di cuore a tutti. Ma sopratutto ringrazio di cuore, la persona di cuore, che mi ha ridato un cuore.

It can only ends once, and everything that happens before that, it is just progress.